ACQUISITION, PROCESSING, AND ANALYSIS OF DIFFUSION TENSOR IMAGING AND ATROPHY MRI IN THE INJURED PEDIATRIC SPINAL CORD

A Dissertation
Submitted to
the Temple University Graduate Board

In Partial Fulfillment
of the Requirements for the Degree
DOCTOR OF PHILOSOPHY

by
Devon M. Middleton

Diploma Date December 2017

Examining Committee Members:

Nancy Pleshko, Ph.D., Advisory Chair, Department of Bioengineering
Feroze B. Mohamed, Ph.D., Examining Chair, Department of Bioengineering
Scott H. Faro, M.D., Professor, Department of Bioengineering
Sayed Ali, M.D., External Member, Professor, Department of Radiology

ABSTRACT

Spinal cord injury has the potential to be debilitating, particularly in the pediatric population. Identification of the exact injury level can be difficult from conventional structural Magnetic Resonance Imaging (MRI) scans, and younger children often have difficulty in participating in the clinical examinations that define neurologic damage. Because of limitations of existing clinical examinations and conventional imaging, more advanced quantitative imaging techniques are important for improvement in diagnostic and prognostic evaluation of spinal cord injury. A quantitative characterization of the full spinal cord injury from both a functional and structural perspective has not been performed in pediatric subjects and has potential to provide important diagnostic and prognostic information. Diffusion tensor imaging (DTI) gives a non-invasive quantification of water diffusion in the spinal cord and can provide insight into white matter integrity, while high resolution volumetric imaging can determine cord cross sectional area reflecting atrophy occurring post injury. Multiple challenges exist in analysis of pediatric spinal cord data, including physiological motion, low signal-to-noise, thermal noise and image artifact, and cumbersome measurements of cord morphology. In this work, a complete pipepline for the acquisition and analysis of both functional DTI data and high resolution structural data is designed, tested, and implemented including MR image acquisition, motion correction, diffusion tensor estimation, region of interest analysis, and semi-automated cord cross sectional area measurement. Data for both healthy subjects and subjects with spinal cord injury is collected and significant correlations are shown between DTI and cord morphology metrics. This characterization of the injured spinal cord using both structural and functional data has the potential to offer important new information for examination of spinal cord injury.

To my wife, Keiko, my mother Kathy, and my father, Andy.

TABLE OF CONTENTS

Page

LIST OF TABLES

LIST OF FIGURES

CHAPTER 1

INTRODUCTION AND BACKGROUND

Injury to the spinal cord can be debilitating, resulting in motor and sensory deficits which are irreversible in many cases. Spinal cord injury (SCI) is a particularly serious problem in the pediatric population with 50% of children with SCI having complete injury with total motor and sensory deficit below the level of cord injury [1]. SCI in children can result from traumatic injury (e.g. falls, motor vehicle accidents) or non-traumatic causes (e.g. spinal tumor, transverse myelitis). The identification of exact injury level can be a complicated process and can involve radiologist examination of structural magnetic resonance imaging (MRI) scans, plain radiography, or computed tomography myelography, as well as clinical examinations assessing motor and sensory function such as the International Standards for Neurological Classification of Spinal Cord Injury (ISNCSCI). The precise injury level can be difficult to determine from one or both of these methods, as non-traumatic injury is not always easily discernible from these imaging methods and younger children often have difficulties participating in clinical examinations [2]. Because of the limitations of existing clinical examinations and conventional medical imaging methods, more advanced quantitative imaging techniques are important for improvement in diagnostic and prognostic evaluation of spinal cord injury. Quantitative analysis of structural and functional image data has the potential to provide greater information than diagnostic imaging or clinical examination alone, and this work will explore the use of two quantitative approaches to pediatric spinal cord imaging: diffusion tensor imaging and spinal cord cross sectional area measurement.

Diffusion tensor imaging (DTI) is an emerging technique in MRI for spinal cord applications. This technique is a type of quantitative functional MRI which is capable of measuring water diffusion in-vivo by examining signal changes between images acquired with diffusion sensitizing magnetic gradients and images acquired without. DTI is an intriguing modality for spinal cord evaluation due to its sensitivity to changes in white matter as demonstrated in the brain. Since DTI allows for the measurement of in-vivo anisotropic water diffusion, it can reveal useful diagnostic information about the microstructural characteristics of different tissues and is particularly effective when examining highly anisotropic structures such as white matter[3-5]. DTI has been used extensively in the brain for examination of white matter pathologies. It has been translated for use in the spinal cord to a lesser extent, but this requires an examination of acquisition and processing strategies due to differences in geometry and physiological motion in the spinal cord as compared with the brain.

The quantitative examination of spinal cord morphology also has the potential to be a valuable tool in diagnosis and prognosis regarding SCI. In addition to the initial damage caused due to injury such as cord compression, hemorrhage, or partial or complete cord transection, several degenerative processes (e.g. Wallerian degeneration, neurotransmitter toxicity, glial scarring [6-8]) continue post stabilization causing some amount of neuronal atrophy in the cord.

The use of these two techniques has potential to improve understanding of SCI in the pediatric population and improve diagnostic and prognostic capabilities.

1.1 Diffusion Tensor Imaging

DTI is based on the principle of quantification of diffusion using spin echo magnetic resonance measurements in the presence of a magnetic gradient. This has been well established since the 1960's in nuclear magnetic resonance spectroscopy. The principle of diffusion measurement is based on the magnetic resonance signal intensity of signals acquired with pulsed magnetic gradients and with no applied gradient. In 1965, an equation was derived by Stejskal and Tanner which relates the intensities of the signals with and without applied gradients to the self-diffusion coefficient[9]. The Stejskal Tanner equation,

$$\ln[A(2\tau)/A(0)] = -\gamma^2 D\delta^2(\Delta - \tfrac{1}{3}\delta)g^2 \tag{1.1}$$

has been used to form the basis for diffusion imaging in MRI. In the equation, the ratio $A(2\tau)/A(0)$ is the ratio of signal amplitude at the echo time to the amplitude at the time of excitation, γ is the gyromagnetic ratio of the nucleus being excited (hydrogen in the case of MRI), g is the amplitude of the pulsed diffusion sensitizing gradient, δ is the gradient application time, and D is the self diffusion coefficient.

This method can be easily illustrated in the case of isotropic diffusion where the problem may be reduced to one dimension allowing for the spatial orientation of the pulsed diffusion gradients to be disregarded. If a 90 degree radio frequency (RF) pulse is applied at the resonant frequency for hydrogen in a static magnetic field, the protons will begin to precess at frequency ω, which is the case in conventional MRI. The application of a magnetic gradient whose strength increases with distance will result in an increase in all protons' frequencies of precession based on their position along the gradient owing to the fact that precession frequency is a function of the local magnetic field strength. Turning off the gradient will result in all protons returning to the same precession frequency, but those toward the stronger end of the gradient will have precessed ahead of those toward the lower end. This results in the protons being labeled positionally by their phase. The 180 degree refocusing pulse used in spin echo measurements is applied, but between the refocus and echo another gradient is pulsed which cancels the first. If no diffusion occurs, there will be no net effect from the gradient pulses and all precessions will be in phase, resulting in a signal equal to that acquired with no diffusion gradients applied (Figure 1-1).

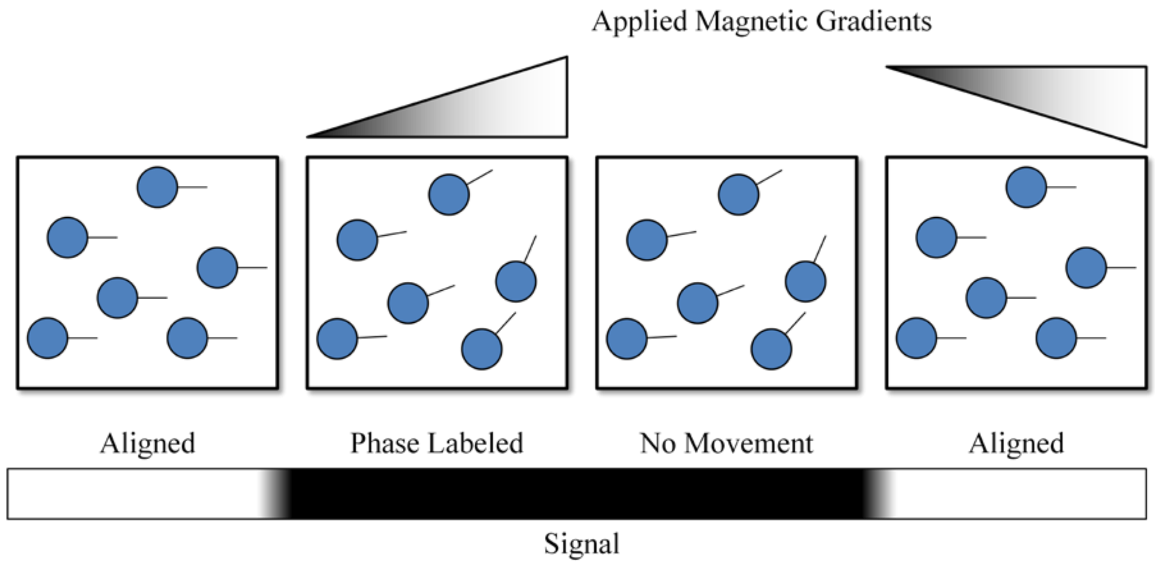

Figure 1-1: Illustration of pulsed diffusion sensitizing gradients in the absence of diffusion and the resulting induced signal from precession; tail direction indicates precession phase.

But if diffusion is occurring, protons will not be subjected to the same gradient strengths in each pulse and the phase changes will not be cancelled. Thus, protons in a given region will not necessarily be in phase and the echo generated will be lower in intensity than that without applied gradients (Figure 1-2). This signal attenuation allows for the measurement.

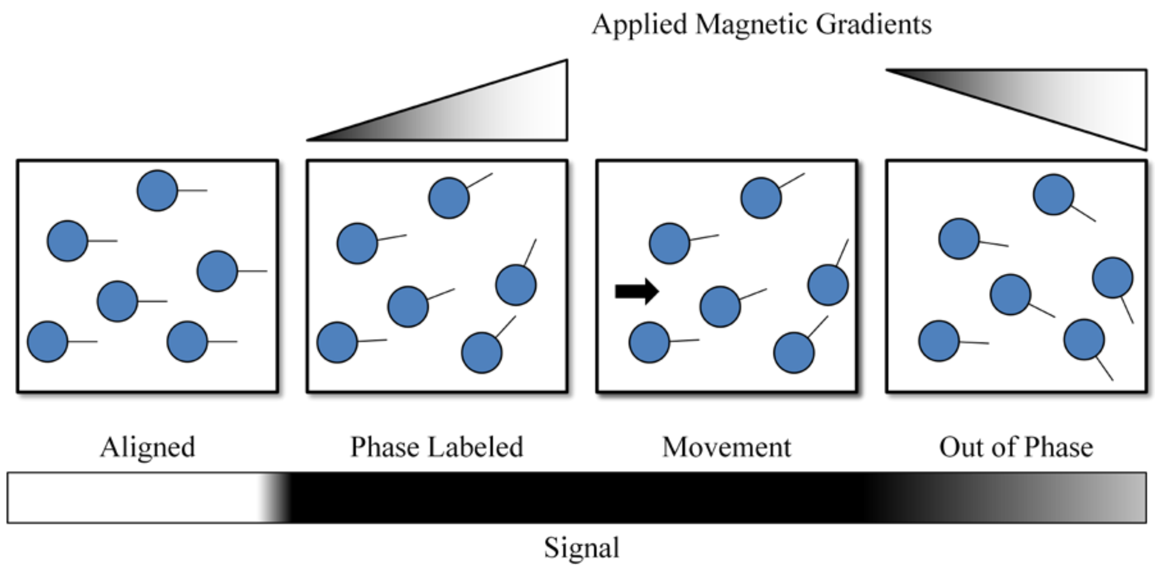

Figure 1-2: Illustration of pulsed diffusion sensitizing gradients with diffusion occurring and the resulting induced signal from precession; tail direction indicates precession phase.

DTI is the application and extension of this concept to characterize directional diffusion in three dimensions. The diffusion tensor D^{eff} is a symmetric 3x3 matrix which relates diffusion J and the concentration gradient ∇C in a medium as:

$$\begin{bmatrix} J_x \\ J_y \\ J_z \end{bmatrix} = -\begin{bmatrix} D_{xx}^{\text{eff}} & D_{xy}^{\text{eff}} & D_{xz}^{\text{eff}} \\ D_{yx}^{\text{eff}} & D_{yy}^{\text{eff}} & D_{yz}^{\text{eff}} \\ D_{zx}^{\text{eff}} & D_{zy}^{\text{eff}} & D_{zz}^{\text{eff}} \end{bmatrix} \begin{bmatrix} \frac{\partial C}{\partial x} \\ \frac{\partial C}{\partial y} \\ \frac{\partial C}{\partial z} \end{bmatrix} \tag{1.2}$$

The diffusion tensor D^{eff} can then be related to the log-transformed ratio of diffusion weighted and unweighted signal intensities for a given direction number **n** from the Stesjkal-Tanner equation as:

$$\begin{aligned} \ln\left[\frac{A(0)}{A(\mathbf{n})}\right] = [& b_{xx}D_{xx}^{\text{eff}} + b_{yy}D_{yy}^{\text{eff}} + b_{zz}D_{zz}^{\text{eff}} + (b_{xy} + b_{yx})D_{xy}^{\text{eff}} \\ & +(b_{xz} + b_{zx})D_{xz}^{\text{eff}} + (b_{yz} + b_{zy})D_{yz}^{\text{eff}}] \end{aligned} \tag{1.3}$$

where $A(0)$ is the unweighted signal intensity, and $A(\mathbf{n})$ is diffusion weighted image signal intensity for gradient direction **n**[3]. The b-matrix represented by b_{ij} is a symmetric 3 x 3 matrix which is calculated for each diffusion direction based on pulse shape, amplitude, and spatial orientation [10].

The diffusion tensor is a 3 x 3 symmetric matrix, therefore six independent elements must be calculated for complete characterization. In order to solve for all independent elements, at least six diffusion weighted images need to be acquired in noncollinear directions, along with a single unweighted image. A vectorized approach is often used to allow for rapid estimation of $\mathbf{D}^{\mathbf{eff}}$:

$$\begin{bmatrix} X_1 \\ X_2 \\ X_3 \\ X_4 \\ X_5 \\ X_6 \end{bmatrix} = \begin{bmatrix} b_{xx}^1 & 2b_{xy}^1 & 2b_{xz}^1 & b_{yy}^1 & 2b_{yz}^1 & b_{zz}^1 \\ b_{xx}^2 & 2b_{xy}^2 & 2b_{xz}^2 & b_{yy}^2 & 2b_{yz}^2 & b_{zz}^2 \\ b_{xx}^3 & 2b_{xy}^3 & 2b_{xz}^3 & b_{yy}^3 & 2b_{yz}^3 & b_{zz}^3 \\ b_{xx}^4 & 2b_{xy}^4 & 2b_{xz}^4 & b_{yy}^4 & 2b_{yz}^4 & b_{zz}^4 \\ b_{xx}^5 & 2b_{xy}^5 & 2b_{xz}^5 & b_{yy}^5 & 2b_{yz}^5 & b_{zz}^5 \\ b_{xx}^6 & 2b_{xy}^6 & 2b_{xz}^6 & b_{yy}^6 & 2b_{yz}^6 & b_{zz}^6 \end{bmatrix} \begin{bmatrix} D_{xx}^{\mathrm{eff}} \\ D_{xy}^{\mathrm{eff}} \\ D_{xz}^{\mathrm{eff}} \\ D_{yy}^{\mathrm{eff}} \\ D_{yz}^{\mathrm{eff}} \\ D_{zz}^{\mathrm{eff}} \end{bmatrix} \tag{1.4}$$

where X_n is the log transformed ratio of unweighted to weighted signal intensity for gradient direction n, and b_{ij}^n is the ijth element of the b-matrix for gradient direction n [11]. Tensor estimation can then be performed by computing $\mathbf{D}^{\mathbf{eff}}$ based on the inverse of the b-matrix as:

$$\mathbf{D}^{\mathbf{eff}} = \mathbf{b}^{-1}\mathbf{X}, \tag{1.5}$$

or using the pseudo inverse of **b** if more than six directions are acquired and **b** is no longer a square matrix as:

$$\mathbf{D}^{\mathbf{eff}} = (\mathbf{B}^{\mathrm{T}}\mathbf{B})^{-1}\mathbf{B}^{\mathrm{T}}\mathbf{X}. \tag{1.6}$$

This tensor estimation is performed on a voxel-by-voxel basis for each slice in an MR image. After tensor estimation is complete, the relevant diffusion indices can be extracted which provide information about water diffusion in the tissue being imaged.

The eigenvalues of the tensor provide basic information regarding axial and radial diffusion magnitude. The primary eigenvalue, λ_1, gives the diffusion magnitude along the axis of the tensor's primary eigenvector. This is commonly referred to as the axial or longitudinal diffusivity (AD). The second and third eigenvalues (λ_2, λ_3) provide the magnitude of diffusion orthogonal to the axis of the primary eigenvector and the average of these two values is called the radial diffusivity (RD). Mean diffusivity (MD) is the average of all three eigenvalues and represents the average diffusion magnitude irrespective of direction.

Fractional anisotropy (FA) is another important diffusion metric and is one of the most frequently examined in DTI. It is calculated from the eigenvalues as:

$$FA = \sqrt{\frac{1}{2}}\frac{\sqrt{(\lambda_1-\lambda_2)^2+(\lambda_1-\lambda_3)^2+(\lambda_2-\lambda_3)^2}}{\sqrt{(\lambda_1^2+\lambda_2^2+\lambda_3^2)}} \tag{1.7}$$

FA is a ratio ranging from zero to one which represents the extent to which a diffusion tensor is anisotropic. A FA value of one indicates complete anisotropy, or diffusion along only one single direction, and a FA of zero is representative of completely isotropic diffusion (Figure 1-3). FA maps are used to show the degree of directionality in imaged tissue, and color FA maps are often used to represent three dimensional diffusion in a two dimensional image. Color FA maps are obtained by the FA value by the magnitudes of the x, y, and z components of the diffusion tensor's primary eigenvector to generate the map's red, green, and blue intensities, respectively (Figure 1-4).

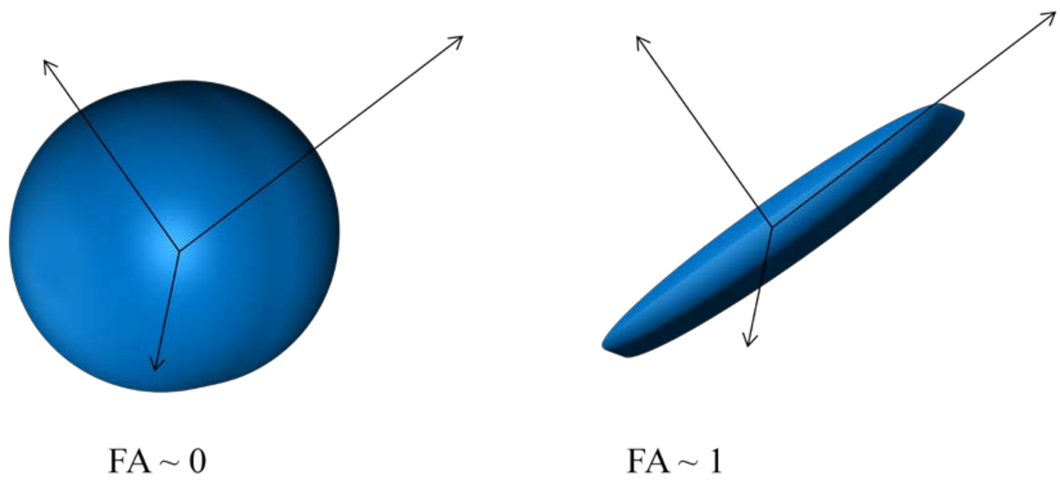

Figure 1-3: Ellipsoids representing diffusion patterns at FA values near zero and one.

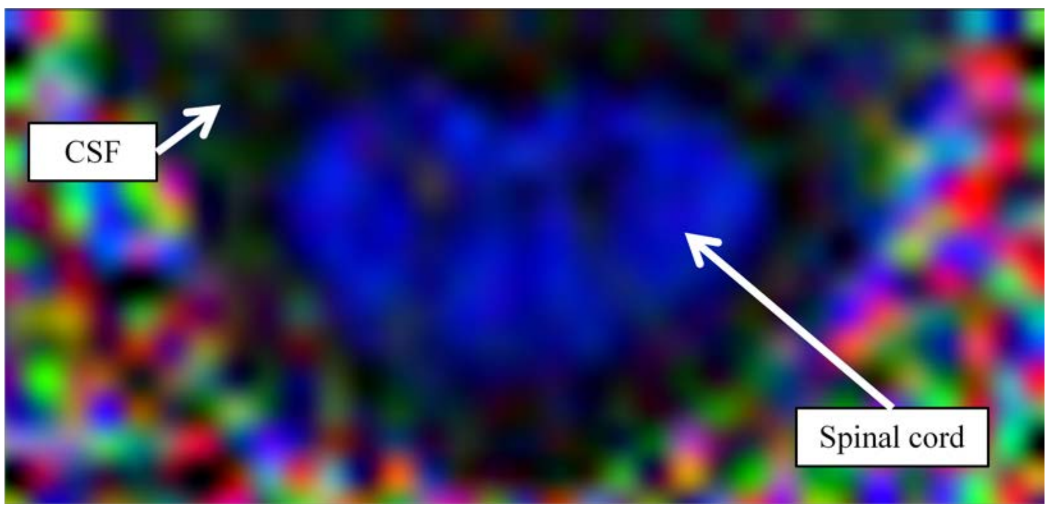

Figure 1-4: Axial color FA map of the spinal cord. The brighter blue color indicates anisotropic diffusion primarily in the z-axis (through plane), and the low intensity, nearly black, in the CSF indicates highly isotropic diffusion due to the lack of microstructural barriers.

1.2 Diffusion Tensor Imaging in the Spinal Cord

DTI has become a popular technique for use in neuroimaging because of its ability to identify abnormalities in white matter via examination of diffusion indices extracted from the diffusion tensor[12, 13]. Healthy white matter is composed of bundles of myelinated axons and the lipid myelin sheathes act as channels which restrict diffusion perpendicular to the axon resulting in higher anisotropy in the direction of the axon. When white matter is compromised by injury or other pathology, the myelin sheath breaks down which results in a loss of anisotropic diffusion as water can more easily diffuse radially (Figure 1-5) [14]. As a result, regions containing more intact axons will exhibit higher FA values than those with damaged axons. Importantly, these changes can be detected in tissue which appears normal using conventional MRI in addition to issues which can be identified as injured/pathological[12].

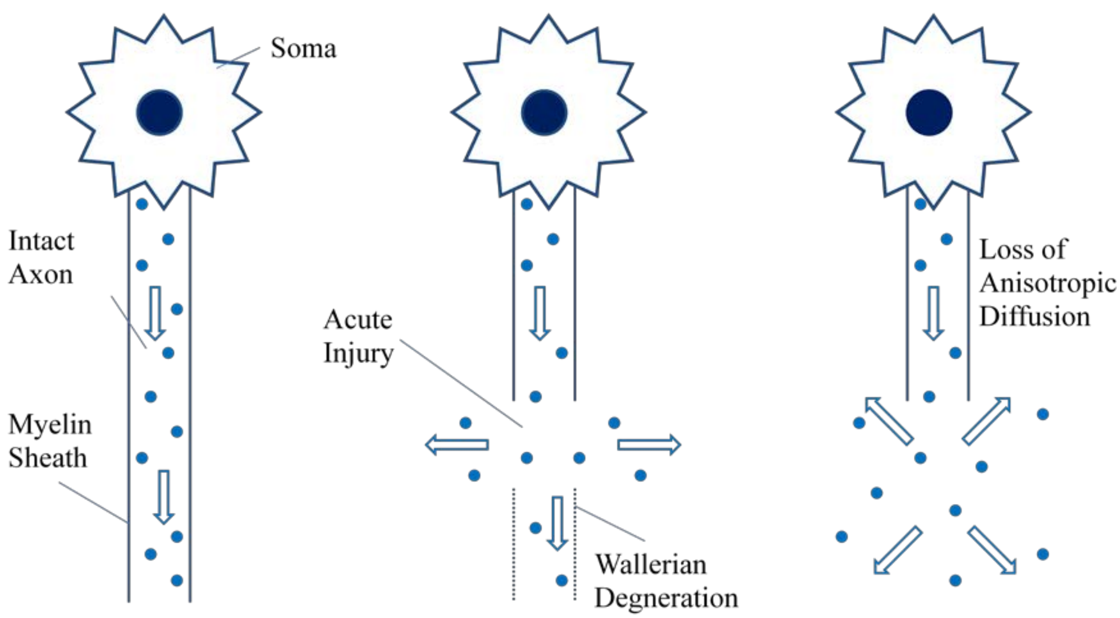

Figure 1-5: Illustration of diffusion changes in damaged axon.

Spinal cord DTI is an expanding area in MR research, including evaluation of acute injury and degenerative conditions [15-31]. Most studies employ FA measurements as a major point of comparison because of its ability to reflect a loss of anisotropic diffusion due to axon transection and degeneration. All studies reviewed showed decreases in FA for the spinal cord in subjects with injury or other degenerative conditions.

In a study of adult subjects with cervical spinal cord injury, Petersen et al. demonstrated significant decreases in FA values for injured subjects and correlations with clinical and electrophysiological measures[32]. Significant decreases in FA values were also found in transverse myelitis patients by Lee et al., including changes in normally appearing spinal cord tissue[33]. A study of adults with cervical spinal cord injury by Freund et al. showed significant decreases in FA for subjects with spinal cord injury, as well as FA changes in the brain[34]. Correlations were shown between DTI metrics and American Spinal Injury Association clinical examination scores for adult subjects with spinal cord injury by Cheran et al. along with significant decreases in FA as compared to healthy subjects[35].

Very limited work has been performed for DTI of the pediatric spinal cord. Mulcahey et al. found good predictive accuracy of DTI with cervical spinal cord injury based on FA and clinical examinations and demonstrated differences including decreased FA between typically developing and injured subjects[36]. DTI values were examined for the pediatric spinal cord in subjects with brain injury were also examined by Orman et al. and found to differ from typically developing subjects[37]. Conklin et al. examined diffusion differences between typically developing subjects and subjects with spinal cord injury using diffusion kurtosis imaging, an extension of DTI[38]. In the typically developing spinal cord, normative values for pediatric spinal cord DTI were acquired by Barakat, et al. [21]. Additionally, Saksena et al. acquired pediatric spinal cord DTI data and demonstrated age related changes in FA and diffusivity values for typically developing subjects with no significant differences based on sex[39].

The spinal cord lends itself well to DTI due to the fact that it is an inherently anisotropic structure, largely comprising long, myelinated axons. Acquiring high-quality undistorted diffusion weighted images of the normal and injured/diseased spinal cord has the potential to aid in diagnosis and treatment, but several technical challenges exist in the acquisition of noise-free images.

A major difficulty is the impact of motion, which can result from patient movement, cord pulsation and oscillation, and respiratory motion [40-42]. Quantitatively, motion can cause artifacts and misalignment which can potentially result in overestimation or underestimation of diffusion magnitude [18], and can also result in poor delineation between the spinal cord and surrounding cerebrospinal fluid. Cardiac and respiratory gating are techniques that can be used to reduce motion artifacts during acquisition in some cases[43]. These gating methods attempt to synchronize the MR acquisition with the subjects cardiac or respiratory cycles based on signal from an EKG, pulse oximiter, or respiratory belt. However, these methods extend scan time as the acquisition must frequently pause in order to resynchronize with a given physiological cycle which in turn can lead to patient discomfort. This is a particular problem in the pediatric population, where subjects frequently have less patience for longer scans and greater difficulty in remaining still than adult subjects. Post-processing motion correction can be an effective means of improving image quality without increased scanning time [44],[45].

Another important issue is the presence of artifact due to magnetic susceptibility of adjacent tissues, motion, and gradient and thermal noise. Additionally, the use of echo-planar imaging in DTI can create geometric distortions and increase susceptibility artifact due to the lower effective bandwidth per pixel. Artifact can impact the tensor fit, and different methods have been developed to address outliers in the fitting process and unexpected negative eigenvalues, which are not physically meaningful, in the diffusion tensor [46-48]. The lack of a gold standard for DTI values complicates the interpretation of results, and when examining DTI datasets, the tensor estimation method chosen has the potential to impact the results of the analysis. It is therefore important to examine the potential impact of different tensor estimation schemes for pediatric spinal cord DTI and select an appropriate method.

1.3 Spinal Cord Atrophy in Injury

In addition to the initial damage caused due to injury such as cord compression, hemorrhage, or partial or complete cord transection, several degenerative processes (e.g. Wallerian degeneration, neurotransmitter toxicity, glial scarring [6-8]) continue post stabilization causing some amount of neuronal atrophy in the cord. Cord atrophy is thought of as the final manifestation of various neurologic pathologies and is generally diagnosed on a qualitative rather than quantitative analysis clinically in MR imaging. In some cases, quantitative measures have been used to depict pathological processes in neurological diseases and are generally estimated by measuring the reduction in Spinal Cord Cross Sectional Area (SCCSA)/cord volume after an injury using high resolution structural MRI scans[49, 50]. Quantitative spinal cord atrophy and volume assessment post injury may provide additional useful biomarkers for injury[51], but literature review on the effects of SCI with respect to cord atrophy and volume changes suggest that this topic is not well studied, particularly in the pediatric population.

Cord cross sectional area and atrophy measurements have been used in the study of spinal cord injury and degenerative conditions such as multiple sclerosis [52-63]. Examination of cord cross section across multiple subjects in a high-resolution 3D volume has previously required considerable effort with manual ROI definition performed by trained personnel and was often unfeasible given the potential for hundreds of ROIs per subject. However, a newly developed method for semi-automated cord SCCSA measurement allows for fast and accurate measurement of the spinal cord from high resolution images with minimal manual input[64]. This method has been used to perform measurements in patients with neuroinflammatory diseases such as human T-cell lymphotropic virus type 1 associated myelopathy/tropical spastic parapesis (HAM/TSP) and multiple sclerosis as well as healthy volunteer subjects. While this technique has been effective for neuroinflammatory conditions, the injured spinal cord presents additional challenges due to variation in cord structure after injury and it must be demonstrated that it can be effectively used to measure SCCSA in injured subjects prior to implementation in a processing pipeline.

1.4 DTI Acquisition for the Pediatric Spinal Cord

DTI of the spinal cord requires an optimized imaging method due to the small size of the spinal cord and the need for high in-plane resolution as compared with brain DTI. Also, DTI techniques employ echo planar imaging (EPI), which uses rapidly switching readout gradients to acquire a complete 2D image in a single repetition time [65]. This rapid acquisition technique is helpful in reducing motion artifacts, but is subject to geometric distortions. In EPI, multiple echoes are acquired during a single excitation with a blipped phase gradient to allow complete acquisition of k-space in a single repetition time. As a consequence of this, the receiver bandwidth per pixel is relatively much lower than that of other types of MRI sequences and susceptibility artifact becomes more severe. In spinal cord DTI, the use of inner field-of-view (iFOV) techniques which reduce phase FOV size have been shown to be effective in reducing distortion [16, 21]. By reducing the phase FOV, fewer k-space phase lines need be acquired and the effective bandwidth per pixel is higher given the same total receiver bandwidth. Additionally, this allows for a substantial reduction in total scan time which is of great importance for clinical feasibility and patient comfort. The optimization of an iFOV acquisition sequence with high in-plane resolution can allow for the effective acquisition of DTI data for the pediatric spinal cord.

1.5 Aims of this Work

Aim 1: This work seeks to address the confounds involved in DTI and morphology measurement in the healthy and injured pediatric spinal cord by designing, testing, and implementing a complete processing and analysis pipeline and use the pipeline to examine relationships between DTI and spinal cord morphology in both typically developing subjects and subjects with spinal cord injury. In order to develop a pipeline, three major challenges have been identified and strategies to deal with them have been developed and tested: spinal cord motion, choice of tensor estimation, and fast, accurate measurement of SCCSA.

Aim 1A: Spinal cord motion resulting from subject sources (e.g., shifting, swallowing), and physiological sources (e.g. cardiac motion, respiratory motion, spinal cord pulsation) is unavoidable during the imaging process and must be corrected prior to analysis. Multiple image registration techniques using different combinations of transformations and cost functions are examined and a reliable methodology for retrospective motion correction of spinal cord DTI data is developed using spinal cord DTI data.

Aim 1B: Tensor estimation is subject to influence from image artifact, misregistration, and other outlier sources, and it is important to understand the impact of the choice of tensor estimation scheme and choose a technique which can best mitigate these undesired influences. Different tensor estimation techniques are evaluated using spinal cord DTI data to determine potential differences in resulting tensor fits and DTI metrics, and a methodology is selected for implementation in the pipeline.

Aim 1C: Fast and accurate segmentation of the spinal cord for SCCSA measurement can be challenging, particularly in the case of subjects with spinal cord injury where the cord may exhibit different signal characteristics and morphology as compared with typically developing subjects. In order to address this, a semi-automated segmentation technique is tested for pediatric spinal cord data to ensure its suitability for use in the processing pipeline.

Aim 2: After addressing these processing challenges, a complete processing and analysis software package is developed to employ the techniques examined. The package is then used to perform motion correction, tensor estimation, and SCCSA measurements for pediatric spinal cord data in typically developing subjects and subjects with spinal cord injury. After processing and analysis is completed, relationships between DTI and SCCSA are examined in typically developing subjects and subjects with spinal cord injury.

CHAPTER 2

DEVELOPMENT AND TESTING OF IMAGE PROCESSING

2.1 Motion Correction

The presence of motion in MRI is always problematic, but since DTI is a technique which depends on quantification of diffusion based on images acquired at different time points motion has the potential to be a major source of error. Misalignment of unweighted b0 images and diffusion weighted images can have a substantial impact on the quantitative results produced during tensor estimation. Motion can also impact the visual quality of the images. This can result in an impaired ability to clearly identify the cord/CSF interface and decrease confidence in ROI definition when examining quantitative data. Because of these issues, it is important to address motion in DTI prior to quantitative analysis in order to ensure the best possible results.

Motion is a concern in all parts of the body during MRI, and the spinal cord has several unique challenges as compared with the brain and many other regions. Major sources of motion in the spinal cord comprise patient movement, cord pulsation, cardiac pulsation, and respiratory motion[40-42]. The spinal cord pulsates regularly in the spinal canal, with the dominant motion in the anterior/posterior (A/P) direction. Some movement also occurs in the right/left (R/L) direction as well as the inferior/superior (I/S) direction[66]. (Figure 2-1) In addition to this, cardiac pulsation can contribute variation to the diffusion tensor trace resulting in the possibility of over-estimation of diffusion[18]. Reports based on brain DTI have demonstrated that motion can impact DTI results at a similar order to image noise when imaging at a field strength of 3T[67].

Respiratory motion can also create artifact which can be difficult to predict and highly variable depending on subject breathing rate and depth. Finally, bulk subject motion can contribute to misalignment whether it results form a sudden twitch or a gradual movement in one direction over the course of a scan.

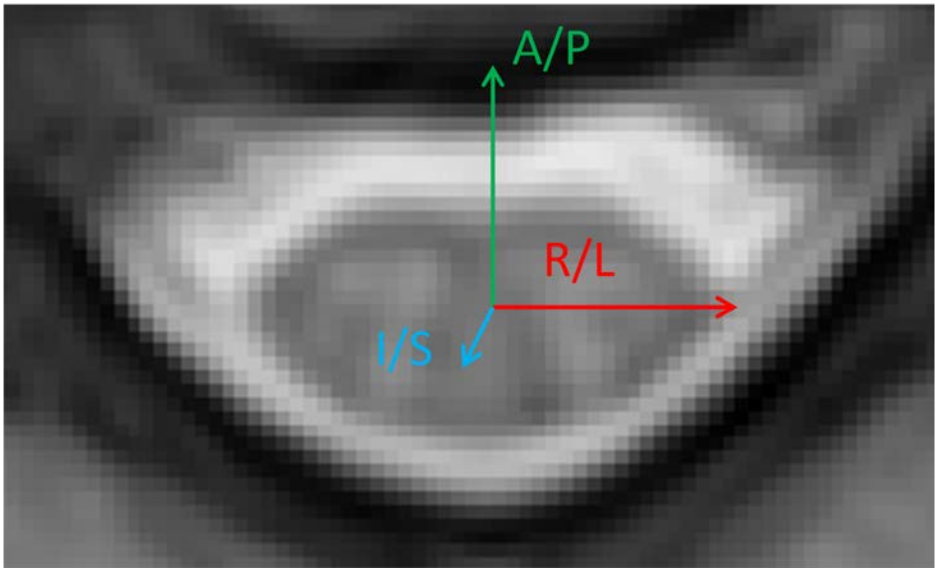

Figure 2-1: Axial view from MR image of the cervical spinal cord indicated axes along which cord pulsation occurs.

Some techniques can be used to reduce the impact of physiological and bulk motion when performing DTI. Cardiac and respiratory gating can be used to time the imaging sequence to align with the cardiac and respiratory cycles, and are a practical motion mitigation method in some cases. However, pediatric subjects often have difficulty tolerating longer scan times and both of these techniques have the potential to considerably increase scan time, as well as set up times due to the need for monitoring equipment such as EKG or respiration measurement belts. Additionally, while healthy adult subjects generally comply well with instructions to remain still, children often have more difficulty, and subjects with SCI may experience muscle spasms during scans in some cases. Due to the difficulties in minimizing motion for DTI when scanning pediatric subjects, it remains important to employ post-processing techniques for the purpose of retrospective motion correction.

Motion correction techniques involve the registration of one image or image volume (the source) to another (the target, or reference). This registration is governed by a transformation type (e.g., rigid body, affine, translation only, non-linear) which determines the degrees of freedom available for transforming the source image. A cost function is used to guide the registration by defining a relationship between the source and target image which serves as the criterion for the success of the registration. Cost functions can be based on different image characteristics including signal intensity, morphological metrics, and texture information.

Much work has been performed in the area of motion correction for brain images in DTI [68-70], but only limited research has been performed with respect to motion correction in the spinal cord, particularly in the case of DTI. Motion correction has become more common in spinal cord DTI with several investigators employing retrospective techniques [15, 19, 45, 71, 72], but it is difficult to find any attempts to systematically examine or quantify the results of motion correction in pediatric DTI. Prior to examination of DTI in the pediatric spinal cord it was necessary to test and evaluate the effectiveness of different retrospective motion correction techniques to achieve the best possible alignment of all acquired volumes including diffusion weighted and unweighted images. Successful motion correction can improve image quality, cord/CSF delineation, and voxel-to-voxel correspondence between images, therefore it was important to examine image quality from expert visual inspection, as well as quantitative information regarding volume displacement to ensure that corrections were reasonable based on known physiological motion.

2.1.1 Imaging, post-processing, and analysis

In order to test motion correction techniques, DTI data from a total of 20 pediatric subjects was examined. DTI datasets for 10 typically developing subjects with a mean age of 16.1 years with no history or evidence of injury to the spinal cord or other spinal cord pathology were used along with DTI data from 10 pediatric subjects (age range 13.2 years) with chronic cervical spinal cord injury (at minimum 6 months post injury). Scanning was performed on a 3.0 T Siemens Verio MR scanner (Siemens Healthcare, Erlangen, Germany) using a 4-channel neck matrix (two anterior, two posterior channels) and an 8-channel spine array. DTI data was acquired using an inner-field-of-view (iFOV) echo-planar (EPI) sequence using spatially selective two-dimensional RF pulses as described previously. Imaging was performed for the entire cervical spinal cord, covering the top of the C1 vertebrae through the C7-T1 disc level. All images were acquired axially with slices prescribed as closely parallel to the cord as possible based on individual cord curvature. Imaging parameters for the DTI images were as follows: FOV size = 250 mm x 43.25 mm, number of diffusion directions = 20, b value = 1000 s/mm^2, voxel size = 1.2 x 1.2 x 3 mm^3, axial slices = 35-45 (depending on subject height), TR = 6100-8000 ms, TE = 115 ms, number of excitations = 3, and acquisition time = 6-8 min. In order to keep scan times as short as possible, cardiac and respiratory gating were not used.

After acquisition, the DTI datasets were corrected for motion using several different combinations of algorithms and cost functions. Two different 3D volume based transformations were examined using the Automated-Image-registration (AIR) package implementation used in DTIstudio (www.mristudio.org)[73], and a 2D slicewise correction technique, FLIRT, implemented in FSL (www.fmrib.ox.ac.uk/fsl/) was used as well. For the 3D techniques, two options were available with respect to degrees of freedom: rigid and affine. Rigid allows for 6 degrees of freedom rigid body transformations only, i.e. only rotation and translation in the x, y, and z axes. The affine transformation allows for 12 degrees of freedom, rotation and translation, plus scaling and shearing along all three axes. The registration process also relies on a cost function used to determine the success of the registration. For both 3D methods, three different cost functions were evaluated as well: Standard Deviation, Least Squares, and Scaled Least Squares. The 2D slicewise method uses only rotation and translation in the x and y directions, and the Correlation Ratio cost function was used. In all cases, all images (diffusion weighted and subsequent b0 images) were registered to the first b0 image.

In order to analyze the 3D transformations quantitatively, the resulting 4 x 4 homogeneous coordinate transformation matrices were examined after registration had completed. Each of the six 3D transform/cost function pairs created a total of 63 transformation matrices: one for the b0 and each gradient direction for a total of 21, with three excitations resulting in a total of 63. These matrices were analyzed using software developed in Matlab which provides a quantification of the registration. This is performed by analyzing a set of transformed points spanning the entire image volume in uniformly spaced increments. The displacements in the right/left (R/L), anterior/posterior (A/P), and superior/inferior (S/I) directions measured for all points in the transformed volume, and the maximum and average amount of displacement in all directions were determined for each transformed image, including all b0 and diffusion weighted volumes. A visual comparison to the image after motion correction was then made to examine whether these quantified displacements corresponded to an improvement in image quality.

Initial inspection of the corrected images showed considerable improvement in image quality in the rigid methods using all three cost functions. Affine transformations showed improvement in some cases, but resulted in considerable distortion in others. Slicewise corrections showed little change in image quality with many artifacts still present in the final images. Image quality was more thoroughly assessed qualitatively by radiologist examination for images corrected by the rigid transformation using the scaled least squares cost function which showed the best combination of quality improvement and acceptable translational metrics based on known physiology. Two board certified neuroradiologists evaluated and scored all images based on two important criteria: cord/CSF delineation, defined as ease of determining the cord edge from surrounding CSF with as little partial volume averaging as possible, and cord homogeneity, representing correction of motion induced artifacts (Figure 2-2). Single sagittal mid-line images were scored pre and post correction for each subject for both criteria on a one to five scale, with reviewers blinded to the correction state (i.e. pre or post correction). Prior to reviewer evaluation, all images were anonymized and presented in random order.

A Wilcoxon signed rank test was used to test for statistical significance between pre and post correction images.

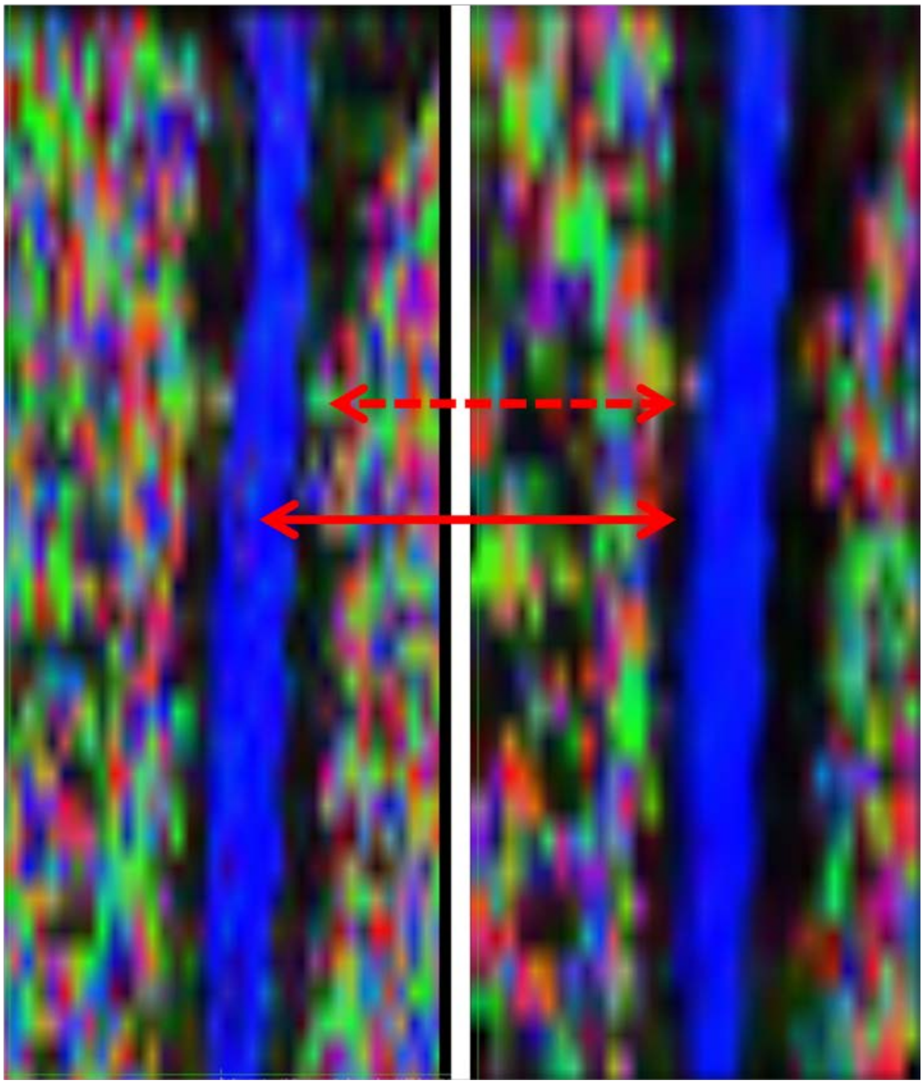

Figure 2-2: Enlarged section of pre correction (left) and post correction (right) color FA maps for a typically developing subject's cervical spinal cord. Greater cord/CSF interface conspicuity (dashed arrow) and cord homogeneity (solid arrow) are easily visible in the corrected image.

Finally, the DTI metrics calculated from both the pre and post correction images were examined to determine if significant differences were present. The diffusion tensor was computed on a voxel-by-voxel basis from axial slices using MedINRIA software (www-sop.inria.fr/asclepios/software/MedINRIA/). After tensor estimation, ROIs were drawn on sagittal mid-line slices on color FA maps which provided superior contrast and cord/CSF delineation compared with b0 or other DTI based maps. ROIs were defined to cover the complete cervical spinal cord, with approximately one voxel sparing at the cord edges to minimize partial volume averaging. Due to differences in subject anatomy, some variation in size and shape of ROIs was present, particularly in the case of subjects with spinal cord injury. Additionally, in cases of complete spinal cord injury, only the intact portion of the cord superior to the injury was included in the ROI. All ROIs were defined by personnel experienced in spinal cord imaging and trained by a board certified neuroradiologist. After completion of ROI definition, DTI metrics FA and MD were calculated for each subject in original uncorrected images, as well as post correction images for each technique used. Post calculation, pre and post correction values were compared using a paired two-tailed t-test to determine if significant differences were found after motion correction.

2.1.2 Examination of Quantitative Transformation Results

A review of the quantitative information obtained from the transformation matrices generated during correction revealed easily observable differences between the rigid and affine transformations. Broadly speaking, affine transformations showed a tendency toward large displacement spikes in some diffusion weighted images which were beyond the scope of what could be considered attributable to physiological motion, or even large subject motion in some cases. In contradistinction, rigid transformations resulted in fewer spikes in displacement, with levels consistent with expectations of physiological motion. For all transformation/cost function pairs tested, the average and maximum displacement along each axis were calculated, and the averages of these over all subjects were compared (Figure 2-3). The largest average and maximum displacement occur in the A/P direction, which is consistent with reported observations of spinal cord motion in literature.

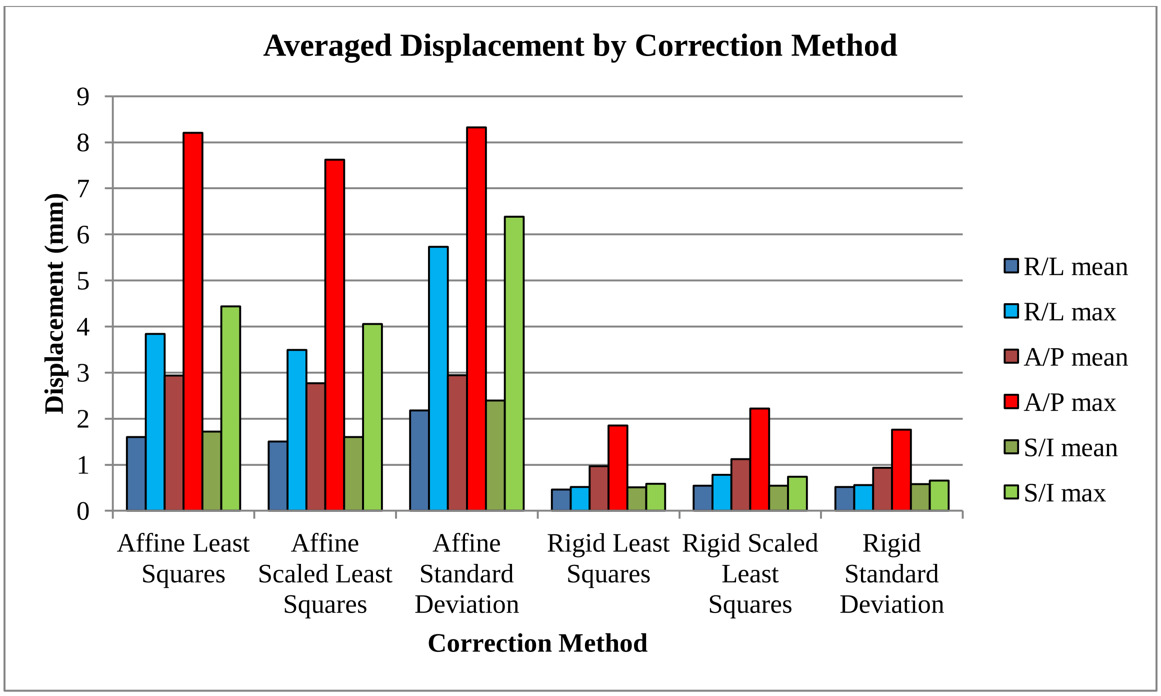

Figure 2-3: Mean and maximum displacements for all transformed images, averaged for all subjects and shown by correction method.

The greater consistency of rigid over affine methods is evident in Figure 2-3, and the fact that such large displacements occurred using affine transformations call into question the suitability of this transform type for spinal cord motion correction. It is possible to question whether these large displacements post-correction are a product of actual large displacements which were accurately corrected, however this is unlikely because they were beyond the scope of physiological motion, and in extreme cases beyond the imaging field-of-view itself. A further review of the resulting DTI maps post correction revealed that large displacement spikes as identified from the transformation matrices corresponded to severely distorted images in DTI maps (Figure 2-4).

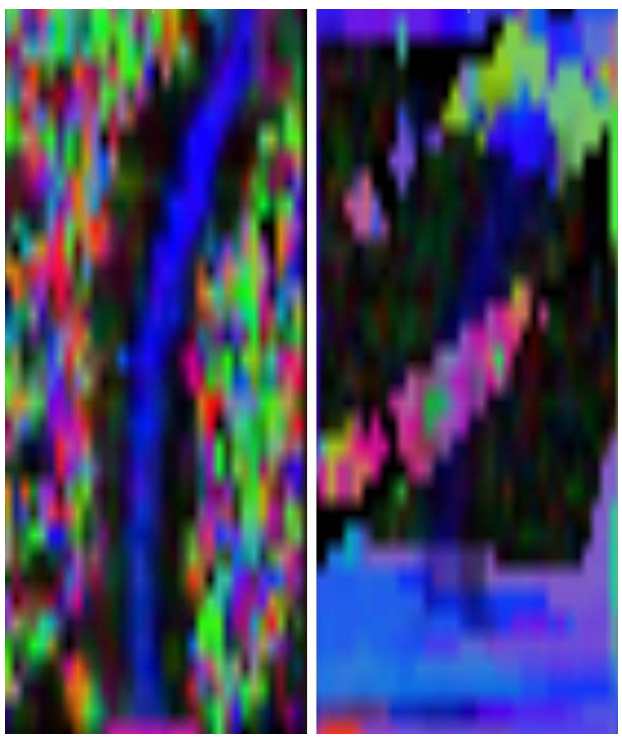

Figure 2-4: Pre (left) and post (right) correction color FA maps for a subject showing distortions resulting from severely displaced diffusion weighted images using affine transformation. Both images are the same sagittal midline slice.

Examination of post-correction diffusion weighted images with large displacement spikes showed primarily volumes with low SNR relative to other diffusion weighted images. In these cases, it is likely that the additional degrees of freedom present in the affine transformation method allow for noise to drive the registration rather than anatomy. The result of this would be some diffusion weighted images being severely misregistered and creating the substantial distortions found in FA maps in these cases. Another possible problem with the affine transformation is the difference in contrast between the b0 and diffusion weighted images. In b0 images, the CSF is hyper-intense relative to the cord and extraneous anatomy, whereas in diffusion weighted images, the cord is intense relative to the CSF, and the CSF is indistinguishable from other anatomy (Figure 2-5). Allowing shearing and scaling components as in affine transformations could allow the spinal cord in diffusion weighted images to be erroneously registered to the CSF regions of the b0 image.

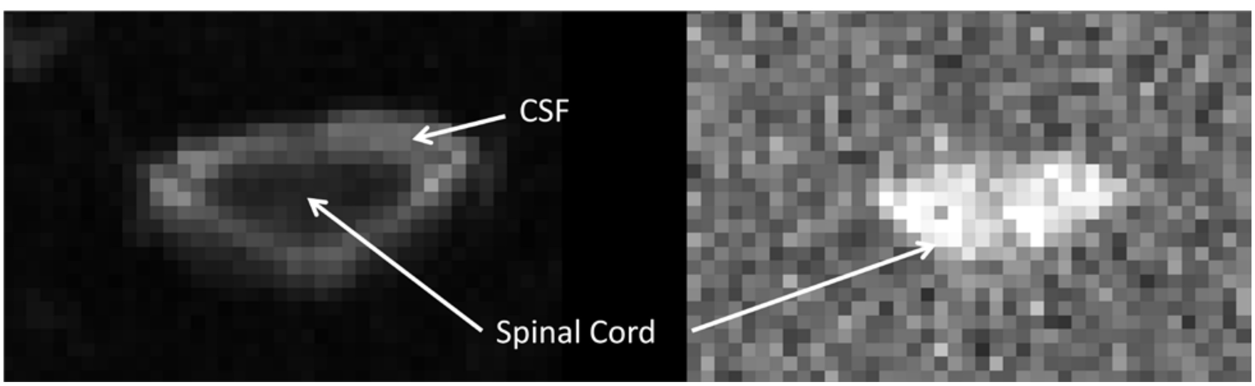

Figure 2-5: Illustration of cord, CSF, and extraneous anatomy intensities in b0 (left) and diffusion weighted (right) images for a single axial slice of the cervical spinal cord.

2.1.3 Results of Qualitative Analysis

Because rigid methods showed better correction than affine and slicewise without distortions or major displacement spikes, and quantitative analysis showed greater consistency and displacements in agreement with expectations for physiological motion they were chosen for further qualitative inspection. Of the three cost functions, scaled least squares showed the most improvement from initial inspection and the images resulting from this correction were chosen for further examination by neuroradiologist. Additionally, the intensity scaling feature of the scaled least squares cost function should provide better performance with differing contrasts as seen between b0 and diffusion weighted images. After radiologist scoring as described previously, corrected images scored higher in cord homogeneity in 20 out of 20 images, and higher in edge conspicuity in 18 out of 20 images. Pre correction images received an average score of 2.40 out of 5 in cord homogeneity, and 2.45 out of 5 in edge conspicuity. Post correction images received an average score of 3.65 in cord homogeneity and 3.45 in edge conspicuity. In the case of two images, one reviewer scored the post correction image lower in edge conspicuity than the original, but the second reviewer scored both post correction images higher. Improvements in both criteria were found to be statistically significant using a Wilcoxon signed rank test ($p < 0.0001$).

While not a quantitative measure of the effects of motion correction, qualitative analysis is useful step, as improvements in image quality (particularly cord/CSF delineation) are important in allowing for greater confidence when placing ROIs for measurement of DTI metrics. With clear separation of the cord from surrounding CSF, boundaries can be clearly drawn and partial volume averaging with CSF can be largely avoided.

2.1.4 DTI Metrics

Examination of DTI metrics FA and MD showed changes, in some cases significant, between pre and post correction images (Table 2-1). The change in FA values averaged for all subjects with spinal cord injury ranged from 11% and 28%, and the change in typically developing subjects was between 2% and 4%. In some cases, the difficulties using affine registrations resulted in severely distorted images which could not be used for DTI measurements as noted in the table. In these cases, the averages comprise only subjects where the registration was successful. P values are given based on a paired two-tailed t-test.

	FA				MD x 10^{-3} (mm^2/s)			
	TD		SCI		TD		SCI	
Correction Method	**Mean ± St.Dev.**	**p value**	**Mean ± St.Dev.**	**p value**	**Mean ± St.Dev.**	**p value**	**Mean ± St.Dev.**	**p value**
No correction	0.57 ± 0.16	-	0.47 ± 0.15	-	0.64 ± 0.17	-	0.66 ± 0.22	-
Affine + Lsq	0.55 ± 0.12[a]	0.027	0.38 ± 0.14[b]	<0.0001	0.60 ± 0.18[a]	0.079	0.74 ± 0.29[b]	0.018
Affine + ScaledLsq	0.55 ± 0.13[c]	0.26	0.41 ± 0.13[d]	0.0013	0.64 ± 0.22[c]	0.072	0.71 ± 0.23[d]	0.69
Affine + Std	0.56 ± 0.13	0.55	0.34 ± 0.11[e]	0.0005	0.59 ± 0.21	0.11	0.74 ± 0.26[e]	0.0017
Rigid + Lsq	0.56 ± 0.13	0.36	0.37 ± 0.12	<0.0001	0.60 ± 0.18	0.057	0.73 ± 0.22	0.34
Rigid + ScaledLsq	0.55 ± 0.13	0.30	0.36 ± 0.12	<0.0001	0.60 ± 0.18	0.056	0.74 ± 0.23	0.26
Rigid + Std	0.55 ± 0.14	0.39	0.37 ± 0.12	<0.0001	0.61 ± 0.2	0.35	0.77 ± 0.26	0.016
Slicewise	0.56 ± 0.15	0.43	0.42 ± 0.14	0.0004	0.67 ± 0.22	0.024	0.77 ± 0.28	0.0024

a - includes only 9 successful registrations out of 10

b - includes only 7 successful registrations out of 10

c - includes only 6 successful registrations out of 10

d - includes only 8 successful registrations out of 10

e - includes only 5 successful registrations out of 10

Table 2-1: Changes in FA and MD pre and post correction for all methods averaged by typically developing (TD) and subjects with spinal cord injury (SCI).

Using rigid scaled least squares correction, statistically significant differences were found between pre and post correction FA for subjects with spinal cord injury ($p < 0.0001$), but not for typically developing subjects ($p = 0.30$). There was no significant difference found between pre and post correction MD for typically developing subjects ($p = 0.056$) or subjects with spinal cord injury ($p = 0.26$). The average change in FA for typically developing subjects using rigid scaled least squares was 2.8%, and 23.6% for subjects with spinal cord injury. The average change in MD using rigid scaled least squares was 5.0% for both typically developing subjects and subjects with spinal cord injury. Additionally, FA variance within individual subjects decreased post correction by 18.3% in typically developing subjects and 19.0% in subjects with spinal cord injury.

The large and statistically significant changes in FA for subjects with spinal cord injury post correction is suggestive that motion correction may be a more critical component of a processing pipeline in subject with spinal cord injury. After injury, it is possible for the spinal cord to exhibit aberrant pulsatile motion[74] due to changes in morphology, and some subjects with spinal cord injury may have an increased likelihood of involuntary motion depending on the nature of the injury. In addition to morphological changes to the cord, glial scarring has the potential to decrease the stiffness of the spinal cord[75] thus making the cord more susceptible to movement in reaction to CSF pulsation and other types of physiological motion. If these factors are present, they can result in increased misregistration in the uncorrected data as compared with typically developing subjects.

2.1.5 Method Refinements and Conclusion

One remaining issue was the difference in contrast between b0 and diffusion weighted images which was not fully addressed by the methods examined thus far. In order to resolve this, the 3D, six degree of freedom rigid transformation was employed utilizing a normalized mutual information cost function. Because mutual information based cost functions use entropy of a joint histogram between the images being registered rather than intensity metrics, they are contrast insensitive and more suitable for registration of images with disparate contrasts. The application of this technique resulted in further improvements in image quality, and in some cases resulted in drastic recovery of otherwise unusable images (Figure 2-6). The corrected images demonstrate on the post processed image on the left show improved signal homogeneity of the spinal cord. The post processed images on the right shows improved cord/CSF and grey matter/white matter conspicuity.

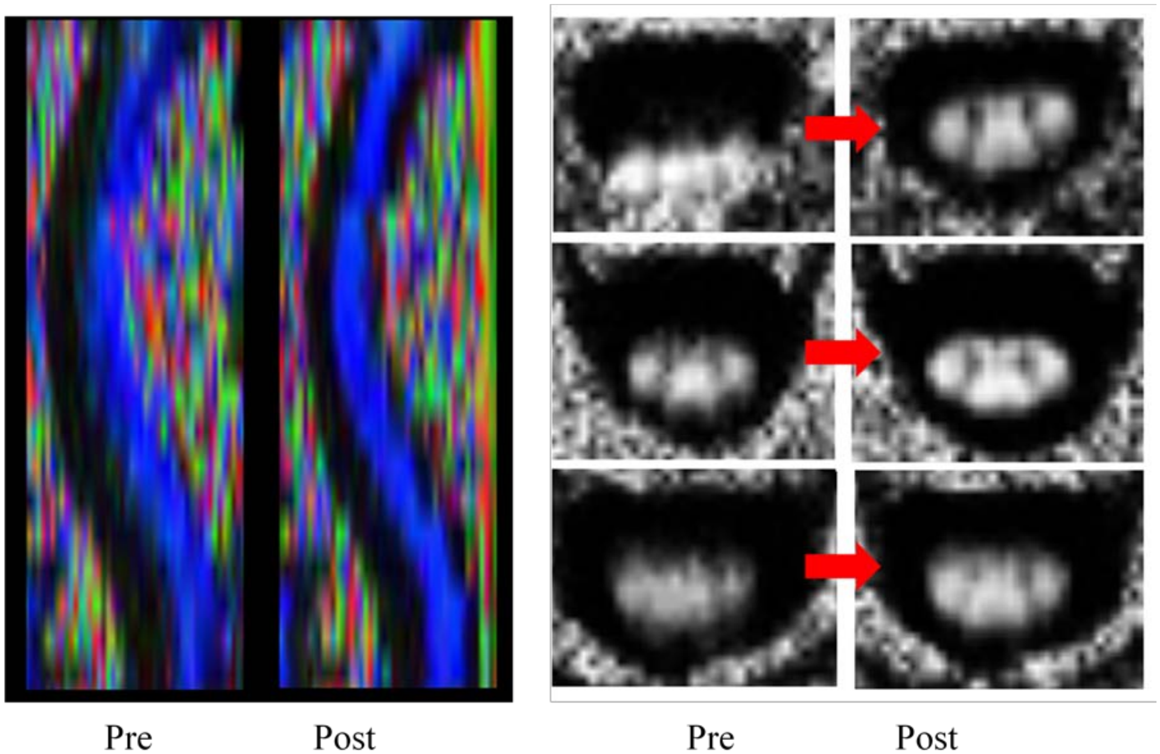

Figure 2-6: Pre and post correction images in sagittal (left) and axial (right) view for FA maps of the cervical spinal cord.

The testing and implementation of an effective motion correction scheme allowed for the collection of high-resolution spinal cord DTI data without cardiac or respiratory gating.

2.2 Tensor Estimation

2.2.1 Complications in Tensor Estimation

The estimation of the diffusion tensor is the final step in DTI analysis post acquisition to allow for the calculation of diffusion indices including FA, MD, AD, and RD. Tensor estimation is in its simplest form a linear least squares fit of an overdetermined system of equations.

In practice, several confounds exist when performing tensor fitting on diffusion weighted MR images. The most substantial of these is motion, whether physiological or subject movement. As discussed previously, retrospective motion correction can resolve much of this; however, some misregistration is still possible, particularly in diffusion weighted images with very low SNR. Additionally, some thermal noise is always present and can affect the final fit. Because of these confounds, it is important to consider the methodology of tensor estimation to prevent noise and artifact in some diffusion weighted images from erroneously driving the fit.

Another consequence of a non ideal fit is the presence of negative eigenvalues in the diffusion tensor. Because the tensor eigenvalues represent diffusion magnitude irrespective of direction along a specific axis, negative eigenvalues should not be possible and are not physically meaningful, but the tensor fitting process can result in their presence. Because of this, any negative eigenvalues must be addressed prior to analysis. The simplest means of dealing with this is setting all negative eigenvalues to zero after estimation. This is not ideal, because some diffusion must be occurring in every direction. Another method is using means of neighboring voxels to interpolate the tensor and resolve the negative values. The assumption in this case is that there is a relationship between the diffusion characteristics of neighboring voxels, but particularly in the case of the spinal cord this is not necessarily accurate. Because the spinal cord contains gray and white matter structures of very small size, it is possible that adjacent voxels do not share commonalities in diffusion characteristics and this method may introduce a sort of partial volume averaging effect. Finally, fitting constraints requiring eigenvalues to be positive can be used.

A final consideration in the tensor estimation process is the matter of heteroscedastity if a linearized, log-transformed approach is used. The non linear formulation of the relationship between the diffusion weighted and unweighted signals and the diffusion tensor can be expressed as:

$$A(\mathbf{n}) = A(0)e^{-\mathbf{bD^{eff}}} \tag{2.1}$$

where $\mathbf{n}$ is the signal for the diffusion weighted image for a given direction, $\mathbf{b}$ is the b-matrix, and $\mathbf{D^{eff}}$ is the diffusion tensor. This is commonly log transformed in order to linearize the estimation process and reduce computation time, resulting in

$$\ln\left[\frac{A(\mathbf{n})}{A(0)}\right] = -\mathbf{bD^{eff}} \tag{2.2}$$

The log transformed form does allow for faster computation, but the linear fit assumes homoscadastity. This is not valid in the case of log transformed data, because the noise component remains constant regardless of signal intensity in the acquired images and thus heteroscadastity is introduced. If a linear least squares approach is still desired, this can be addressed by creating a weight W based on signal intensity $A(\mathbf{n})$ and noise variance σ^2 as:

$$W(\mathbf{n}) = \frac{(A(\mathbf{n}))^2}{\sigma^2} \tag{2.3}$$

and minimizing:

$$\chi^2 = \sum_{\mathbf{n}} W(\mathbf{n})(y_{\mathbf{n}} - y(x_{\mathbf{n}})) \tag{2.4}$$

where $y_{\mathbf{n}}$ and $y(x_{\mathbf{n}})$ are the measured and predicted signals, respectively. One potential issue with this method unique to the inner field-of-view imaging technique used in this study of the spinal cord is the fact that a pure noise region does not exist in the images. In full field-of-view MR images, some amount of space outside the subject (i.e. air) generally exists where noise can be measured without inhomogeneity from tissues imaged contributing to the variance. In inner field-of-view imaging, no outside region exists and therefore noise can only be estimated by a reasonably homogeneous region in the anatomy, providing a reasonable but imperfect estimate of the noise characteristics.

2.2.2 Comparison of Estimation Techniques

In order to understand the potential impact of tensor estimation techniques in DTI of the healthy and injured pediatric spinal cord, a comparison of three techniques was performed on DTI datasets for typically developing subjects and subjects with spinal cord injury. DTI data for the cervical spinal cord (C1 through C7 vertebral levels) from 14 pediatric subjects, 7 typically developing with no evidence of spinal cord pathology and 7 with chronic spinal cord injury at least six months post injury. The images were acquired using the inner field-of-view echo-planar DTI pulse sequence described previously on a 3.0T Siemens Verio MR scanner. The imaging parameters are: 20 diffusion directions, b=1000s/mm^2, voxel size = 1.2x1.2x3mm^3, axial slices = 35-45 (depending on subject's height), TR = 6100-8000 ms, TE = 115 ms, and number of averages = 3. After acquisition, motion correction was performed on the diffusion weighted images using a rigid body 3D transformation as described in the previous chapter. Tensor estimation was performed using three different methods, ordinary linear least squares, a method using log-Euclidean metrics for non-positive eigenvalues removal, and a weighted nonlinear least squares method using a robust outlier rejection technique.

The ordinary linear least squares (OLLS) method has been used extensively in DTI, and makes no attempts to correct for outliers or data heteroscedastity. This method is a simple linear fit and was used as a baseline comparison for the other more sophisticated techniques. The second method (log-Euclidean) relies on the computation of the diffusion tensor by performing operations on the matrix logarithm $\mathbf{L} = \log(\mathbf{D}^{\mathbf{eff}})$ and converting back to the tensor via matrix exponential. Performing operations in the log-Euclidean framework is computationally similar to the Euclidean framework and ensures the absence of negative eigenvalues[47]. The third method is a robust outlier-rejection technique (RESTORE) using a non-linear tensor fit. This technique addresses negative eigenvalues via a constrained fit, but additionally incorporates an outlier rejection scheme which iteratively downweights specific diffusion weighted images with larger residuals during the minimization process using the Geman-McClure Estimator[46, 48]. This outlier rejection makes the estimation robust to noise and misregistration in individual diffusion weighted images.

After tensor estimation was performed for all subjects using all three methods, DTI metrics FA and MD were examined. Sagittal ROIs were defined on a midline image of the cervical spinal cord, with approximately one voxel sparring to prevent partial volume averaging with CSF. The mean and standard deviation for FA and MD were calculated for each subject (Table 2-2). Changes in FA and MD within subjects were relatively lower in typically developing subjects compared with subjects with spinal cord injury (Table 2-3). Subjects with spinal cord injury exhibited greater changes in some cases, with maximum changes of 13.7% in FA and 54.7% for MD. These large changes indicate that the choice of tensor estimation method has the potential to substantively affect the analysis in the data acquired for the pediatric spinal cord.

	OLLS				RESTORE				log-Euclidean			
	FA		MD ($x10^{-3}mm^2/s$)		FA		MD ($x10^{-3}mm^2/s$)		FA		MD ($x10^{-3}mm^2/s$)	
Subject	**Mean**	**StdDev**	**Mean**	**StdDev**	**Mean**	**StdDev**	**Mean**	**StdDev**	**Mean**	**StdDev**	**Mean**	**StdDev**
SCI 1	0.27	0.07	0.81	0.14	0.27	0.07	0.81	0.14	0.27	0.07	0.83	0.15
SCI 2	0.61	0.18	0.71	0.28	0.61	0.18	0.71	0.28	0.59	0.15	0.72	0.28
SCI 3	0.31	0.08	0.71	0.11	0.32	0.10	0.70	0.12	0.30	0.08	0.72	0.11
SCI 4	0.36	0.14	0.77	0.22	0.36	0.14	0.76	0.23	0.36	0.14	0.77	0.24
SCI 5	0.38	0.17	0.67	0.30	0.40	0.21	1.03	0.16	0.37	0.17	0.68	0.31
SCI 6	0.49	0.13	0.80	0.18	0.55	0.17	0.77	0.25	0.48	0.13	0.80	0.21
SCI 7	0.34	0.15	0.45	0.24	0.32	0.15	0.47	0.24	0.31	0.13	0.47	0.26
Average	0.39	0.13	0.70	0.21	0.41	0.15	0.75	0.20	0.38	0.12	0.71	0.22

	OLLS				RESTORE				log-Euclidean			
	FA		MD ($x10^{-3}mm^2/s$)		FA		MD ($x10^{-3}mm^2/s$)		FA		MD ($x10^{-3}mm^2/s$)	
Subject	**Mean**	**StdDev**	**Mean**	**StdDev**	**Mean**	**StdDev**	**Mean**	**StdDev**	**Mean**	**StdDev**	**Mean**	**StdDev**
TD 1	0.53	0.13	0.92	0.22	0.55	0.13	0.92	0.19	0.51	0.13	0.91	0.25
TD 2	0.52	0.12	0.67	0.17	0.54	0.15	0.68	0.19	0.51	0.11	0.68	0.18
TD 3	0.56	0.17	0.50	0.18	0.56	0.17	0.50	0.18	0.54	0.13	0.51	0.18
TD 4	0.54	0.14	0.48	0.13	0.51	0.11	0.52	0.11	0.52	0.12	0.49	0.14
TD 5	0.54	0.11	0.63	0.12	0.56	0.12	0.62	0.12	0.53	0.11	0.64	0.14
TD 6	0.62	0.15	0.46	0.13	0.58	0.13	0.51	0.12	0.61	0.14	0.47	0.14
TD 7	0.64	0.15	0.55	0.15	0.63	0.13	0.56	0.14	0.63	0.14	0.55	0.17
Average	0.56	0.14	0.60	0.16	0.56	0.14	0.62	0.15	0.55	0.12	0.61	0.17

Table 2-2: FA and MD measurements for subjects with spinal cord injury (top), and typically developing subjects (bottom) for three tensor estimation methods.

	% Change vs OLLS					% Change vs OLLS			
	FA		MD			FA		MD	
Subject	RESTORE	log-Euclidean	RESTORE	log-Euclidean	Subject	RESTORE	log-Euclidean	RESTORE	log-Euclidean
SCI1	0.0%	-1.0%	0.0%	2.0%	TD1	4.2%	-2.8%	0.0%	-0.6%
SCI2	0.0%	-3.4%	0.0%	2.1%	TD2	3.7%	-1.0%	1.0%	1.2%
SCI3	2.4%	-1.7%	-0.6%	1.4%	TD3	0.0%	-4.8%	0.0%	2.4%
SCI4	-0.6%	-1.7%	-0.2%	1.0%	TD4	-4.9%	-3.3%	8.3%	2.2%
SCI5	7.8%	-1.9%	54.7%	1.7%	TD5	4.2%	-1.3%	-1.2%	1.1%
SCI6	13.7%	-0.8%	-3.6%	0.7%	TD6	-6.0%	-2.4%	9.6%	2.1%
SCI7	-4.1%	-6.9%	4.7%	5.3%	TD7	-2.1%	-1.6%	3.3%	1.5%

Table 2-3: Percentage change using RESTORE and log-Euclidean tensor fitting methods compared with OLLS within subjects for subjects with spinal cord injury (left) and typically developing subjects (right).

As discussed in the previous chapter, several factors exist which may result in greater changes in DTI metrics using different processing techniques. Changes in cord morphology and mechanical properties following injury may create aberrant physiological motion and subjects may be more likely to spasm or exhibit other involuntary motion. Despite the overall efficacy of motion correction techniques, the addition of a robust outlier-rejection scheme can add an important means of handling unsuccessful registrations of very low SNR diffusion weighted images, as well as noise from thermal sources or potential signal spikes.

2.3 Spinal Cord Morphology Measurement

The morphology of the spinal cord is an important feature for consideration in the examination of spinal cord injury. Aside from changes due to traumatic injury, cord atrophy will occur in chronic spinal cord injuries due to multiple degenerative processes resulting in a decrease in total volume of the spinal cord. spinal cord atrophy has potential as a useful biomarker in cases of traumatic and non-traumatic injury, but measurement requires high resolution imaging and segmentation of the cord; both of which can be time consuming. In order to address this it is necessary to develop and implement an imaging protocol and analysis technique which will allow for fast and accurate measurement of cord morphology.

2.3.1 Imaging

There are three major requirements for effective imaging to allow for accurate spinal cord segmentation and measurement: high resolution, high cord/CSF contrast, and reasonable acquisition time. To allow for high resolution, a 3D pulse sequence with a 1 mm isotropic voxel size was selected. Despite the somewhat increased scan time required for 3D imaging compared with 2D, the improvements in SNR resulting from 3D encoding are necessary to provide the desired 1 mm isotropic voxel. A turbo-spin-echo (TSE) readout was selected with echo and repetition times appropriate for T2 weighted contrast in order to provide good cord/CSF delineation. The TSE readout acquires multiple echoes during a single TR by applying a series of refocusing pulses after the initial excitation (Figure 2-7). This series of echoes (the echo train) within a single TR allows for more rapid collection of lines in k-space and therefore a shorter total acquisition time. As an added benefit, the TSE readout results in an increased contrast between CSF and spinal cord tissue as the length of the echo train increases. This is because the additional RF pulses used to generate the echo train are refocusing pulses and therefore the net magnetization in the transverse plane will continue to decay along the echo train according to the T2 relaxation characteristics of the imaged tissue. The effect of this is relatively small in tissues with long T2 relaxation times such as CSF, but more prominent in tissues such as white matter which have relatively shorter T2 relaxation times. The result of this is a darkening of the spinal cord (comprising largely white and grey matter) and a bright CSF region. The exaggerated contrast provided is not ideal in the case of diagnostic imaging, but is excellent for the purposes of segmenting the spinal cord and surrounding CSF.

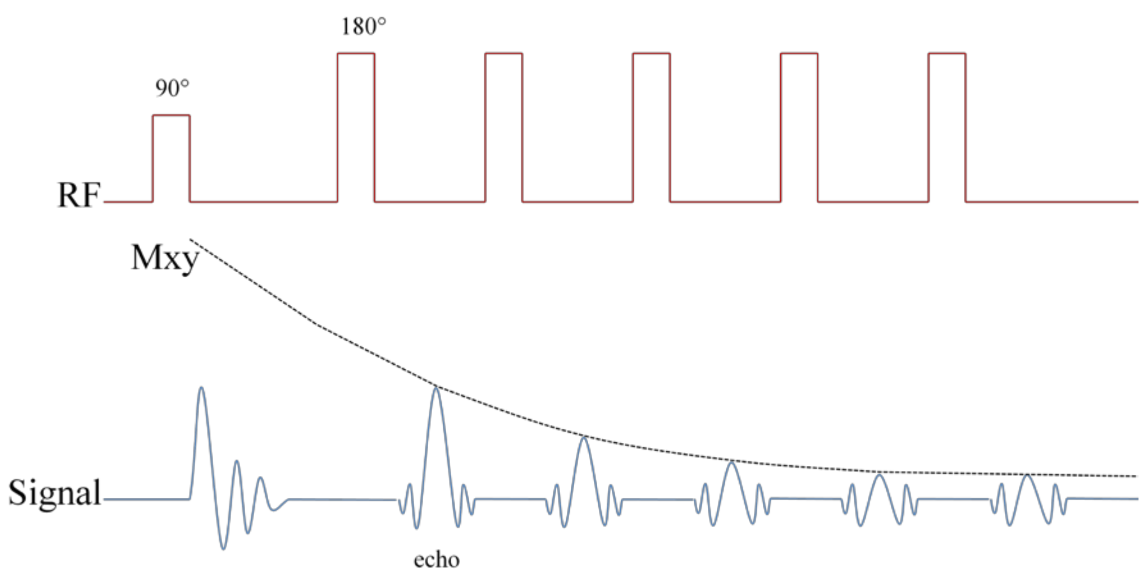

Figure 2-7: Illustration of TSE echo train generation and transverse magnetization decay along the echo train based on the tissue T2 relaxation rate.

The final sequence parameters were set as TE = 122 ms, TR = 1500 ms, voxel size 1 x 1 x 1 mm^3, bandwidth = 751 Hz/pixel, FOV = 256 x 256 mm, acquisition matrix 256 x 256 x 30, and acquisition time = 3:21. To cover the entire cervical and thoracic spinal cord two acquisitions were required, one covering the cervical to upper thoracic cord and the second providing coverage from upper thoracic to lower thoracic. Each set of two volumes was prescribed in such that a minimum range of C1 through the T12-L1 disc was imaged with an overlap of at least one vertebral body to ensure effective stitching of the two volumes (Figure 2-8).

Figure 2-8: Upper (left) and lower (right) volumes acquired using the 3D TSE sequence

2.3.2 Processing and Measurement

After acquisition, the two volumes were stitched together based on scanner provided coordinates using a custom developed script in FSL (www.fmrib.ox.ac.uk/fsl/) to create a single contiguous volume which contained the entire cervical and thoracic spinal cord. Images were reviewed visually after the stitching process to verify that the stitching process was performed successfully and that the resulting volume contained a contiguous cord without gaps.

In order to allow for rapid measurement of spinal cord cross sectional area (SCCSA) a recently developed semi-automatic technique for spinal cord segmentation and SCCSA measurement was implemented in Matlab (The Mathworks, Natick, MA). The process begins with Canny edge detection on a sagittal mid-line image of the stitched contiguous spinal cord and either the anterior or posterior edge of the cord is selected, creating a contour matching contour of the spinal cord (Figure 2-9). In cases where the spinal cord was angled such that it was not fully visible on a midline image, the volume was rotated to ensure parallel alignment of the cord and the viewing plane. After edge selection and contour definition was performed the start and end points of the segmentation were selected as the top of the C1 vertebral body through the T12-L1 disc level. Canny edge detection is then performed in the reformatted axial plane and the cord edge was then identified automatically using the initially generated spinal cord contour as a starting point and selecting the complete enclosed edge in the axial plane which encloses the spinal cord. The result of this segmentation are then displayed for inspection (Figure 3b) and if detection of the spinal cord is successful the algorithm continues along the cord contour until the end point at the T12-L1 disc. In cases where the segmentation failed in detection of a completed cord edge for five continuous slices, manual segmentation was performed and the process was then allowed to continue.

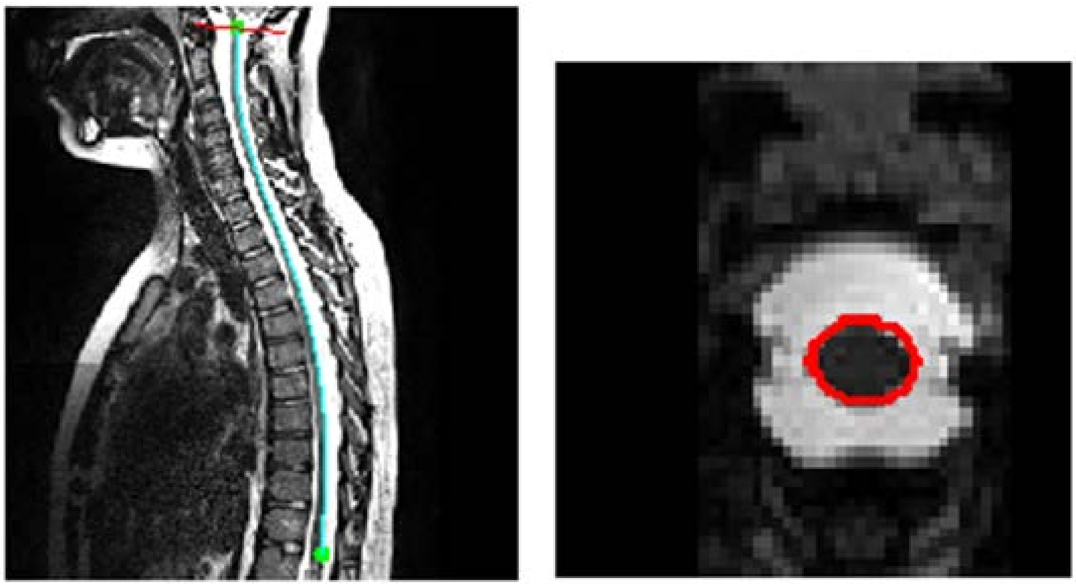

Figure 2-9: (left) Spine contour generated by edge detection/selection (light blue); (right) Segmentation of spinal cord in axial plane (red)

After completion of the segmentation process, SCCSA was calculated at each slice where segmentation was successful. Each vertebral level was identified by selecting the midpoint of each vertebral body and the measurement results could then be plotted for inspection. Due to differences in cord length and subject height, the average SCCSA between midpoints was used to create a metric for comparison which was independent of total cord length.

Clinical evaluation was completed using the International Standards for Neurological Classification of Spinal Cord Injury (ISNCSCI) examination. The ISNCSCI examination is the standard clinical method used to evaluate the neurological consequence of spinal cord injury and is used globally and endorsed by spinal cord injury clinical trials and spinal cord injury centers of excellence. The ISNCSCI examination comprises testing of muscle strength in 20 muscles (5 per arm, 5 per leg), testing of sharp/dull sensation discrimination and light touch in 56 dermatomes, and testing of motor and sensory sacral sparing[76]. The results of this examination allow for the classification of the neurological level, motor and sensory levels (right side, left side, highest level), and severity (complete, incomplete) for the subject with spinal cord injury. Motor function is scored from 0 (total paralysis) to 5 (active movement with full resistance) and sensory function is scored as 0 (absent), 1 (altered), or 2 (normal). The ISNCSCI examination was originally developed for adults, but reliability has been established for pediatric subjects six years and older[2]. Figure 2-10 shows the examination worksheet which is completed during the ISNCSCI exam.

Subjects with spinal cord injury were evaluated by trained examiners using ISNCSCI motor, sensory, and anaorectal examinations to establish the clinical neurological level of injury, including right motor score, left motor score, right light touch, left light touch, right pin prick, and left pin prick. Statistical analysis as described in the following section was performed to determine group differences, as well as correlation between SCCSA and ISNCSCI clinical endpoints and the anatomical findings on MRI.

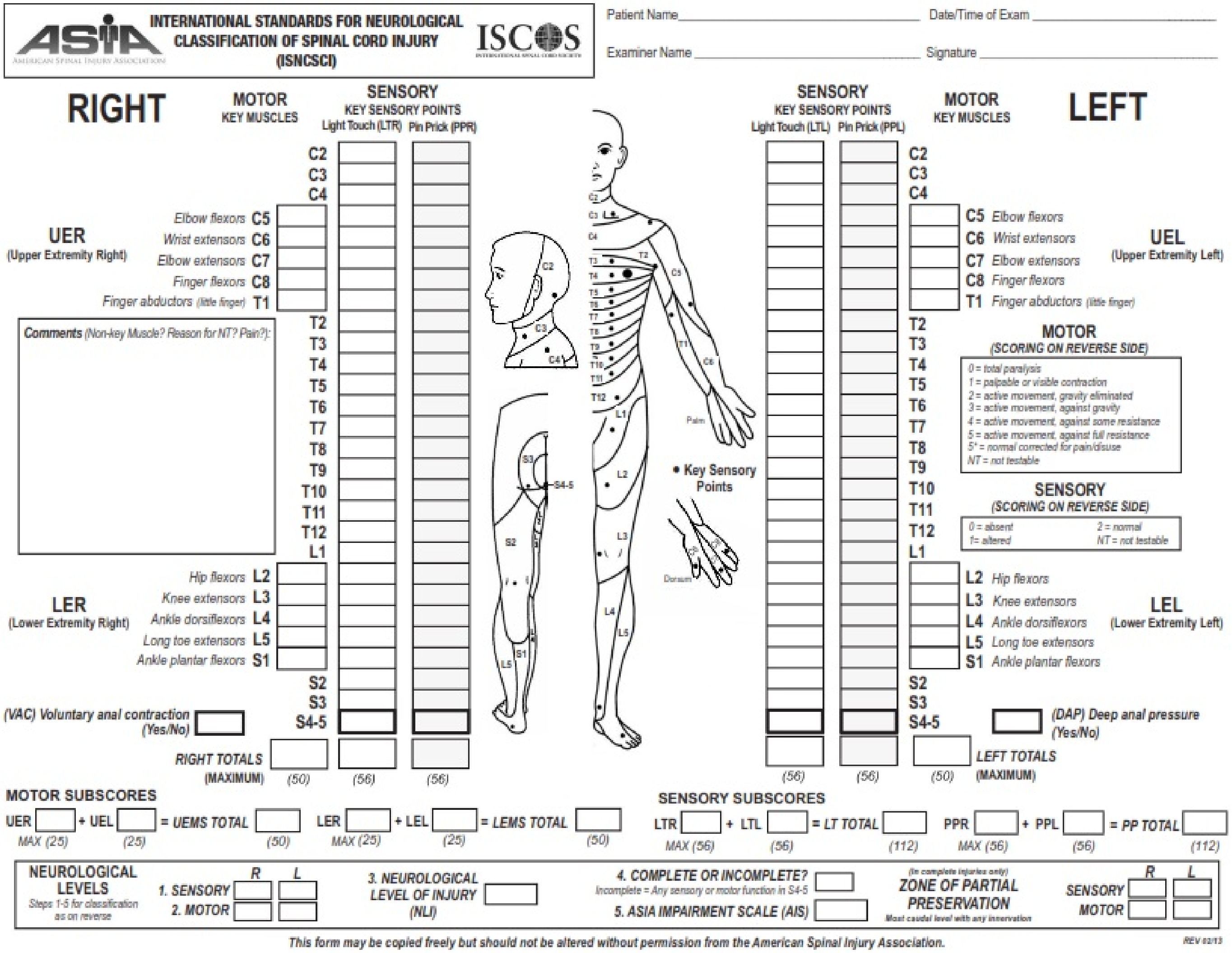
INTERNATIONAL STANDARDS FOR NEUROLOGICAL CLASSIFICATION OF SPINAL CORD INJURY (ISNCSCI)

Patient Name ____________ Date/Time of Exam ____________

Examiner Name ____________ Signature ____________

RIGHT

MOTOR KEY MUSCLES | SENSORY KEY SENSORY POINTS Light Touch (LTR) Pin Prick (PPR)

C2 C3 C4

UER (Upper Extremity Right): Elbow flexors C5, Wrist extensors C6, Elbow extensors C7, Finger flexors C8, Finger abductors (little finger) T1

Comments (Non-key Muscle? Reason for NT? Pain?):

T2 T3 T4 T5 T6 T7 T8 T9 T10 T11 T12 L1

LER (Lower Extremity Right): Hip flexors L2, Knee extensors L3, Ankle dorsiflexors L4, Long toe extensors L5, Ankle plantar flexors S1

S2 S3 S4-5

(VAC) Voluntary anal contraction (Yes/No)

RIGHT TOTALS (MAXIMUM) (50) (56) (56)

LEFT

SENSORY KEY SENSORY POINTS Light Touch (LTL) Pin Prick (PPL) | MOTOR KEY MUSCLES

C2 C3 C4

UEL (Upper Extremity Left): C5 Elbow flexors, C6 Wrist extensors, C7 Elbow extensors, C8 Finger flexors, T1 Finger abductors (little finger)

T2 T3 T4 T5 T6 T7 T8 T9 T10 T11 T12 L1

MOTOR (SCORING ON REVERSE SIDE)
0 = total paralysis
1 = palpable or visible contraction
2 = active movement, gravity eliminated
3 = active movement, against gravity
4 = active movement, against some resistance
5 = active movement, against full resistance
5* = normal corrected for pain/disuse
NT = not testable

SENSORY (SCORING ON REVERSE SIDE)
0 = absent 2 = normal
1 = altered NT = not testable

LEL (Lower Extremity Left): L2 Hip flexors, L3 Knee extensors, L4 Ankle dorsiflexors, L5 Long toe extensors, S1 Ankle plantar flexors

S2 S3 S4-5

(DAP) Deep anal pressure (Yes/No)

LEFT TOTALS (MAXIMUM) (56) (56) (50)

• Key Sensory Points

MOTOR SUBSCORES

UER ___ + UEL ___ = UEMS TOTAL ___ MAX (25) (25) (50)

LER ___ + LEL ___ = LEMS TOTAL ___ MAX (25) (25) (50)

SENSORY SUBSCORES

LTR ___ + LTL ___ = LT TOTAL ___ MAX (56) (56) (112)

PPR ___ + PPL ___ = PP TOTAL ___ MAX (56) (56) (112)

NEUROLOGICAL LEVELS (Steps 1-5 for classification as on reverse): 1. SENSORY R L; 2. MOTOR R L

3. NEUROLOGICAL LEVEL OF INJURY (NLI)

4. COMPLETE OR INCOMPLETE? Incomplete = Any sensory or motor function in S4-5

5. ASIA IMPAIRMENT SCALE (AIS)

ZONE OF PARTIAL PRESERVATION (In complete injuries only) Most caudal level with any innervation: SENSORY R L; MOTOR R L

This form may be copied freely but should not be altered without permission from the American Spinal Injury Association.

REV 02/13

Figure 2-10: Worksheet for the ISNCSCI examination

2.3.3 SCCSA Measurement Results

Initial review of the segmentation and SCCSA measurement showed the data following expected patterns based on known anatomy, with the cervical enlargement clearly visible, as well as the beginning of the lumbar enlargement in the lower cord. In general, subjects with SCI showed a smaller SCCSA at each level than healthy subjects with an average difference of 10.8 mm^2 for all levels between means for healthy and SCI subjects. SCI subjects also exhibited an approximately 22% greater standard deviation on average for all vertebral levels as compared with healthy subjects due to the local variations in SCCSA resulting from injury. The differences between SCI subjects and healthy subjects were found to be statistically significant ($p<0.0001$) in group level means for SCCSA using ANOVA for repeated measures. Changes in spinal cord morphology among individual SCI subjects were observable from visual inspection by a distinct decrease in SCCSA near the level of injury, a lower SCCSA throughout the length of the spinal cord, or both.

Quantitative examination of the relationship between SCCSA by vertebral level and level of injury as determined by MRI or clinical examination showed significant correlations for individual subjects. All but one test score from the ISNSCI examination exhibited at minimum weak significant correlation to SCCSA with Spearman rho > 0.2 and $p < 0.01$. The strongest correlation was found with the left pin prick ($r = 0.47$, $p < 0.0001$) and right pin prick ($r = 0.36$, $p < 0.0001$) tests from the ISNSCI examination. For MRI level, there was a weak correlation between SCCSA and MRI abnormality ($r = 0.30$, $p < 0.0001$). Table 2-4 shows the results of the Spearman Correlation analysis.

	MRI	Right Motor Score	Left Motor Score	Right Light Touch	Left Light Touch	Right Pin Prick	Left Pin Prick
Spearman's rho	0.3	0.24	0.29	0.23	0.18	0.36	0.47
p-value	<0.0001	0.0008	<0.0001	<0.0001	<0.0001	<0.0001	<0.0001

Table 2-4: Spearman correlations between SCCSA and MRI results/ISNSCI examination results

2.3.4 Discussion of Results

The use of this novel semi-automated SCCSA measurement technique allows for fast and effective characterization of spinal cord atrophy in subjects with SCI. Atrophy of the spinal cord is expected in all cases of injury, where degenerative processes occur from the sub-acute through chronic phases of injury resulting in a loss of cord tissue and consequently a decrease in SCCSA. In this study, the semi-automated technique used was successful in detecting/measuring atrophy of the spinal cord when compared with healthy subjects as evidenced by significant differences in group mean SCCSA between healthy and SCI subjects and examination of individual cases compared with healthy averages. While sudden changes near injury were observed in several cases, virtually all subjects with SCI exhibited some degree of spinal cord atrophy as evidenced by smaller SCCSA when compared with the average SCCSA for healthy subjects. The increase in variance in SCCSA for SCI subjects is also consistent with expectations as different injury locations and severities should result in differing degrees of atrophy throughout the spinal cord.

Encouragingly, significant correlations were also observed between SCCSA and clinical examination results. The decrease in SCCSA following lower scores on the ISNSCI examination as well as positive MRI pathology findings suggest that SCCSA may have potential as a useful biomarker for injury. Further, distinct sudden changes in SCCSA were observable at or immediately superior to the level of injury in addition to decreased overall SCCSA for SCI subjects. Figure 3 shows two representative subjects demonstrating decreased overall SCCSA as well as sharp changes near the injury as determined by MRI.

However, Spearman correlations were generally weak to weak-moderate adjusted for individual subjects. Part of the difficulty in establishing strong correlations with clinical results may be differences in injury mechanism and severity between subjects. While atrophy should be expected in all SCI cases, highly focal injuries will be more likely to create sudden changes in SCCSA as compared with non-traumatic injuries which may manifest as a slightly lower SCCSA throughout the cord. Further examination of these correlations with a larger population stratified by injury mechanism and INSCSCI impairment scores would be important in examining atrophy changes with injury.

2.4 Completed Pipeline and Software Development

After development and testing of the strategies for data acquisition, motion correction, DTI tensor estimation, and SCCSA measurement, the completed pipeline was implemented (Figure 2-11). The complete dataset including DTI and structural images is acquired in a single scanning session lasting approximately 45 minutes per subject. After acquisition, structural and DTI data are put through the appropriate processing steps. DTI data is motion corrected, tensor estimation is performed, and ROIs are defined on axial slices for the whole cord. Structural data is stitched and SCCSA measurements are performed using the semi-automated method described previously.

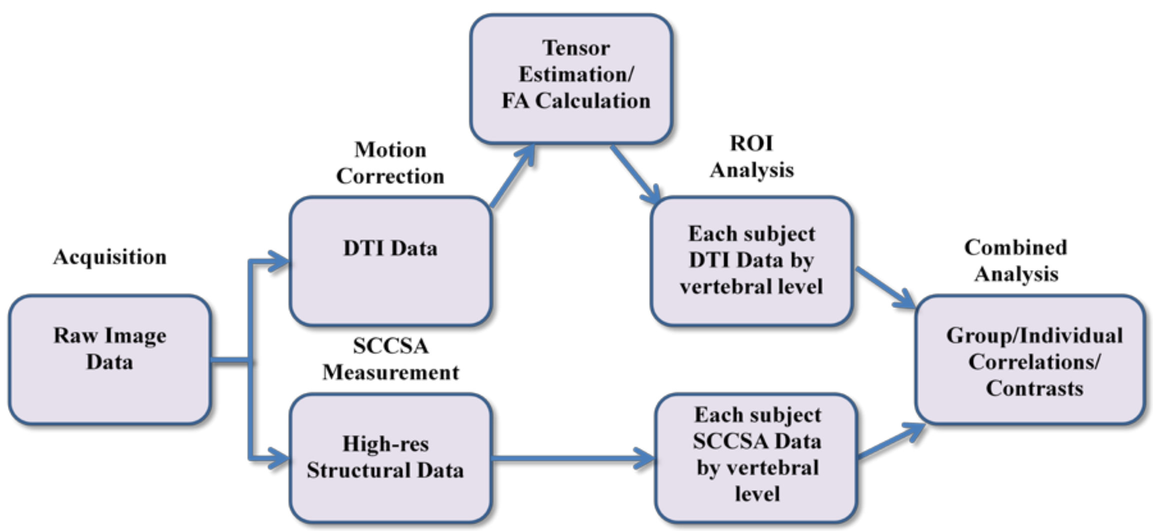

Figure 2-11: Block diagram for acquisition, processing, and analysis of spinal cord data

In order to perform motion correction, tensor estimation, and ROI analysis, a complete custom software package was developed in Matlab. The package implements

3-D rigid body transformations based on normalized mutual information cost functions, tensor estimation using the RESTORE robust outlier rejection algorithm, and provides a graphical interface for visualization and ROI definition to allow for measurement of DTI indices and export of measurement data (Figure 2-12).

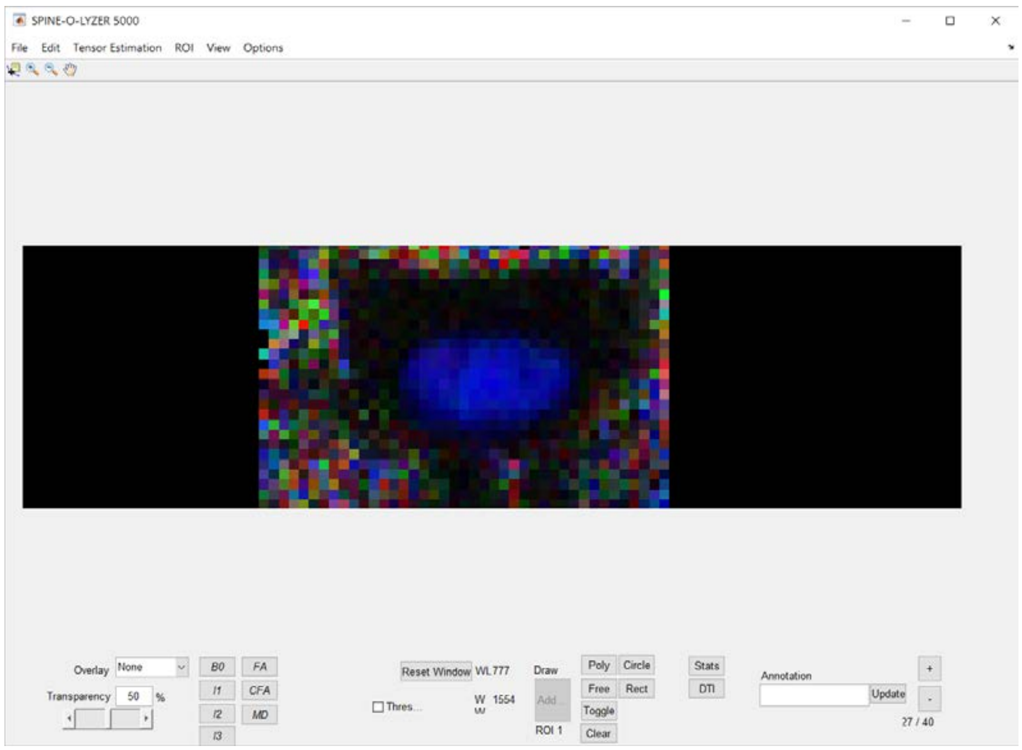

Figure 2-12: Screenshot of custom processing and analysis software developed for use with spinal cord DTI.

CHAPTER 3

DATA COLLECTION, PROCESSING, AND ANALYSIS WITH PIPELINE

3.1 Subjects

After implementation of the completed pipeline, image analysis was performed to examine relationships between DTI metrics and SCCSA in subjects with spinal cord injury and typically developing subjects. Ten pediatric subjects with spinal cord injury and ten typically developing pediatric subjects were selected for analysis. Subjects with spinal cord injury were included if they met the following criteria: 1) stable, chronic spinal cord injury at minimum six months post injury, 2) no surgically implanted metal instrumentation or stabilization hardware, and 3) ability to comfortably tolerate the scanning protocol. All subjects and their parents provided informed assent and consent of the protocol which was approved by Temple University's IRB.

Subject injury level was defined by both radiologist examination (Radiological Level) and clinical ISNCSCI examination (Neurological Level). Injury levels for all ten subjects are shown in Table 3-1. In some cases, the examiner (clinical or radiological) was unable to determine the level of injury with confidence and these cases are noted as such.

Subject	Injury Level	
	Neurological	**Radiological**
SCI1	C6	C6
SCI2	T4	T6-T7
SCI3	C1	Undetermined
SCI4	C5	Undetermined
SCI5	T9	T8-T9
SCI6	Undetermined	T9-T10
SCI7	T12	Undetermined
SCI8	Undetermined	T6
SCI9	Undetermined	C6-C7
SCI10	T10	T9-T10

Table 3-1: Subjects with spinal cord injury and their associated injury level as determined by ISNCSCI (Neurological) and radiologist evaluation (Radiological). Undetermined indicates that the level of injury could not be confidently established by the examination.

3.2 Imaging

All imaging was performed on a 3.0T Siemens Verio MR scanner located at Temple University Hospital. DTI imaging was performed using the iFOV EPI sequence described previously in order to provide short scan time, reduced geometric distortion, and improved SNR[16]. DTI data was collected in 6 mm axial slices parallel to the spinal cord. Two slabs were acquired, one covering the cervical to upper/mid-thoracic, and a second covering the upper/mid-thoracic to the T12-L1 disc with a minimum of one level of vertebral overlap to ensure complete coverage. Imaging parameters for the DTI sequence were TE = 110 ms, TR = 7900 ms, diffusion weighted directions = 20, b = 800 s/mm^2, voxel size = 0.8 x 0.8 x 6 mm^3, axial slices = 40, averages = 3, b0 acquisitions =

6. Cardiac and respiratory gating were not used in order to keep scans as short as possible. In addition to DTI, slice matched T2 weighted gradient echo structural images were acquired in order to aid in anatomic localization.

Structural data for SCCSA measurement was acquired using the previously described sagittal 3D TSE T2 weighted SPACE sequence with parameters TR = 1500 ms, TE = 122 ms, voxel size = 1 x 1 x 1 mm^3, sagittal slices = 30, bandwidth = 751 Hz/px, and FOV = 256 x 256 mm. As with the DTI data, two slabs were required to cover the entire spinal cord. The first slab was prescribed to provide coverage from above the C1 vertebrae through the upper/mid-thoracic with the second slab covering upper/mid-thoracic through at least the T12-L1 disc level. In order to ensure proper stitching, the upper and lower slabs were prescribed with at least one vertebral body of overlap.

3.3 Processing

After acquisition, DTI data was first motion corrected. A central mask was applied to the DTI data to remove extraneous anatomy at the lateral sides of the spinal canal. After masking, all six b0 volumes were co-registered using a 3-D rigid body transformation and normalized mutual information cost function in order to create a mean b0 image providing increased SNR relative to individual b0 images (Figure 3-1). This is an important step, as signal attenuation in diffusion weighted images relative to the b0 image is the determining factor in tensor estimation and obtaining the best possible unweighted image is critical to accuracy. After creation of the mean b0, all diffusion weighted volumes were registered to the mean b0 using a 3-D rigid body transformation and normalized mutual information cost function as described in the previous chapter.

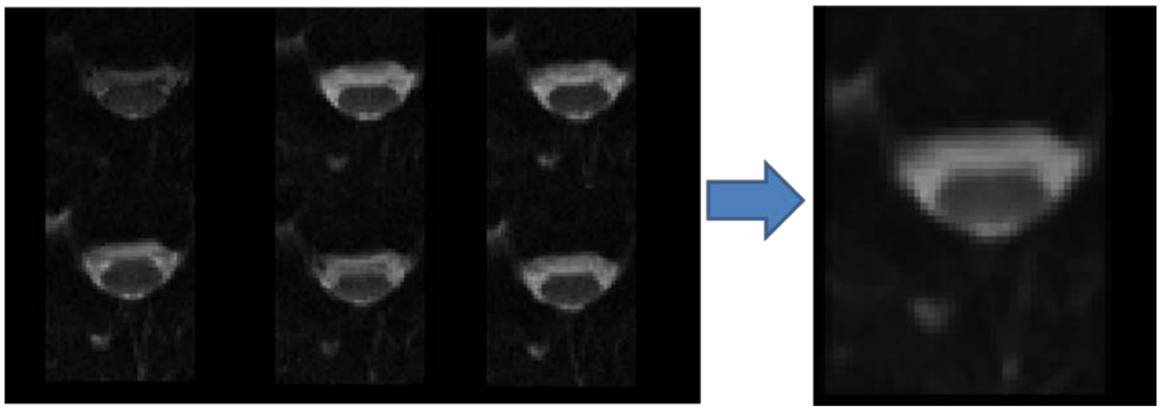

Figure 3-1: Six b0 images at the same slice for a single subject (left) and the resulting mean b0 after co-registration and averaging (right).

After motion correction, tensor estimation was performed using a non-linear fit implementation of the RESTORE robust outlier rejection algorithm to mitigate the impact of image artifact, noise, or misregistration that may occur in a given diffusion weighted image. As described previously, the RESTORE algorithm uses the Geman-McClure estimator to re-weight components with large residuals after fitting in order to reduce the influence of outliers on the final fit. The process is performed iteratively until convergence criteria are met, and components with residuals outside the specified tolerances are rejected as outliers (Figure 3-2).

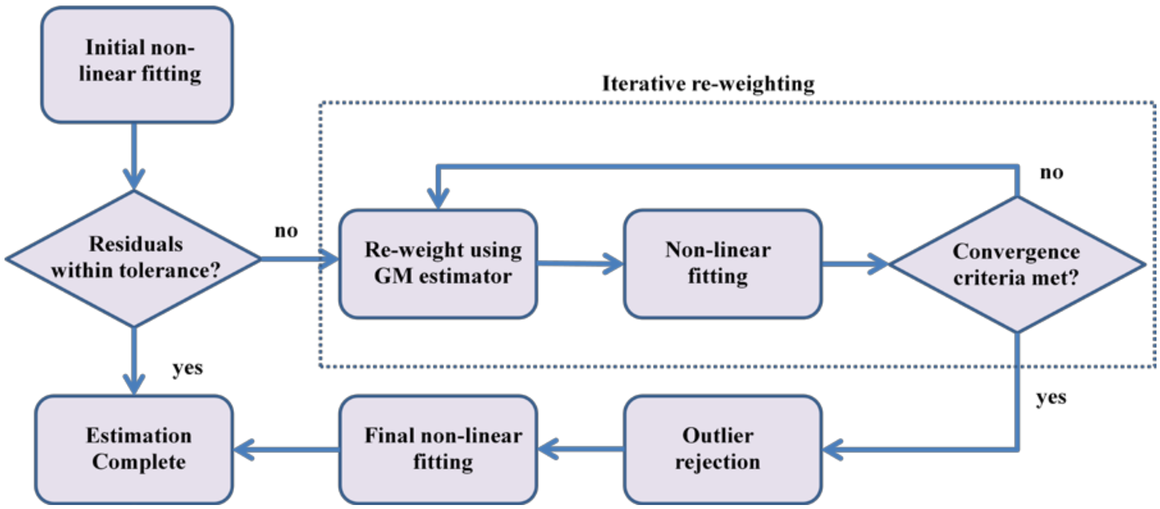

Figure 3-2: Flow diagram for tensor estimation using the RESTORE algorithm including iterative re-weighting and outlier rejection.

After completion of tensor estimation, maps for DTI metrics FA, MD, AD, and RD were generated from the calculated diffusion tensors. Whole cord ROIs were drawn on the axial color FA maps with approximately one voxel of sparing to prevent partial volume averaging with surrounding CSF. After ROI definition, average values for all DTI metrics were exported and assigned to the appropriate vertebral level based on evaluation of the slice matched T2 weighted GRE images by a board certified neuroradiologist.

Structural 3D T2 weighted SPACE images were then processed in order to measure SCCSA for subjects. The upper and lower slabs were stitched together to create a contiguous spinal cord image (Figure 3-3) and measurements were taken using the semi-automated segmentation algorithm described in the previous chapter based on contour identification and automated edge detection in the reformatted axial plane along the length of the cord. After measurement, vertebral bodies were identified manually from sagittal midline images and SCCSA measurement data was exported for analysis.

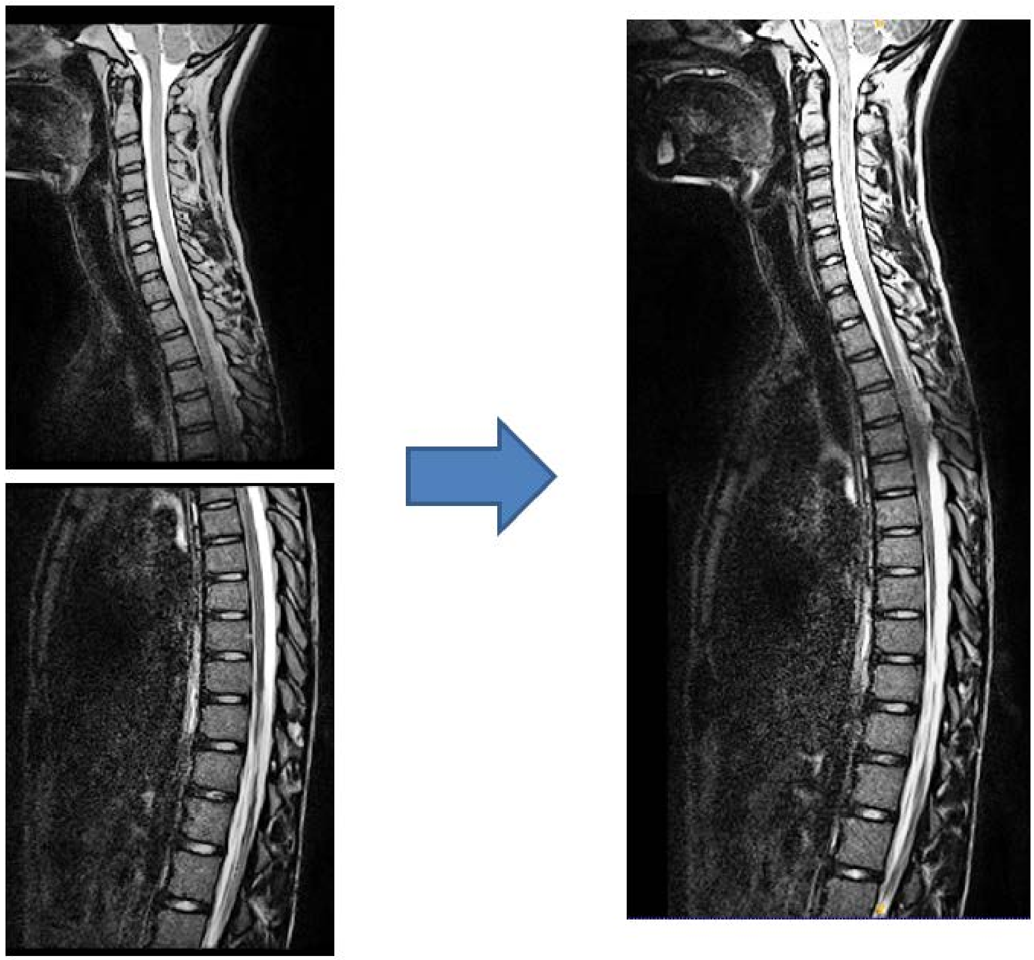

Figure 3-3: Upper and lower T2 weighted SPACE acquisitions (left) and resulting stitched image (right).

3.4 Results

3.4.1 Group Differences Between TD and SCI subjects

For the full cord, group differences were immediately identifiable for DTI metrics and SCCSA between typically developing subjects and subjects with spinal cord injury (Figure 3-4). Whole cord FA was significantly higher ($p<0.01$) for the typically developing group at an average value of 0.58 ± 0.04 compared to 0.49 ± 0.08. SCCSA was also significantly higher ($p = 0.03$) for the typically developing group with an average of 48.05± 4.25 mm^2 as compared to 39.50 ± 9.86 mm^2 across all levels for subjects with spinal cord injury. Diffusivity values MD and RD were significantly higher for subjects with spinal cord injury, and AD values were higher but not significant. Table 3-2 summarizes these group comparisons.

	TD		**SCI**		
	Average	**StdDev**	**Average**	**StdDev**	**p-value**
FA	**0.58**	**0.04**	**0.49**	**0.08**	**<0.01**
MD ($x10^{-3}$ mm^2/s)	**0.97**	**0.09**	**1.12**	**0.19**	**0.04**
AD ($x10^{-3}$ mm^2/s)	1.67	0.15	1.75	0.21	0.34
RD ($x10^{-3}$ mm^2/s)	**0.62**	**0.08**	**0.81**	**0.20**	**0.01**
SCCSA (mm^2)	**48.05**	**4.25**	**39.50**	**9.86**	**0.03**

Table 3-2: Average full cord values for DTI metrics and SCCSA for typically developing subjects and subjects with spinal cord injury. Significant differences (bold text) were found between all metrics except AD by unpaired two tailed t-test.

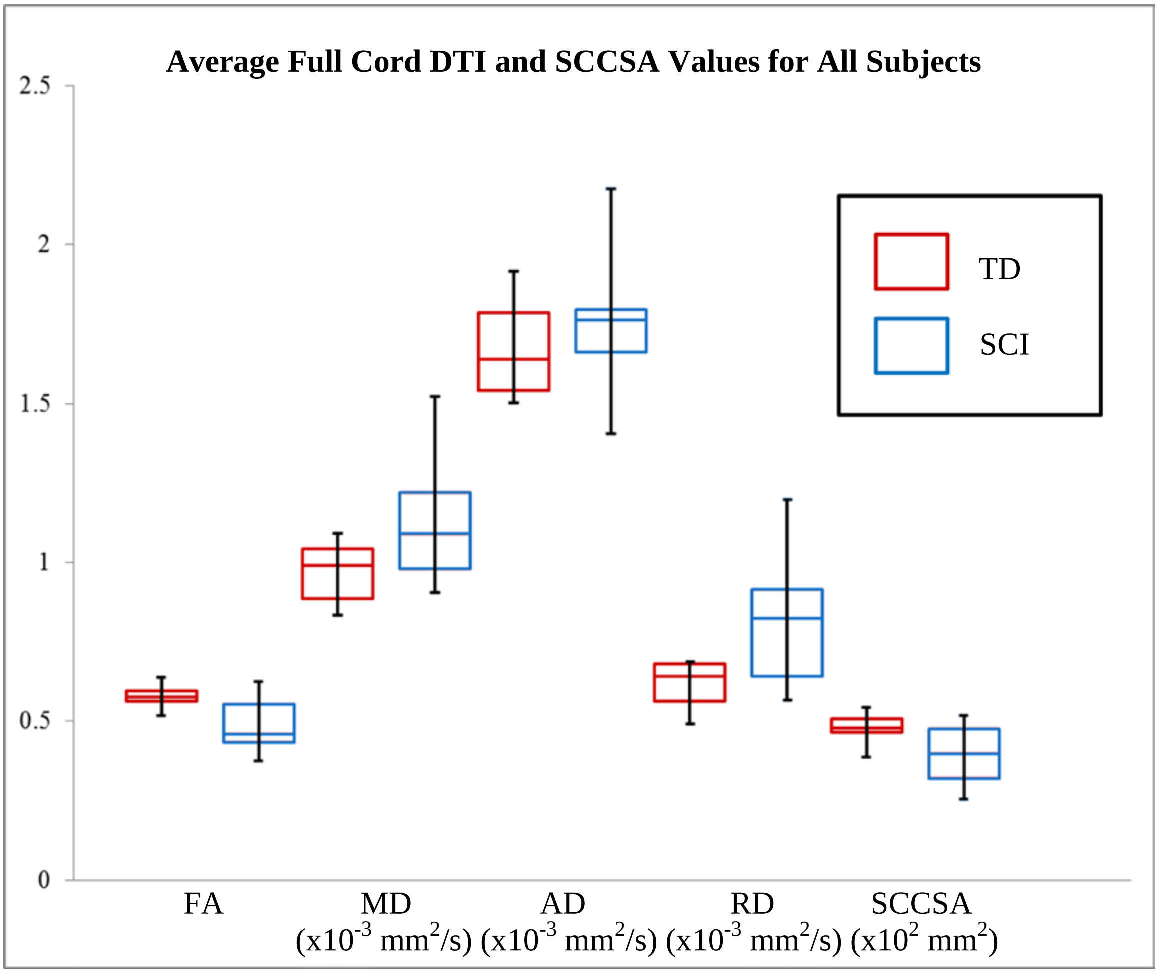

Figure 3-4: Box-whisker plots showing whole cord values for TD and SCI subjects.

The changes in DTI metrics and SCCSA with spinal cord injury are consistent with expectations based on the traumatic axonal injury processes and degenerative processes which occur after injury. Axonal transection and subsequent Wallerian degeneration will cause a decrease in diffusion restrictions, creating more isotropic diffusion. This should result in lower FA values, and increased RD as diffusion can more easily occur in directions perpendicular to the spinal cord, both of which are exhibited in the group for subjects with spinal cord injury. Additionally, these degenerative processes occur in both retrograde and anterograde directions, so the manifestation of atrophy along the entire cord is consistent with known patterns in chronic injury.

Examining group differences by vertebral level provides additional information on changes between typically developing subjects and subjects with spinal cord injury. FA values tend to diverge along the length of the spinal cord with the decrease in FA in subjects with spinal cord injury growing more pronounced (Figure 3-5). MD and RD show similar divergence, with the pattern reversed as subjects with spinal cord injury show increased diffusivity (Figure 3-6,3-7). AD patterns remain relatively similar between both groups along the entire length of the spinal cord (Figure 3-8). SCCSA shows an overall decrease along the entire length of the cord in subjects with spinal cord injury compared with typically developing subjects (Figure 3-9). Complete graphs for each typically developing subject and subject with spinal cord injury showing all DTI metrics and SCCSA by level are provided in the Appendix.

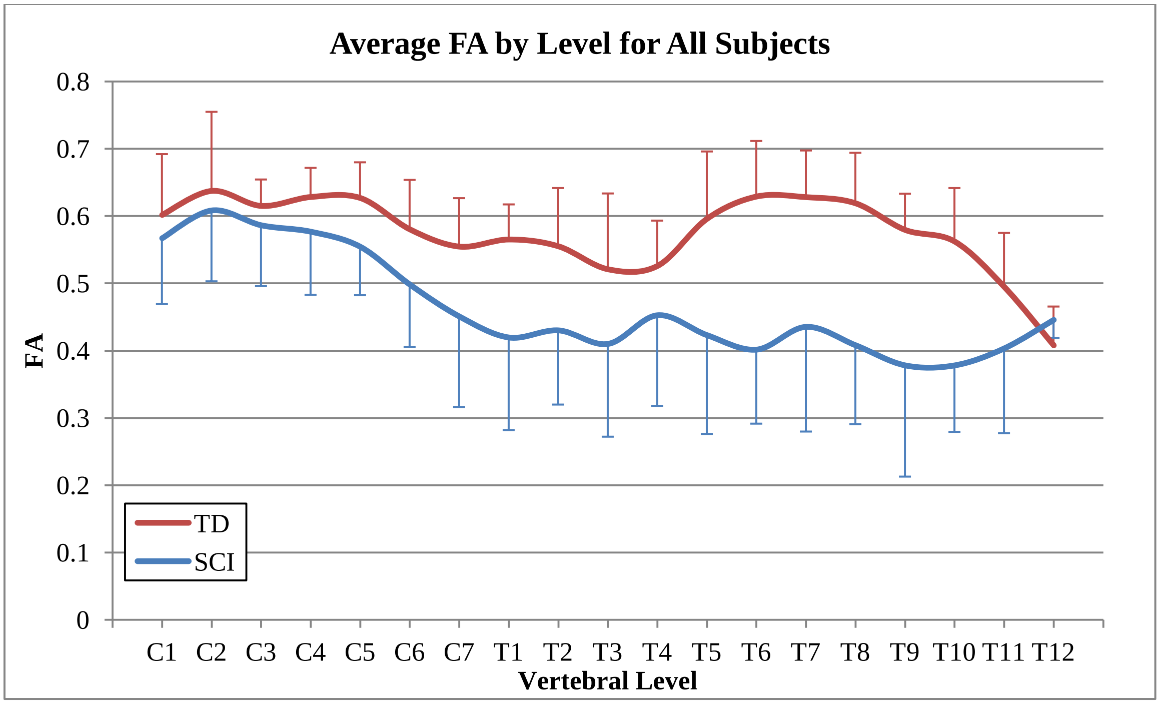

Figure 3-5: Average FA by vertebral level for TD and SCI groups. Error bars indicate standard deviation.

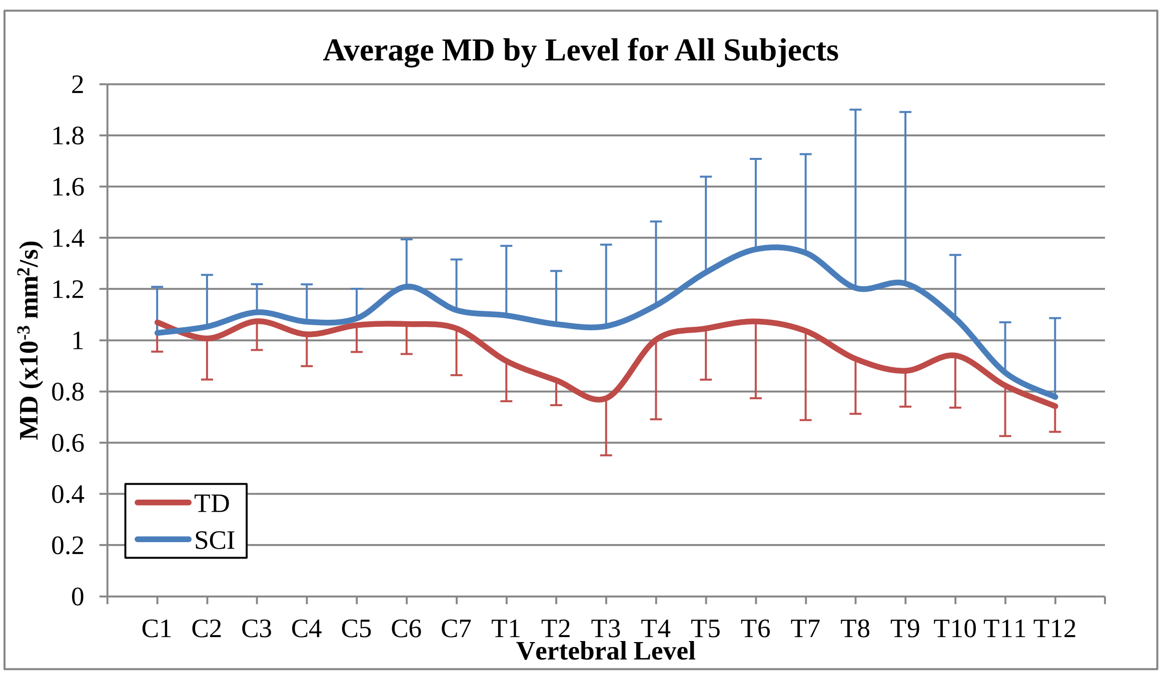

Figure 3-6: Average MD by vertebral level for TD and SCI groups. Error bars indicate standard deviation.

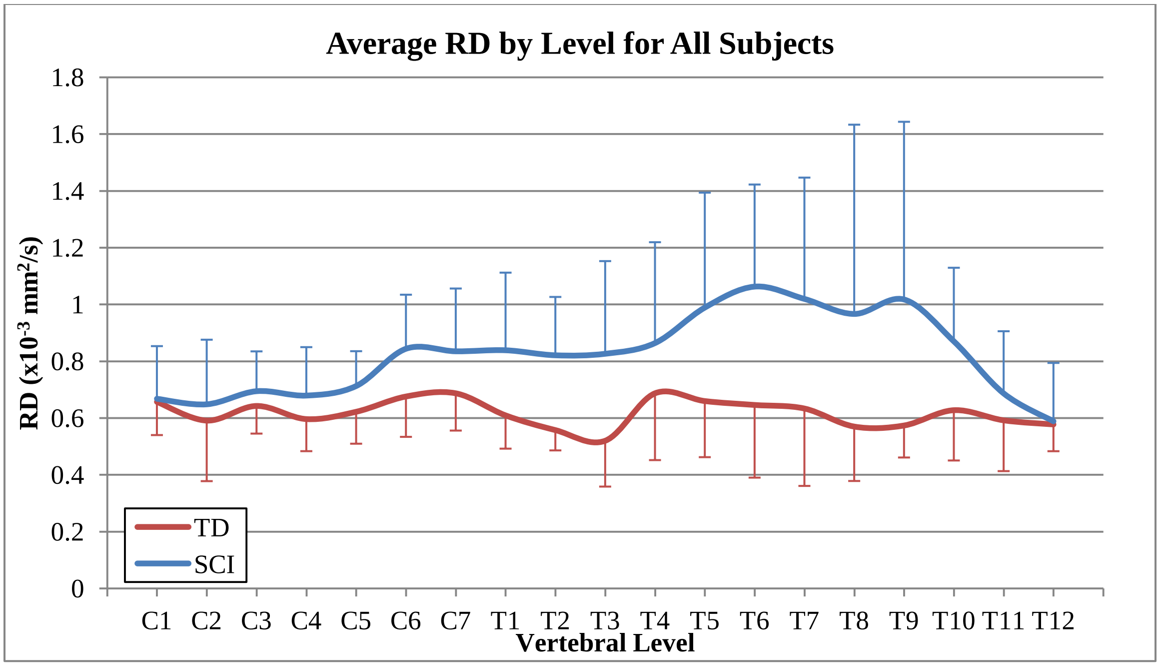

Figure 3-7: Average RD by vertebral level for TD and SCI groups. Error bars indicate standard deviation.

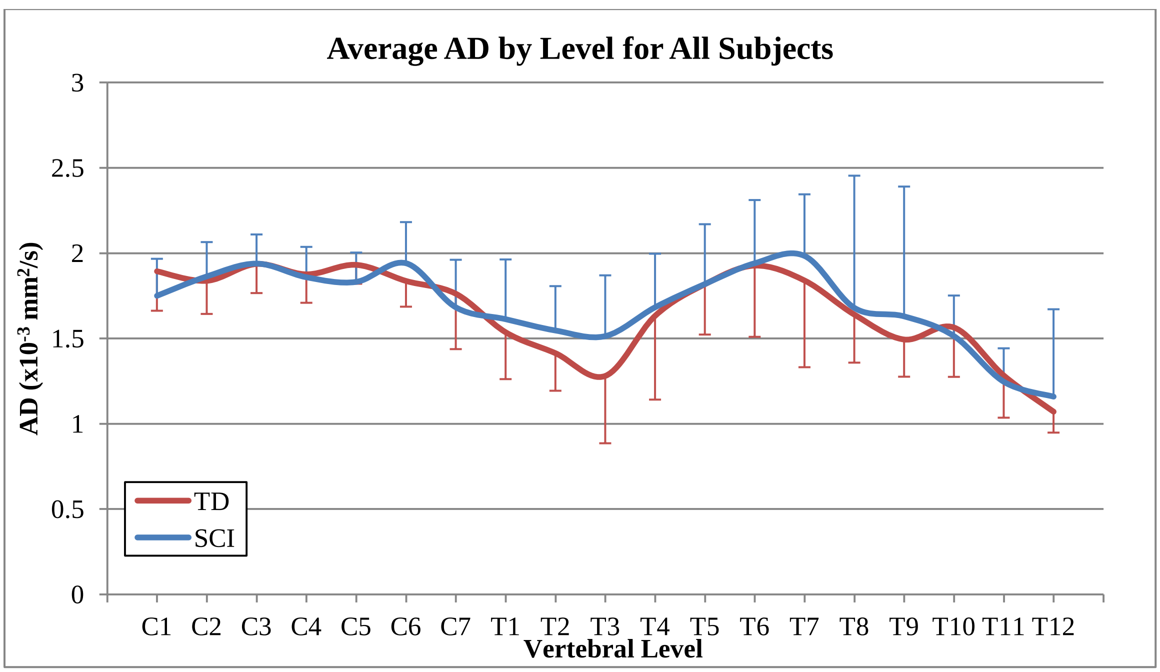

Figure 3-8: Average AD by vertebral level for TD and SCI groups. Error bars indicate standard deviation.

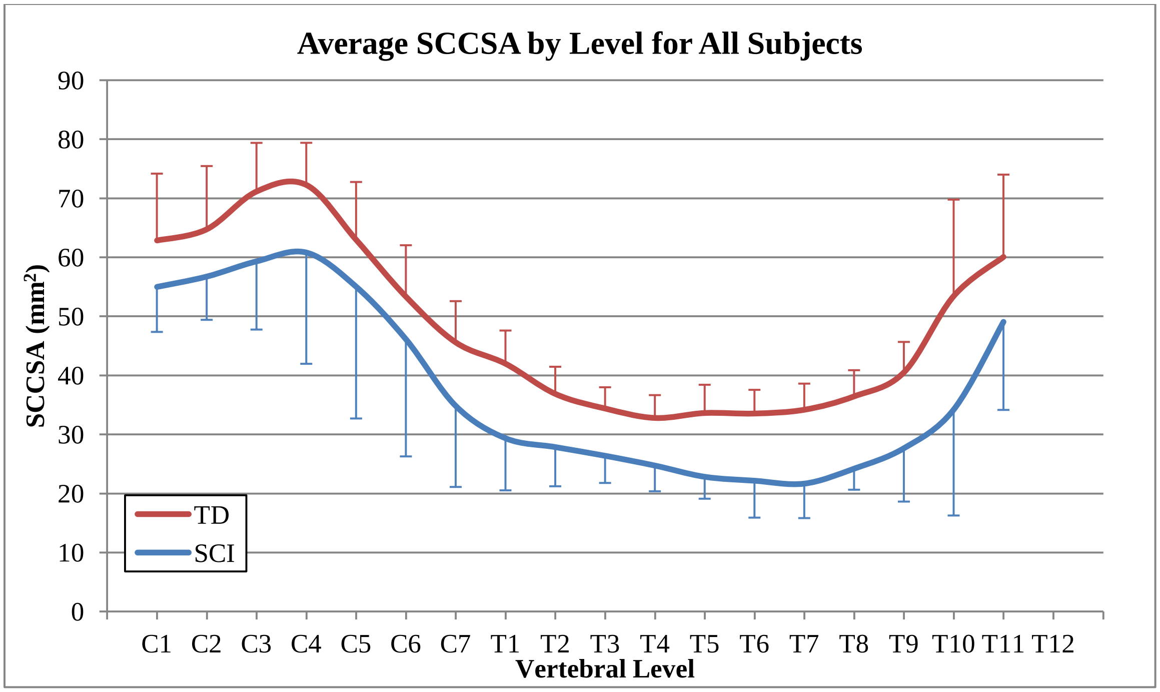

Figure 3-9: Average SCCSA by vertebral level for TD and SCI groups. Error bars indicate standard deviation.

3.4.2 Analysis of DTI Metrics and SCCSA Relationships

As an initial step, comparisons of average DTI metrics with average SCCSA for the full cervical and thoracic spinal cord were performed for subjects with SCI as a group to examine relationships between DTI and SCCSA over the entire spinal cord. Spearmann's rank correlation coefficient (Spearmann's rho) and associated p-values were computed for subject average SCCSA and DTI metrics for the full spinal cord. For the full spinal cord, FA and SCCSA were very strongly positively correlated ($r = 0.81$, $p < 0.01$), RD and SCCSA had a strong negative correlation ($r = -0.68$, $p = 0.02$), and MD and AD were moderately negatively and weakly positively correlated, respectively, but without significance (Table 3-3).

	FA	MD	AD	RD
Spearmann's rho	**0.81**	-0.38	0.15	**-0.68**
p-value	**<0.01**	0.19	0.35	**0.02**

Table 3-3: Correlations between DTI metrics and SCCSA averaged for the entire spinal cord for all subjects with spinal cord injury; significant correlations in bold.

The presence of strong, significant correlations with FA and RD for the full spinal cord are of particular interest in examination of the injured spinal cord. Because the spinal cord comprises primarily long, myelinated axons, its microstructure inherently creates restrictions to water diffusion in perpendicular directions and tends toward highly anisotropic diffusion. The fact that these restrictions appear related to the physical size of the cord is a very useful piece of information. During conventional examination of structural spinal cord images, atrophy can be qualitatively or quantitatively assessed based on the size of the cord, but no information as to the microstructural environment can be determined. These correlations may provide evidence of microstructural changes occurring during the atrophy process which would otherwise be unobservable. The lack of significant correlation with AD and MD is not surprising as well. Because diffusion is relatively unrestricted axially in the intact spinal cord, it is not unexpected that axonal damage would have limited impact on AD. The fact that AD is the largest contributor to MD allows the lack of significance in MD/SCCSA correlations to be explained similarly.

The relationship between DTI metrics and SCCSA was also examined for the full cord in typically developing subjects, again using Spearmann’s rank correlation coefficient. FA showed no correlation with SCCSA in typically developing subjects (r = 0.01), but diffusivities showed moderate to strong negative correlations, ranging from r = -0.41 to r = -0.79 (Table 3-4).

	FA	MD	AD	RD
Spearmann's rho	-0.01	**-0.73**	**-0.79**	-0.41
p-value	0.39	**0.01**	**<0.01**	0.17

Table 3-4: Correlations between DTI metrics and SCCSA averaged for the entire spinal cord for all typically developing subjects; significant correlations in bold.

The lack of correlation between FA and SCCSA in typically developing subjects is expected, as the intact spinal cord should maintain highly directional diffusion regardless of morphology. Interestingly, correlations between SCCSA and AD/MD were significant. This may be due to higher degrees of myelination as the cord develops. As the myelin sheath grows, inter-axonal space decreases and this may result in decreased overall diffusion as the inter-axonal water compartment becomes increasingly restricted.

3.4.3 Vertebral Level Analysis for SCI Group

Finally, data for subjects with spinal cord injury was analyzed on a vertebral level basis to examine potential intra-subject relationships between DTI metrics and SCCSA. Spearmann rank correlation coefficients were calculated for all DTI metrics (FA, MD, AD, RD) with SCCSA by vertebral level for each subject with spinal cord injury (Table 3-5).

Subject		**FA**	**MD**	**AD**	**RD**
SCI1	Spearmann's rho	**0.64**	**-0.69**	-0.41	**-0.69**
	p-value	**<0.01**	**<0.01**	0.08	**<0.01**
SCI2	Spearmann's rho	**0.92**	-0.23	0.23	**-0.62**
	p-value	**<0.01**	0.25	0.25	**<0.01**
SCI3	Spearmann's rho	**0.50**	-0.38	0.17	**-0.57**
	p-value	**0.03**	0.10	0.31	**0.01**
SCI4	Spearmann's rho	0.19	0.04	0.20	-0.15
	p-value	0.29	0.39	0.28	0.33
SCI5	Spearmann's rho	**0.68**	0.26	**0.77**	-0.32
	p-value	**<0.01**	0.26	**<0.01**	0.20
SCI6	Spearmann's rho	**0.55**	-0.03	0.47	-0.36
	p-value	**0.04**	0.39	0.08	0.16
SCI7	Spearmann's rho	0.36	0.43	**0.74**	0.01
	p-value	0.20	0.14	**<0.01**	0.39
SCI8	Spearmann's rho	0.45	**-0.78**	-0.41	**-0.73**
	p-value	0.09	**<0.01**	0.12	**<0.01**
SCI9	Spearmann's rho	0.25	-0.03	0.03	-0.16
	p-value	0.22	0.39	0.39	0.31
SCI10	Spearmann's rho	**0.79**	**-0.66**	-0.38	**-0.71**
	p-value	**<0.01**	**<0.01**	0.12	**<0.01**

Table 3-5: Correlations by vertebral level for DTI metrics and SCCSA for all subjects with spinal cord injury; significant correlations in bold.

On a vertebral level basis, FA was significantly correlated with SCCSA for six out of ten subjects, MD for three out of ten, AD for two out of ten, and RD for five out of ten. FA remains the most closely associated metric with SCCSA, followed by RD as with comparisons performed considering the full cord. These results are somewhat less consistent than the previously described correlations for the entire spinal cord, but not entirely unexpected. All injuries under consideration in this work are chronic and as such are subject to retrograde and anterograde degeneration from the actual injury site. During these processes, the entire spinal cord will have a tendency to undergo changes in its diffusion and morphological characteristics, and in the case of less focally traumatic injuries it is possible that these changes are less distinct at the injury site and whole cord values may provide a better description of the state of the spinal cord.

CHAPTER 4

CONCLUSIONS AND FUTURE WORK

4.1 Conclusions

The goal of this work was to design, test, and implement a complete acquisition, processing, and analysis pipeline for both DTI and structural data for the pediatric spinal cord, and to use the pipeline to examine relationships between DTI metrics and spinal cord morphology in typically developing subjects and subjects with spinal cord injury. The challenges in processing originally stated (spinal cord motion, choice of tensor estimation, and fast-accurate measurement of SCCSA) were examined and addressed with processing strategies which were implemented in the processing pipeline.

Spinal cord motion in DTI was addressed by examining multiple retrospective motion correction techniques using different transformations and cost functions. The results of the analysis showed a rigid body 3D transformation to be most suitable based on quantitative and qualitative analysis, and this was combined with a normalized mutual information cost function to provide contrast insensitivity. This retrospective technique was implemented in the final software package and applied to all DTI data being examined.

Examination of tensor estimation showed potential for considerable difference in resulting DTI metrics depending on the choice of tensor fitting technique. In order to limit the influence of noise, misregistration, and image artifact, a robust, outlier-rejection estimation scheme (RESTORE) was selected as the final method for tensor fitting and was used for all data analysis.

A semi-automated technique for the measurement of SCCSA based on spinal cord contour identification and automated edge detection was tested for both typically developing subjects and subjects with spinal cord injury to ensure its suitability for use with pediatric subjects with spinal cord injury. The method tested was found to be fast, effective, and reliable for measurement of SCCSA in pediatric subjects.

After establishment of the preceding strategies for processing of pediatric spinal cord DTI and structural data, a complete processing and analysis software package was developed to allow for motion correction, tensor estimation, and ROI analysis of DTI data for the spinal cord. This package was then used to analyze data from both typically developing subjects and subjects with spinal cord injury.

The presence of significant group level differences between typically developing subjects is consistent with expectations and reports of DTI in spinal cord injury in adults and children[32-34, 36]. Significant decreases in FA and increases in RD for subjects with spinal cord injury reflect the injury and associated degenerative processes. Axonal injury will result in an immediate focal loss of anisotropic diffusion and increased radial diffusion, and subsequent retrograde and anterograde degenerative processes cause this to propagate along the cord. The significant decrease in SCCSA for subjects with spinal cord injury demonstrates the morphological changes which occur during these processes.

The relationships between DTI and SCCSA also provide useful insight regarding the state of the spinal cord post-injury. While conventional structural MR imaging can determine atrophy quantitatively based on cord size, it cannot allow for any determinations of the microstructural changes within the spinal cord. The significant correlations found between DTI and SCCSA in subjects with spinal cord injury provide valuable information in terms of the relationship between atrophy and microstructural changes.

4.2 Future Work

The ability to effectively collect and analyze a combination of DTI and SCCSA data has the potential to provide better understanding of spinal cord injury. With additional data collection and analysis, it may be possible to improve diagnostic accuracy and provide a more complete characterization of the injured spinal cord based on functional and structural data together. To that end, it is important to continue to collect data for both subjects with spinal cord injury and typically developing subjects. Particularly in the case of typically developing subjects, a larger normative dataset is needed. Because developmental processes in the spinal cord (e.g. myelination) are ongoing in pediatric subjects, it is important to have an age-stratified normative data set as large as possible in order to allow the most accurate possible comparisons between typically developing subjects and subjects with spinal cord injury.

Advancements in pulse sequence design for acquisition can also greatly improve several aspects of diffusion imaging. Multiband imaging which allows for the simultaneous collection of multiple slices is becoming more widely available and can reduce the acquisition time needed for DTI considerably. This reduction in time is important for clinical feasibility, particularly in acute injury cases, and also for reducing the impact of motion in the imaging process.

The subjects with spinal cord injury in this study were all imaged during the chronic injury phase. If data is collected from the acute, subacute, and chronic phase as a longitudinal study, the pipeline developed in this work could be used to examine the recovery process with respect to structural and functional data. Data from such a study could be valuable in improving understanding of microstructural changes during this process and possibly provide prognostic information on recovery after spinal cord injury.

Additionally, higher order diffusion models such as diffusion kurtosis imaging and NODDI may offer useful information with respect to spinal cord imaging while simultaneously providing DTI metrics[38, 77]. The inclusion of additional MR imaging techniques such as magnetization transfer could allow for greater understanding via a larger, multispectral analysis. If a multispectral approach proves more sensitive to injury level, it could be used as a biomarker to stratify spinal cord injury patients into different physical therapy treatments as well as new developing treatment's. This new developing treatments include artificial limb robotics and stem cell therapy. With regard to stem cell therapy these advanced multispectral techniques may be used to help guide the placements of stem cells into viable spinal cord tissue and also to monitor the microstructural changes of the treated spinal cord over time.

REFERENCES CITED

[1] C. Roche and H. Carty, "Spinal trauma in children," *Pediatr.Radiol.*, vol. 31, no. 10, 10/01, pp. 677-700.

[2] M.J. Mulcahey, J.P. Gaughan, R.S. Chafetz, L.C. Vogel, A.F. Samdani and R.R. Betz, "Interrater Reliability of the International Standards for Neurological Classification of Spinal Cord Injury in Youths With Chronic Spinal Cord Injury," *Arch.Phys.Med.Rehabil.*, vol. 92, no. 8, 8, pp. 1264-1269.

[3] P.J. Basser, J. Mattiello and D. Lebihan, "Estimation of the Effective Self-Diffusion Tensor from the NMR Spin Echo," *Journal of Magnetic Resonance, Series B*, vol. 103, no. 3, 3, pp. 247-254.

[4] P.J. Basser, J. Mattiello and D. LeBihan, "MR diffusion tensor spectroscopy and imaging," *Biophys.J.*, vol. 66, no. 1, 1, pp. 259-267.

[5] D. Le Bihan, J. Mangin, C. Poupon, C.A. Clark, S. Pappata, N. Molko and H. Chabriat, "Diffusion tensor imaging: Concepts and applications," *Journal of Magnetic Resonance Imaging*, vol. 13, no. 4, pp. 534-546.

[6] A. Buss, G.A. Brook, B. Kakulas, D. Martin, R. Franzen, J. Schoenen and Noth,J.,Schmitt,A.B., "Gradual loss of myelin and formation of an astrocytic scar during Wallerian degeneration in the human spinal cord," *Brain*, vol. 127:1, pp. 34-44.

[7] D.W. Choi, "Glutamate neurotoxicity and diseases of the nervous system," *Neuron*, vol. 1, no. 8, 10, pp. 623-634.

[8] H. Aldskogius, L. Liu and M. Svensson, "Glial responses to synaptic damage and plasticity," *J.Neurosci.Res.*, vol. 58, no. 1, pp. 33-41.

[9] E. Stejskal, "Spin Diffusion Measurements: Spin Echoes in the Presence of a Time Dependent Field Gradient," *J. Chem. Phys.*, vol. 42, no. 1, 2004-07-02T14:35:44, pp. 288-5.

[10] J. Mattiello, P.J. Basser and D. Le Bihan, "The b matrix in diffusion tensor echo-planar imaging," *Magnetic Resonance in Medicine*, vol. 37, no. 2, pp. 292-300.

[11] D.K. Jones, "Gaussian Modeling of the Diffusion Signal,", pp. 37-52.

[12] D.J. Werring, C.A. Clark, G.J. Barker, A.J. Thompson and D.H. Miller, "Diffusion tensor imaging of lesions and normal-appearing white matter in multiple sclerosis," *Neurology*, vol. 52, no. 8, May 01, pp. 1626-1626.

[13] M. Doran, J.V. Hajnal, N.V. Bruggen, M.D. King, I.R. Young and G.M. Bydder, "Normal and Abnormal White Matter Tracts Shown by MR Imaging using Directional Diffusion Weighted Sequences," *J.Comput.Assist.Tomogr.*, vol. 14, no. 6, November/December, pp. 865-873.

[14] C. Pierpaoli, A. Barnett, S. Pajevic, R. Chen, L. Penix, A. Virta and P. Basser, "Water Diffusion Changes in Wallerian Degeneration and Their Dependence on White Matter Architecture," *Neuroimage*, vol. 13, no. 6, 6, pp. 1174-1185.

[15] J. Cohen-Adad, M.M. El Mendili, S. Lehericy, P.F. Pradat, S. Blancho, S. Rossignol and H. Benali, "Demyelination and degeneration in the injured human spinal cord detected with diffusion and magnetization transfer MRI," *Neuroimage*, vol. 55, no. 3, Apr 1, pp. 1024-1033.

[16] J. Finsterbusch, "High-resolution diffusion tensor imaging with inner field-of-view EPI," *J.Magn.Reson.Imaging*, vol. 29, no. 4, Apr, pp. 987-993.

[17] J. Finsterbusch, F. Eippert and C. Büchel, "Single, slice-specific z-shim gradient pulses improve T2*-weighted imaging of the spinal cord," *Neuroimage*, no. 0.

[18] H.S. Kharbanda, D.C. Alsop, A.W. Anderson, G. Filardo and D.B. Hackney, "Effects of cord motion on diffusion imaging of the spinal cord," *Magn.Reson.Med.*, vol. 56, no. 2, Aug, pp. 334-339.

[19] F. Laun, B. Stieltjes, M. Schluter, R. Rupp and L.R. Schad, "Reproducible evaluation of spinal cord DTI using an optimized inner volume sequence in combination with probabilistic ROI analysis," *Z.Med.Phys.*, vol. 19, no. 1, pp. 11-20.

[20] X. Santarelli, G. Garbin, M. Ukmar and R. Longo, "Dependence of the fractional anisotropy in cervical spine from the number of diffusion gradients, repeated acquisition and voxel size," *Magn.Reson.Imaging*, vol. 28, no. 1, Jan, pp. 70-76.

[21] N. Barakat, F.B. Mohamed, P. Shah, S.H. Faro, A. Samdani, J. Finsterbusch, R. Betz, J. Gaughan and M. Mulcahey, "Diffusion Tensor Imaging of the Normal Pediatric Spinal Cord using an inner-FoV EPI Sequence," *AJNR*, vol. 33, pp. 1127-1133.

[22] C. Rossi, A. Boss, T.M. Lindig, P. Martirosian, G. Steidle, W. Maetzler, C.D. Claussen, U. Klose and F. Schick, "Diffusion Tensor Imaging of the Spinal Cord at 1.5 andÂ 3.0 Tesla," *Fortschr Rontgenstr*, vol. 179, no. 03, pp. 219-224.

[23] D. Ducreux, P. Fillard, D. Facon, A. Ozanne, J. Lepeintre, J. Renoux, M. Tadié and P. Lasjaunias, "Diffusion Tensor Magnetic Resonance Imaging and Fiber Tracking in Spinal Cord Lesions: Current and Future Indications," *Neuroimaging Clinics of North America*, vol. 17, no. 1, February 2007, pp. 137-147.

[24] M. Akter, T. Hirai, R. Minoda, R. Murakami, S. Saiki, T. Okuaki, M. Kitajima, H. Fukuoka, A. Sasao, S. Nishimura, E. Yumoto, K. Awai and Y. Yamashita, "Diffusion Tensor Tractography in the Head-and-Neck Region Using a Clinical 3-T MR Scanner," *Academic Radiology*, vol. 16, no. 7, July 2009, pp. 858-865.

[25] W. Van Hecke, G. Nagels, G. Emonds, A. Leemans, J. Sijbers, J. Van Goethem and P.M. Parizel, "A diffusion tensor imaging group study of the spinal cord in multiple sclerosis patients with and without T2 spinal cord lesions," *Journal of Magnetic Resonance Imaging*, vol. 30, no. 1, pp. 25-34.

[26] C.A. Clark, D.J. Werring and D.H. Miller, "Diffusion imaging of the spinal cord in vivo: Estimation of the principal diffusivities and application to multiple sclerosis," *Magnetic Resonance in Medicine*, vol. 43, no. 1, pp. 133-138.

[27] K. Fujiyoshi, T. Konomi, M. Yamada, K. Hikishima, O. Tsuji, Y. Komaki, S. Momoshima, Y. Toyama, M. Nakamura and H. Okano, "Diffusion tensor imaging and tractography of the spinal cord: From experimental studies to clinical application," *Experimental Neurology*, vol. 242, April 2013, pp. 74-82.

[28] S.M. Hesseltine, M. Law, J. Babb, M. Rad, S. Lopez, Y. Ge, G. Johnson and R.I. Grossman, "Diffusion Tensor Imaging in Multiple Sclerosis: Assessment of Regional Differences in the Axial Plane within Normal-Appearing Cervical Spinal Cord," *Am.J.Neuroradiol.*, vol. 27, no. 6, 06/14, pp. 1189.

[29] A. Banaszek, J. Bladowska, P. Szewczyk, P. Podgarski and M. Sasiadek, "Usefulness of diffusion tensor MR imaging in the assessment of intramedullary changes of the cervical spinal cord in different stages of degenerative spine disease," *European Spine Journal*, vol. 23, no. 7, 07/01, pp. 1523-1530.

[30] R. Wadhwa and P.V. Mummaneni, "Correlation of Diffusion Tensor Magnetic Resonance Imaging Metrics with Clinical Outcomes," *World Neurosurgery*, vol. 83, no. 4, April 2015, pp. 494-495.

[31] K. Shanmuganathan, R.P. Gullapalli, J. Zhuo and S.E. Mirvis, "Diffusion Tensor MR Imaging in Cervical Spine Trauma," *Am.J.Neuroradiol.*, vol. 29, no. 4, 04/08, pp. 655.

[32] J.A. Petersen, B.J. Wilm, J. von Meyenburg, M. Schubert, B. Seifert, Y. Najafi, V. Dietz and S. Kollias, "Chronic Cervical Spinal Cord Injury: DTI Correlates with Clinical and Electrophysiological Measures," *J.Neurotrauma*, vol. 29, no. 8, 05/20; 2017/08, pp. 1556-1566.

[33] J.W. Lee, K.S. Park, J.H. Kim, J. Choi, S.H. Hong, S. Park and H.S. Kang, "Diffusion Tensor Imaging in Idiopathic Acute Transverse Myelitis," *Am.J.Roentgenol.*, vol. 191, no. 2, 08/01; 2017/08, pp. W52-W57.

[34] P. Freund, T. Schneider, Z. Nagy, C. Hutton, N. Weiskopf, K. Friston, C. Wheeler-Kingshott and A.J. Thompson, "Degeneration of the Injured Cervical Cord Is Associated with Remote Changes in Corticospinal Tract Integrity and Upper Limb Impairment," *PLoS ONE*, vol. 7, no. 12, 11/05, pp. e51729.

[35] S. Cheran, K. Shanmuganathan, J. Zhuo, S.E. Mirvis, B. Aarabi, M.T. Alexander and R.P. Gullapalli, "Correlation of MR Diffusion Tensor Imaging Parameters with ASIA Motor Scores in Hemorrhagic and Nonhemorrhagic Acute Spinal Cord Injury," *J.Neurotrauma*, vol. 28, no. 9, 09/01; 2017/08, pp. 1881-1892.

[36] M.J. Mulcahey, A.F. Samdani, J.P. Gaughan, N. Barakat, S. Faro, P. Shah, R.R. Betz and F.B. Mohamed, "Diagnostic accuracy of diffusion tensor imaging for pediatric cervical spinal cord injury," *Spinal Cord*, vol. 51, no. 7, print, pp. 532-537.

[37] G. Orman, K.Y. Wang, X. Li, C. Thompson, T.A.G.M. Huisman and I. Izbudak, "Diffusion tensor imaging of the cervical spinal cord in children," *Child s Nervous System*, vol. 31, no. 8, 08/01, pp. 1239-1245.

[38] C.J. Conklin, D.M. Middleton, M. Alizadeh, J. Finsterbusch, D.L. Raunig, S.H. Faro, P. Shah, L. Krisa, R. Sinko, J.Z. Delalic, M.J. Mulcahey and F.B. Mohamed, "Spatially selective 2D RF inner field of view (iFOV) diffusion kurtosis imaging (DKI) of the pediatric spinal cord," *NeuroImage : Clinical*, vol. 11, 01/09, pp. 61-67.

[39] S. Saksena, D.M. Middleton, L. Krisa, P. Shah, S.H. Faro, R. Sinko, J. Gaughan, J. Finsterbusch, M.J. Mulcahey and F.B. Mohamed, "Diffusion Tensor Imaging of the Normal Cervical and Thoracic Pediatric Spinal Cord," *AJNR Am.J.Neuroradiol.*, Jul 14.

[40] F. Giove, G. Garreffa, G. Giulietti, S. Mangia, C. Colonnese and B. Maraviglia, "Issues about the fMRI of the human spinal cord," *Magn.Reson.Imaging*, vol. 22, no. 10, Dec, pp. 1505-1516.

[41] G. Schroth and U. Klose, "Cerebrospinal fluid flow I. Physiology of cardiac-related pulsation" *Neuroradiology*, vol. 35, no. 1, pp. 1-9.

[42] G. Schroth and U. Klose, "Cerebrospinal fluid flow. II. Physiology of respiration-related pulsations." *Neuroradiology*, vol. 35, no. 1, pp. 10-15.

[43] S. Skare and J.L.R. Andersson, "On the effects of gating in diffusion imaging of the brain using single shot EPI," *Magnetic Resonance Imaging*, vol. 19, no. 8, October 2001, pp. 1125-1128.

[44] N. Barakat, D.M. Middleton, L. Hunter, J. Finsterbusch, S.H. Faro, M. Mulcahey, A. Samdani and F.B. Mohamed, "An Investigation of Motion Correction Algorithms for Pediatric Spinal Cord DTI in Normals and Patients with SCI," *ISMRM Montreal*, pp. 6282.

[45] S. Mohammadi, P. Freund, T. Feiweier, A. Curt and N. Weiskopf, "The impact of post-processing on spinal cord diffusion tensor imaging," *Neuroimage*, vol. 70, Apr 15, pp. 377-385.

[46] L.C. Chang, D.K. Jones and C. Pierpaoli, "RESTORE: robust estimation of tensors by outlier rejection," *Magn.Reson.Med.*, vol. 53, no. 5, May, pp. 1088-1095.

[47] P. Fillard, X. Pennec, V. Arsigny and N. Ayache, "Clinical DT-MRI estimation, smoothing, and fiber tracking with log-Euclidean metrics," *IEEE Trans.Med.Imaging*, vol. 26, no. 11, Nov, pp. 1472-1482.

[48] L.C. Chang, L. Walker and C. Pierpaoli, "Informed RESTORE: A method for robust estimation of diffusion tensor from low redundancy datasets in the presence of physiological noise artifacts," *Magn.Reson.Med.*, vol. 68, no. 5, Nov, pp. 1654-1663.

[49] M.H. Tuszynski, K. Gabriel, K. Gerhardt and S. Szollar, "Human Spinal Cord Retains Substantial Structural Mass in Chronic Stages After Injury," *J Neurotrauma*, vol. 16(6), pp. 523-531.

[50] W.L. Curati, D.P.E. Kingsley, B.E. Kendall and I.F. Moseley, "MRI in chronic spinal cord trauma," *Neuroradiology*, vol. 35, no. 1, 01/01, pp. 30-35.

[51] J.Y. Kim, S.J. Kim and M.S. Bang, "Spinal Cord Atrophy and Early Motor Recovery following Transverse Myelitis in Pediatric Patients," *Ann.Rehabil.Med.*, vol. 36, no. 3, Jun, pp. 328-333.

[52] N.A. Losseff, S.L. Webb, J.I. O Riordan, R. Page, L. Wang, G.J. Barker, P.S. Tofts, W.I. McDonald, D.H. Miller and A.J. Thompson, "Spinal cord atrophy and disability in multiple sclerosis," *Brain*, vol. 119, no. 3, Oxford University Press, pp. 701-708.

[53] X. Lin, C.R. Tench, B. Turner, L.D. Blumhardt and C.S. Constantinescu, "Spinal cord atrophy and disability in multiple sclerosis over four years: application of a reproducible automated technique in monitoring disease progression in a cohort of the interferon β-1a (Rebif) treatment trial," *Journal of Neurology, Neurosurgery & Psychiatry*, vol. 74, no. 8, August 01, pp. 1090-1094.

[54] M.A. Horsfield and M. Filippi, "Spinal cord atrophy and disability in multiple sclerosis over four years," *Journal of Neurology, Neurosurgery & Psychiatry*, vol. 74, no. 8, August 01, pp. 1014-1015.

[55] M. El Mendili, T. Lenglet, T. Stojkovic, A. Behin, R. Guimarales-Costa, F. Salachas, V. Meininger, G. Bruneteau, N. Le Forestier, P. Laforat, S. Leharicy, H. Benali and P. Pradat, "Cervical Spinal Cord Atrophy Profile in Adult SMN1-Linked SMA," *PLoS ONE*, vol. 11, no. 4, 03/14, pp. e0152439.

[56] J. Hou, Z. Xiang, R. Yan, M. Zhao, Y. Wu, J. Zhong, L. Guo, H. Li, J. Wang, J. Wu, T. Sun and H. Liu, "Motor recovery at 6 months after admission is related to structural and functional reorganization of the spine and brain in patients with spinal cord injury," *Hum.Brain Mapp.*, vol. 37, no. 6, pp. 2195-2209.

[57] Y. Liu, C. Lukas, M.D. Steenwijk, M. Daams, A. Versteeg, Y. Duan, K. Li, F. Weiler, H.K. Hahn, M.P. Wattjes, F. Barkhof and H. Vrenken, "Multicenter Validation of Mean Upper Cervical Cord Area Measurements from Head 3D T1-Weighted MR Imaging in Patients with Multiple Sclerosis," *Am.J.Neuroradiol.*, vol. 37, no. 4, 04/12, pp. 749.

[58] G. Kim, F. Khalid, V.V. Oommen, S. Tauhid, R. Chu, M.A. Horsfield, B.C. Healy and R. Bakshi, "T1- vs. T2-based MRI measures of spinal cord volume in healthy subjects and patients with multiple sclerosis," *BMC Neurology*, vol. 15, 07/17, pp. 124.

[59] E. Bernitsas, F. Bao, N. Seraji-Bozorgzad, J. Chorostecki, C. Santiago, A. Tselis, C. Caon, I. Zak, S. Millis and O. Khan, "Spinal cord atrophy in multiple sclerosis and relationship with disability across clinical phenotypes," *Multiple Sclerosis and Related Disorders*, vol. 4, no. 1, January 2015, pp. 47-51.

[60] R. Schlaeger, N. Papinutto, V. Panara, C. Bevan, I.V. Lobach, M. Bucci, E. Caverzasi, J.M. Gelfand, A.J. Green, K.M. Jordan, W.A. Stern, H.-. von Büdingen, E. Waubant, A.H. Zhu, D.S. Goodin, B.A.C. Cree, S.L. Hauser and R.G. Henry, "Spinal cord gray matter atrophy correlates with multiple sclerosis disability," *Ann.Neurol.*, vol. 76, no. 4, pp. 568-580.

[61] P. Freund, N. Weiskopf, N.S. Ward, C. Hutton, A. Gall, O. Ciccarelli, M. Craggs, K. Friston and A.J. Thompson, "Disability, atrophy and cortical reorganization following spinal cord injury," *Brain*, vol. 134, no. 6, 03/28, pp. 1610-1622.

[62] R.S. Mann, C.S. Constantinescu and C.R. Tench, "Upper cervical spinal cord cross-sectional area in relapsing remitting multiple sclerosis: Application of a new technique for measuring cross-sectional area on magnetic resonance images," *Journal of Magnetic Resonance Imaging*, vol. 26, no. 1, pp. 61-65.

[63] C.R. Tench, P.S. Morgan, T. Jaspan, D.P. Auer and C.S. Constantinescu, "Spinal Cord Imaging in Multiple Sclerosis," *Journal of Neuroimaging*, vol. 15, pp. 94S-102S.

[64] W. Liu, G. Nair, L. Vuolo, A. Bakshi, R. Massoud, D.S. Reich and S. Jacobson, "In vivo imaging of spinal cord atrophy in neuroinflammatory diseases," *Ann.Neurol.*, vol. 76, no. 3, pp. 370-378.

[65] P. Mansfield, "Multi-planar image formation using NMR spin echoes," *J Phys C: Solid State Phys*, vol. 10, pp. L55-L58.

[66] C.R. Figley and P.W. Stroman, "Investigation of human cervical and upper thoracic spinal cord motion: implications for imaging spinal cord structure and function," *Magn.Reson.Med.*, vol. 58, no. 1, Jul, pp. 185-189.

[67] R.H. Tijssen, J.F. Jansen and W.H. Backes, "Assessing and minimizing the effects of noise and motion in clinical DTI at 3 T," *Hum.Brain Mapp.*, vol. 30, no. 8, Aug, pp. 2641-2655.

[68] M. Kavec, N. Sadeghi, D. Baleriaux and T. Metens, "A Monte Carlo simulation of image misalignment effects in diffusion tensor imaging," *Magn.Reson.Imaging*, vol. 28, no. 6, Jul, pp. 834-841.

[69] G.K. Rohde, A.S. Barnett, P.J. Basser, S. Marenco and C. Pierpaoli, "Comprehensive approach for correction of motion and distortion in diffusion-weighted MRI," *Magn.Reson.Med.*, vol. 51, no. 1, Jan, pp. 103-114.

[70] J. Ling, F. Merideth, A. Caprihan, A. Pena, T. Teshiba and A.R. Mayer, "Head injury or head motion? Assessment and quantification of motion artifacts in diffusion tensor imaging studies," *Hum.Brain Mapp.*, vol. 33, pp. 50-62.

[71] P.W. Stroman, C.R. Figley and C.M. Cahill, "Spatial normalization, bulk motion correction and coregistration for functional magnetic resonance imaging of the human cervical spinal cord and brainstem," *Magn.Reson.Imaging*, vol. 26, no. 6, Jul, pp. 809-814.

[72] G. Nair, J.D. Carew, S. Usher, D. Lu, X.P. Hu and M. Benatar, "Diffusion tensor imaging reveals regional differences in the cervical spinal cord in amyotrophic lateral sclerosis," *Neuroimage*, vol. 53, no. 2, Nov 1, pp. 576-583.

[73] H. Jiang, P.C. van Zijl, J. Kim, G.D. Pearlson and S. Mori, "DtiStudio: resource program for diffusion tensor computation and fiber bundle tracking," *Comput.Methods Programs Biomed.*, vol. 81, no. 2, Feb, pp. 106-116.

[74] P.M. Jokich, J.M. Rubin and G.J. Dohrmann, "Intraoperative ultrasonic evaluation of spinal cord motion," *J.Neurosurg.*, vol. 60, no. 4, Apr, pp. 707-711.

[75] T. Saxena, J. Gilbert, D. Stelzner and J. Hasenwinkel, "Mechanical Characterization of the Injured Spinal Cord after Lateral Spinal Hemisection Injury in the Rat," *J Neurotrauma*, vol. 29, pp. 1747-1757.

[76] S.C. Kirshblum, W. Waring, F. Biering-Sorensen, S.P. Burns, M. Johansen, M. Schmidt-Read, W. Donovan, D.E. Graves, A. Jha, L. Jones, M.J. Mulcahey and A. Krassioukov, "Reference for the 2011 revision of the international standards for neurological classification of spinal cord injury," *J.Spinal Cord Med.*, vol. 34, no. 6, 11/01; 2015/09, pp. 547-554.

[77] S. By, J. Xu, B.A. Box, F.R. Bagnato and S.A. Smith, "Application and evaluation of NODDI in the cervical spinal cord of multiple sclerosis patients," *NeuroImage: Clinical*, vol. 15, 2017, pp. 333-342.

APPENDIX

INDIVIDUAL SUBJECT DTI AND SCCSA BY VERTEBRAL LEVEL

The following graphs provide data for DTI metrics FA, MD, AD, and RD alongside SCCSA by vertebral level for all subjects with spinal cord injury and typically developing subjects.

Subject SCI1

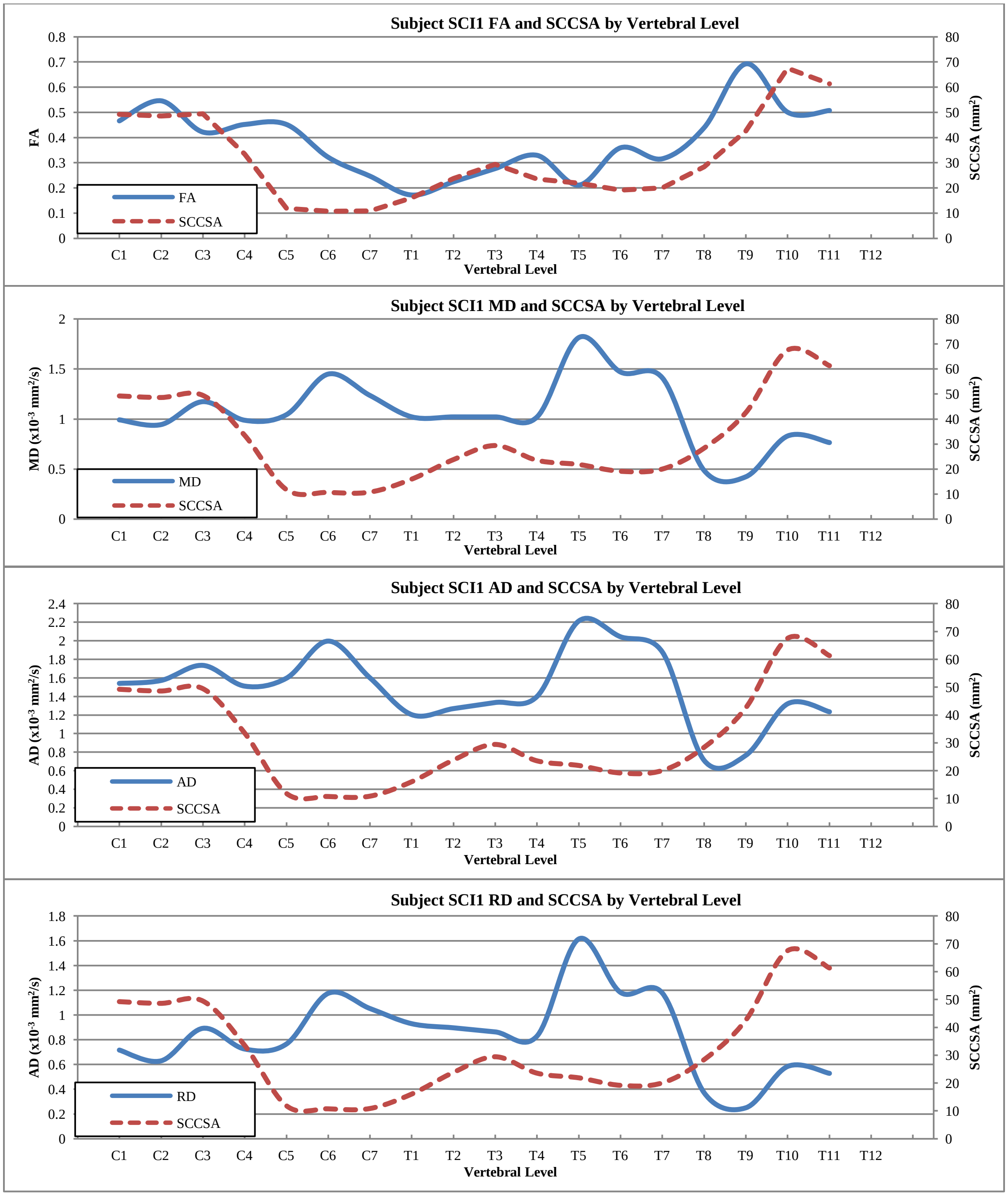

Figure A-1: FA, MD, AD, and RD with SCCSA by vertebral level for subject SCI1

Subject SCI2

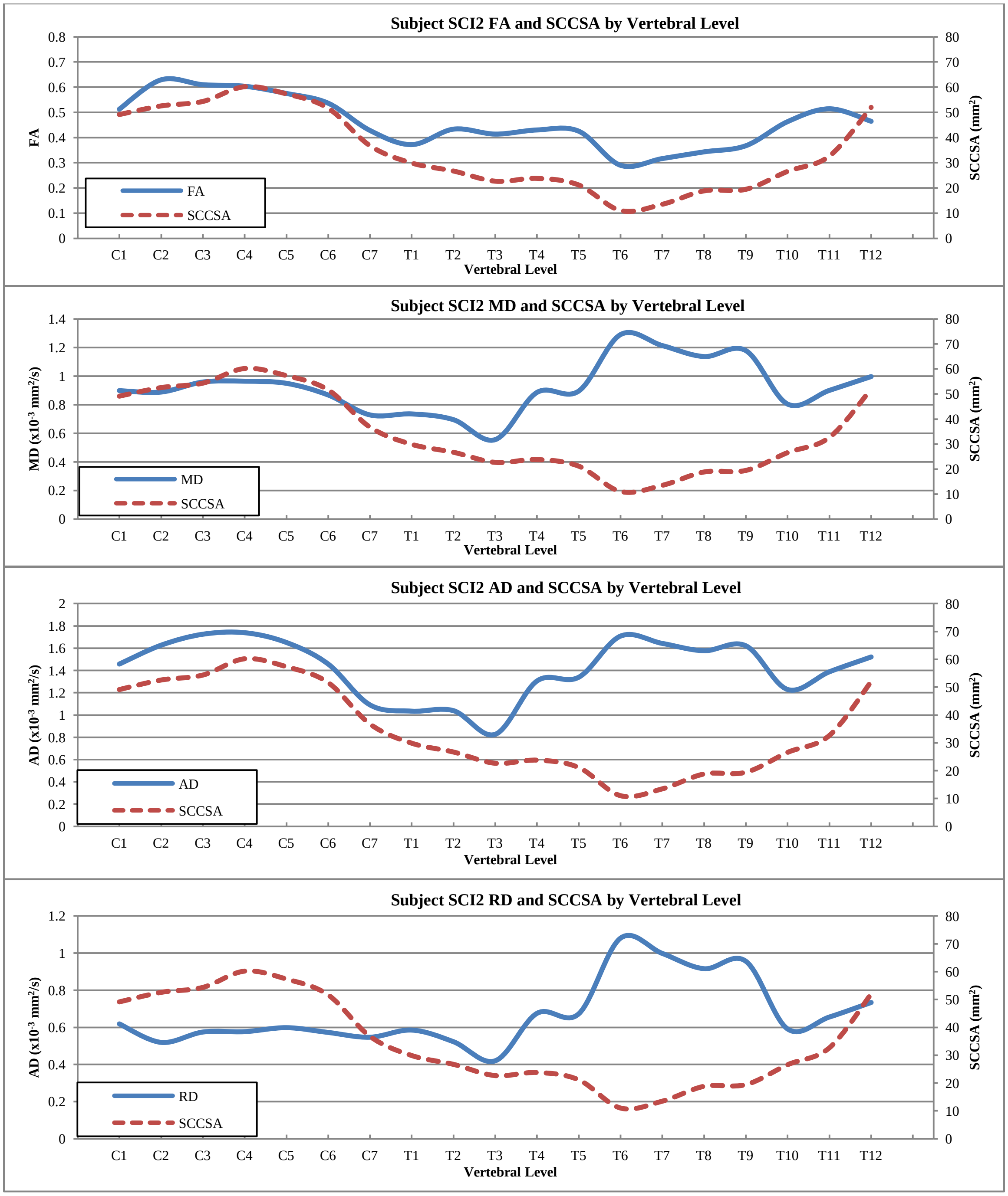

Figure A-2: FA, MD, AD, and RD with SCCSA by vertebral level for subject SCI2

Subject SCI3

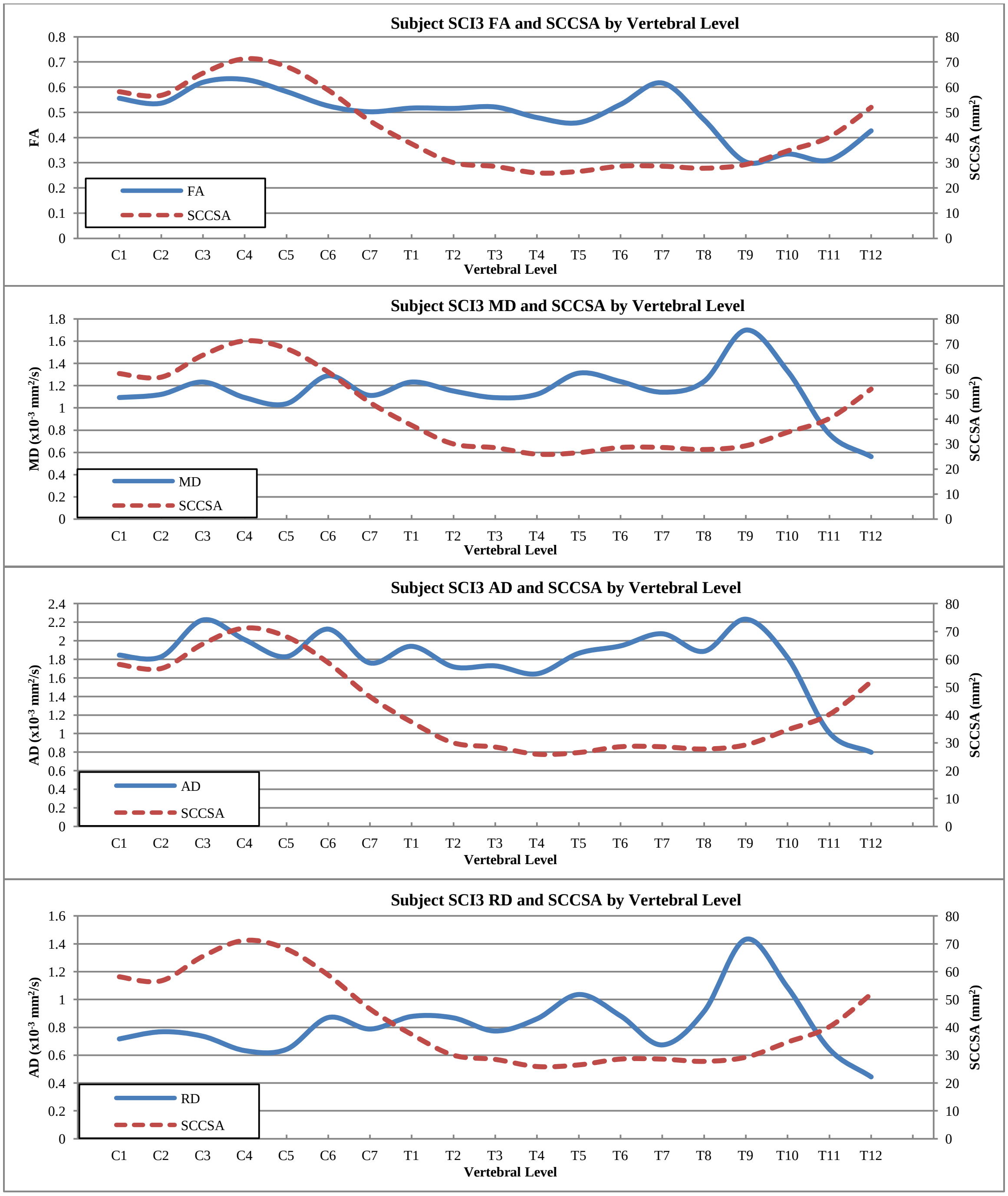

Figure A-3: FA, MD, AD, and RD with SCCSA by vertebral level for subject SCI3

Subject SCI4

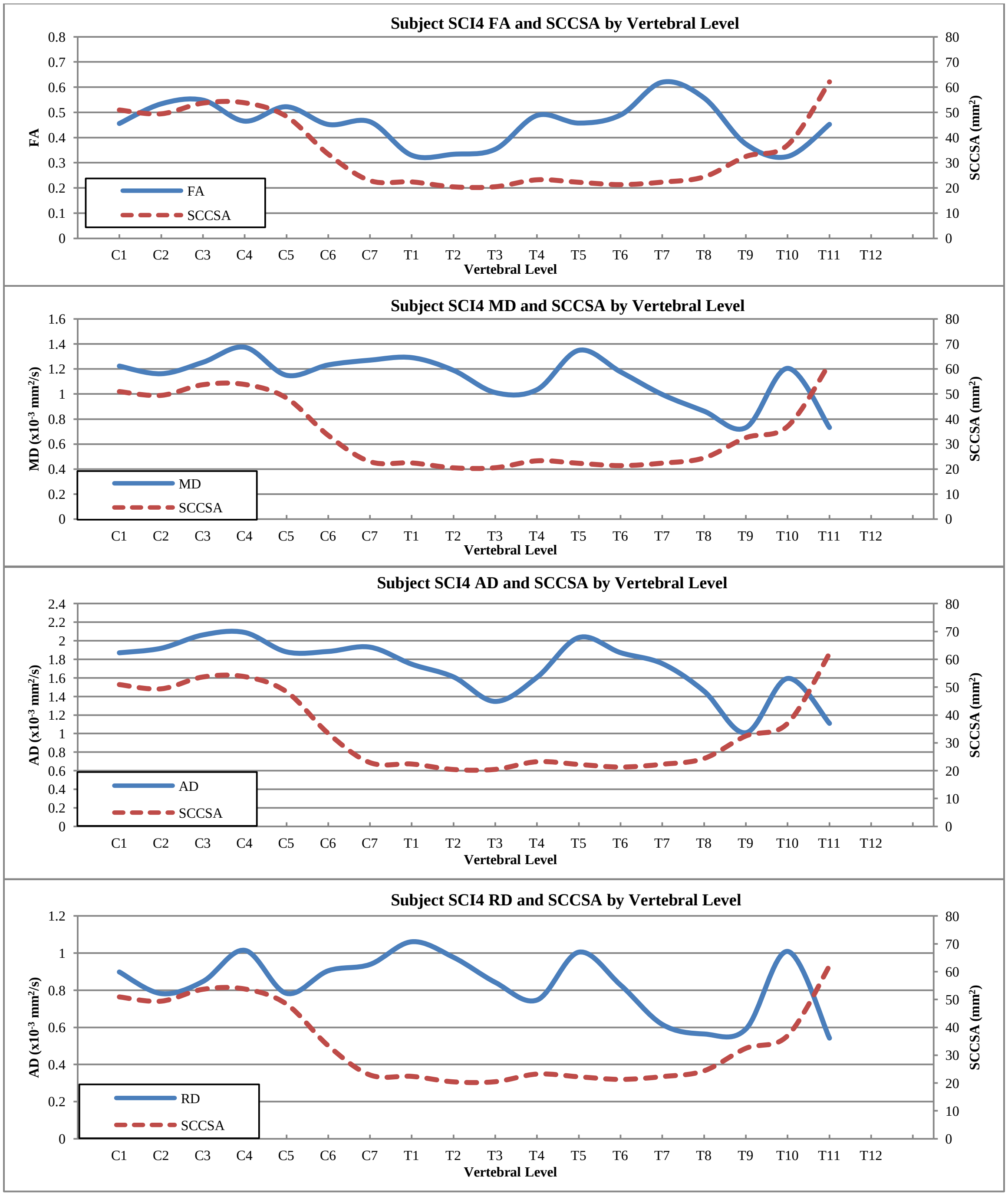

Figure A-4: FA, MD, AD, and RD with SCCSA by vertebral level for subject SCI4

Subject SCI5

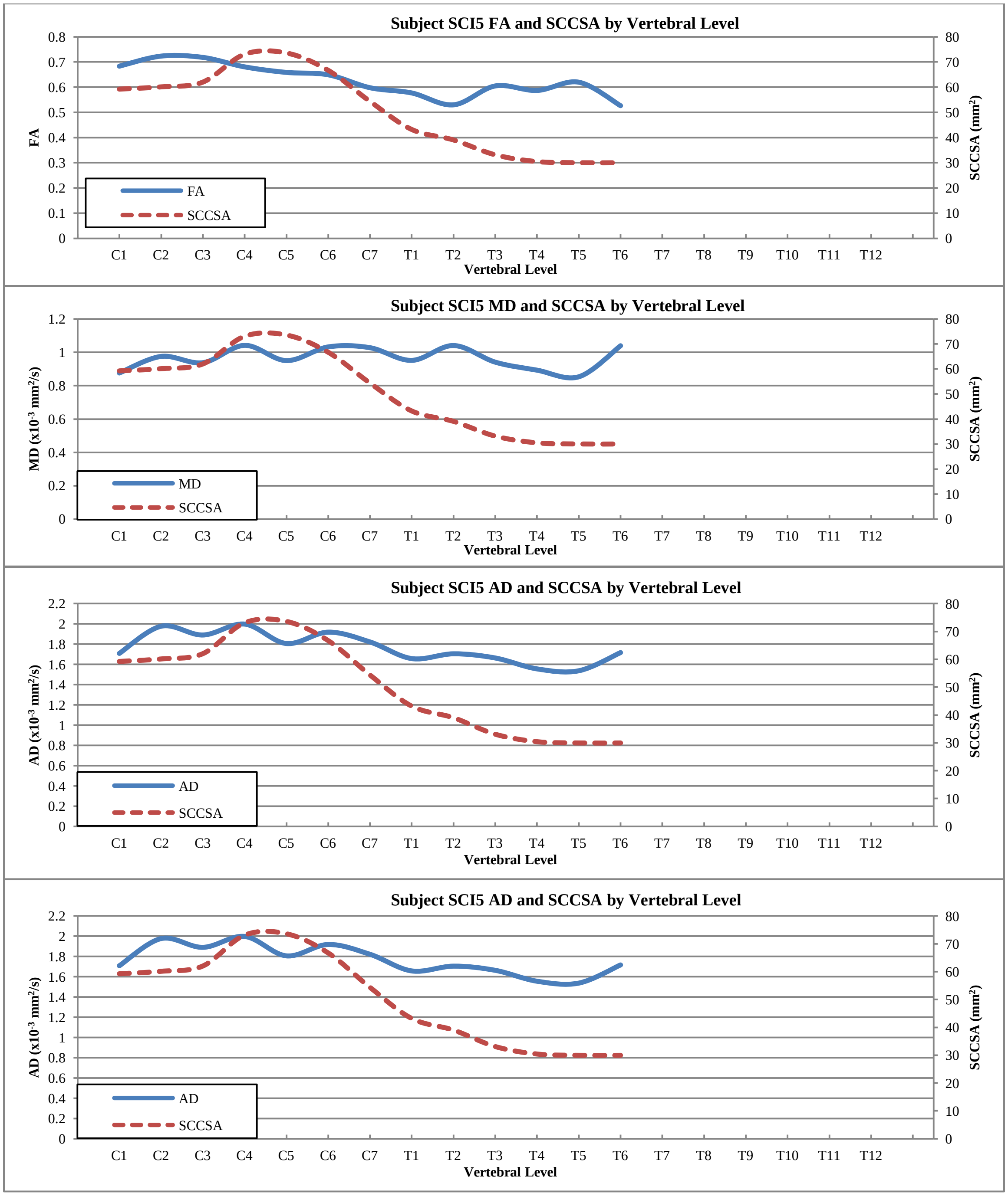

Figure A-5: FA, MD, AD, and RD with SCCSA by vertebral level for subject SCI5

Subject SCI6

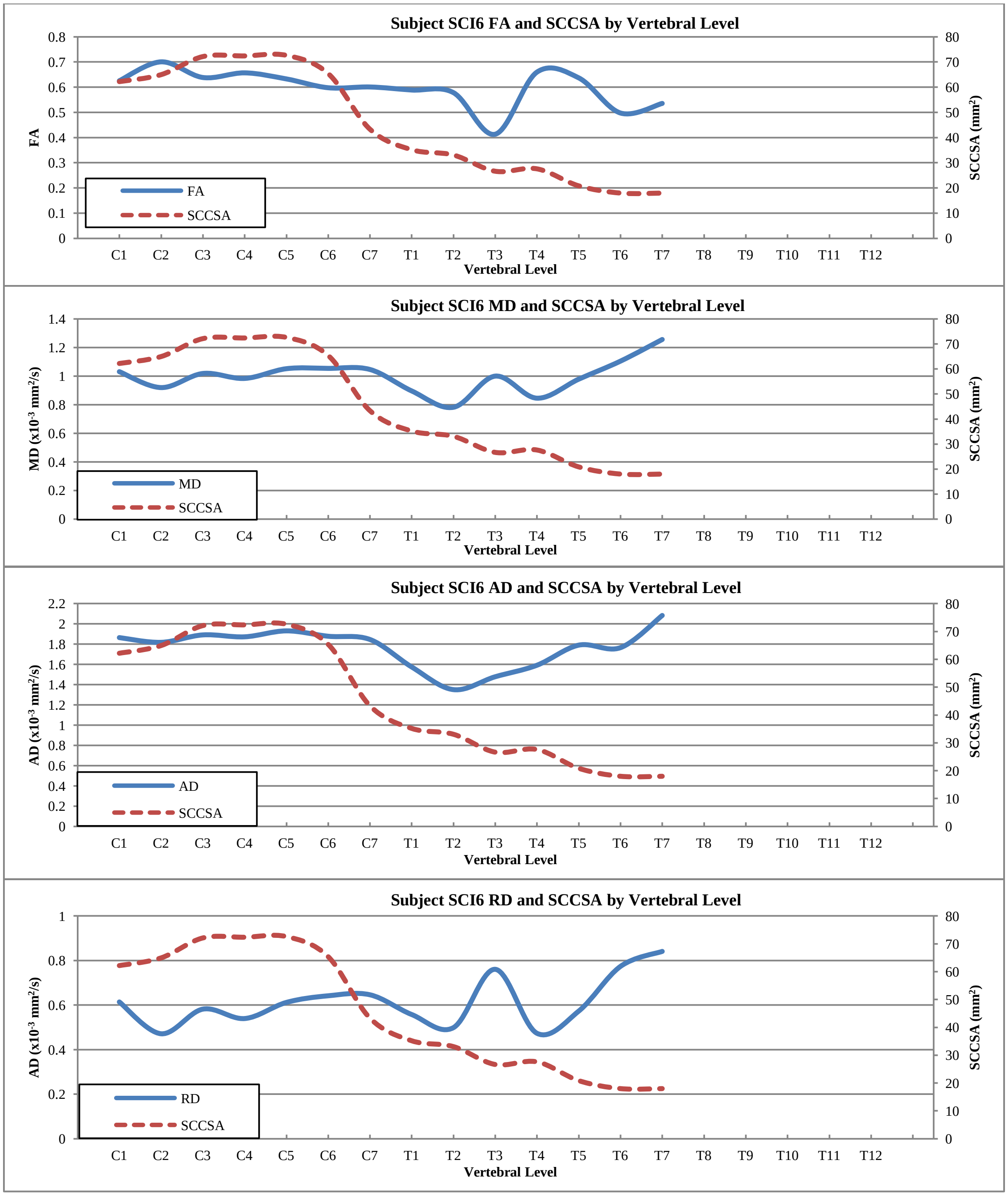

Figure A-6: FA, MD, AD, and RD with SCCSA by vertebral level for subject SCI6

Subject SCI7

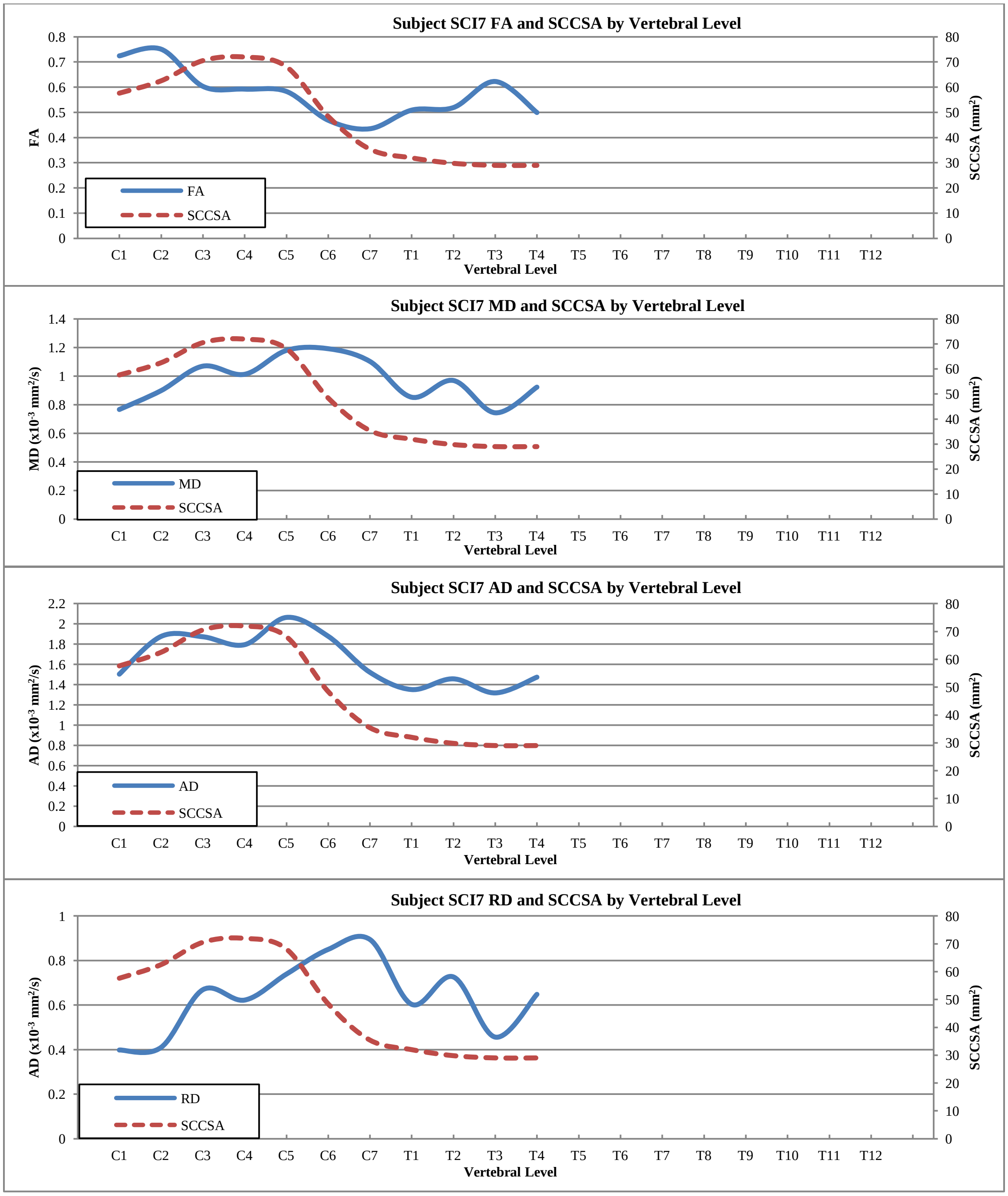

Figure A-7: FA, MD, AD, and RD with SCCSA by vertebral level for subject SCI7

Subject SCI8

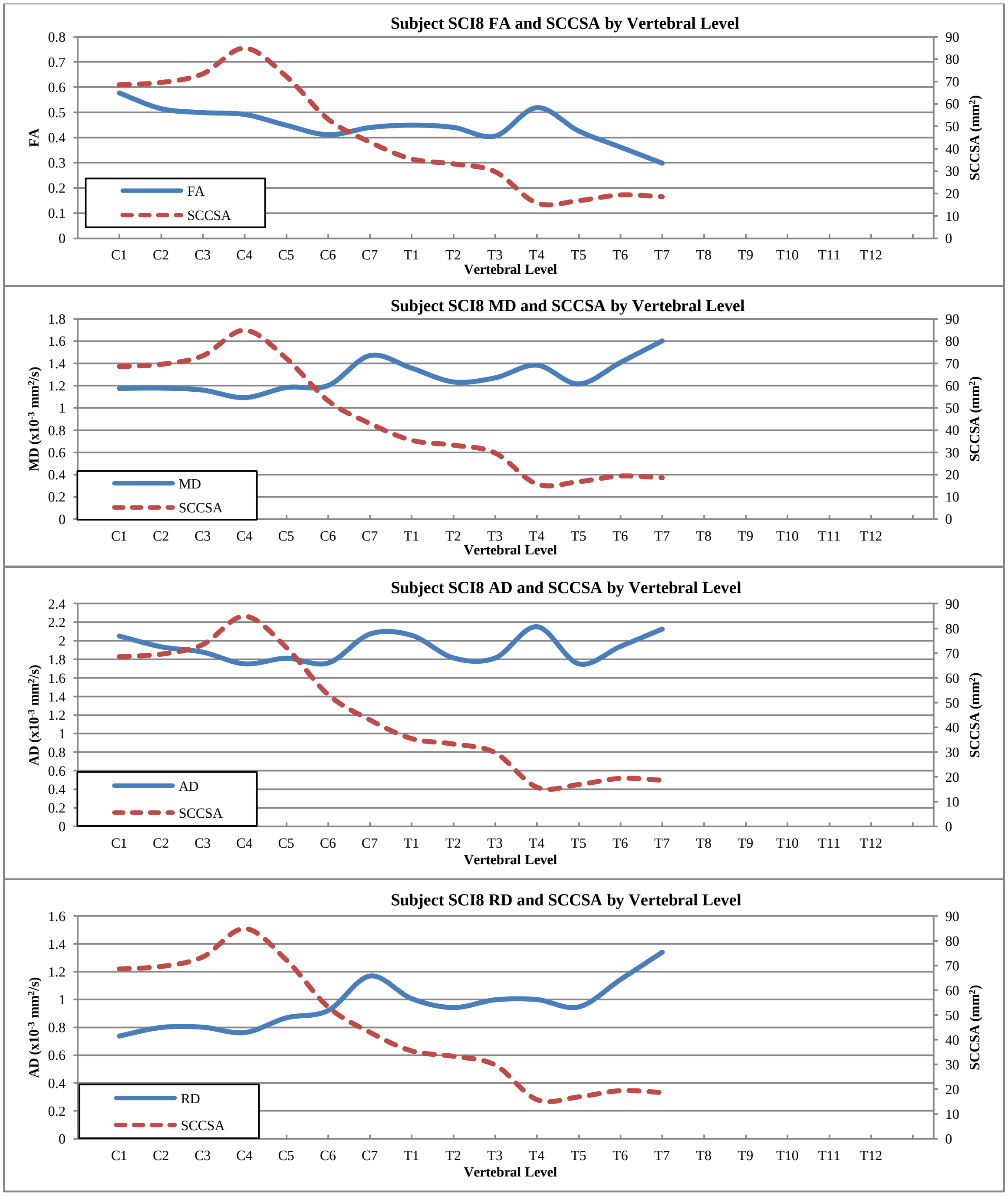

Figure A-8: FA, MD, AD, and RD with SCCSA by vertebral level for subject SCI8

Subject SCI9

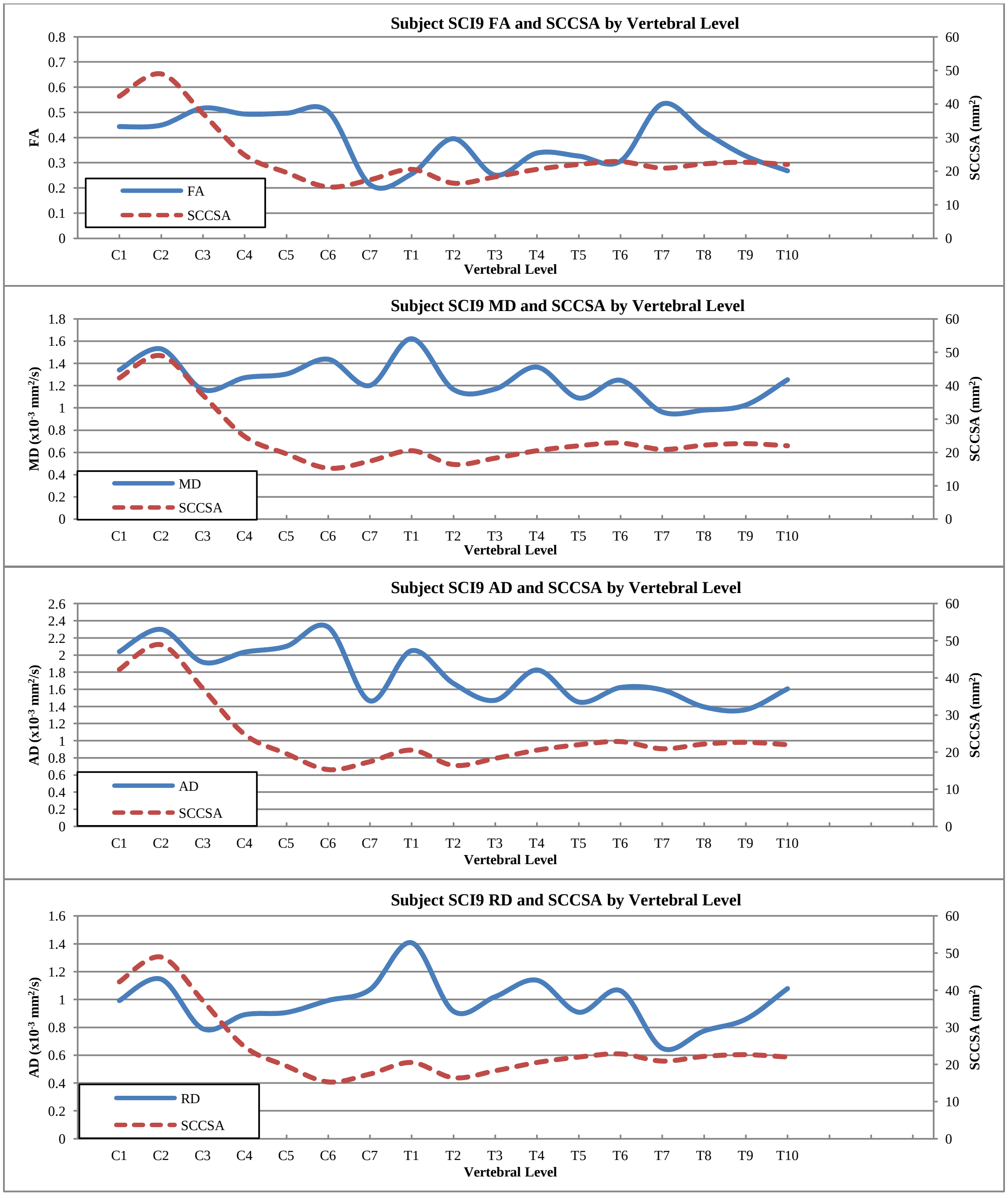

Figure A-9: FA, MD, AD, and RD with SCCSA by vertebral level for subject SCI9

Subject SCI10

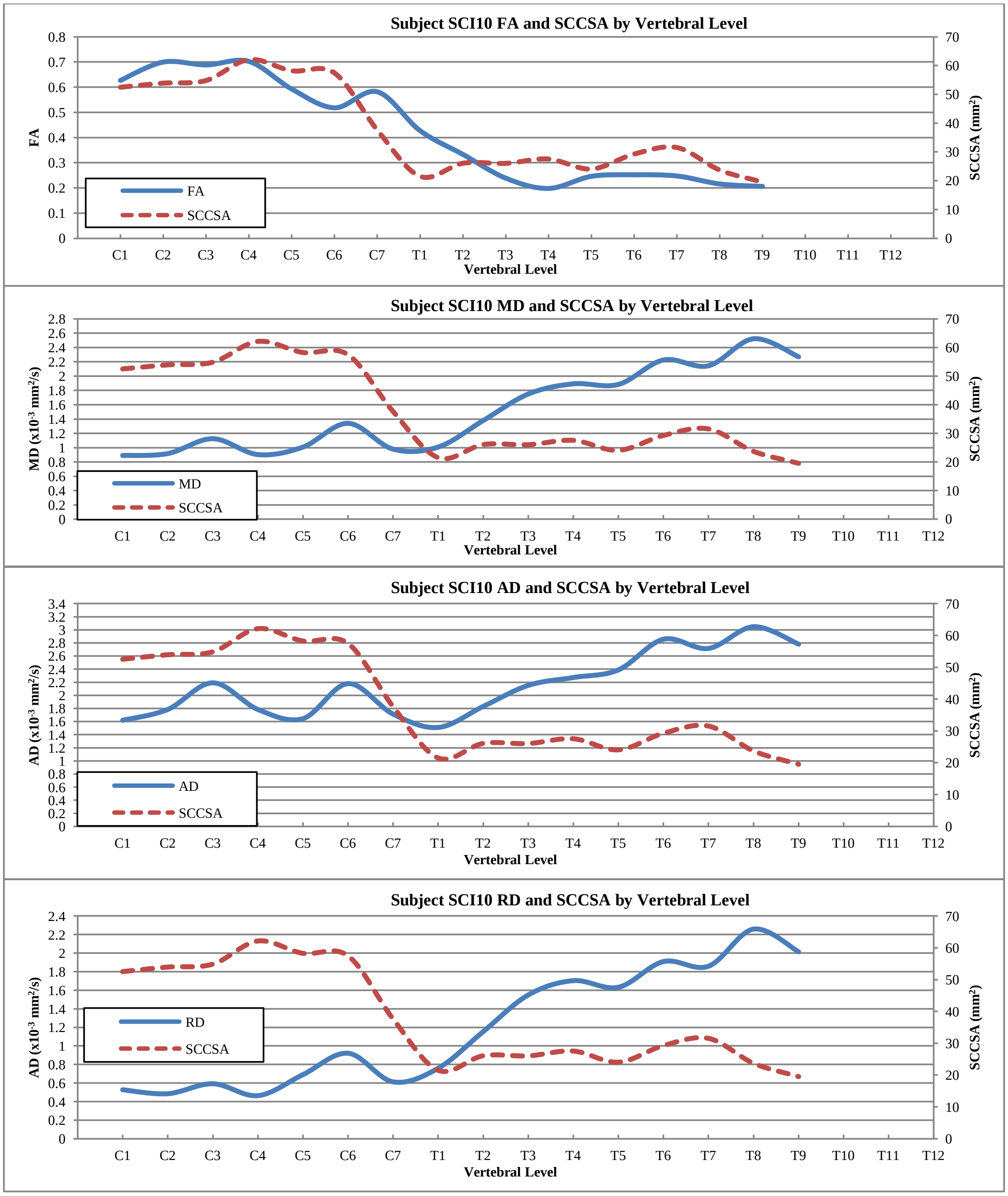

Figure A-10: FA, MD, AD, and RD with SCCSA by vertebral level for subject SCI10

Subject TD1

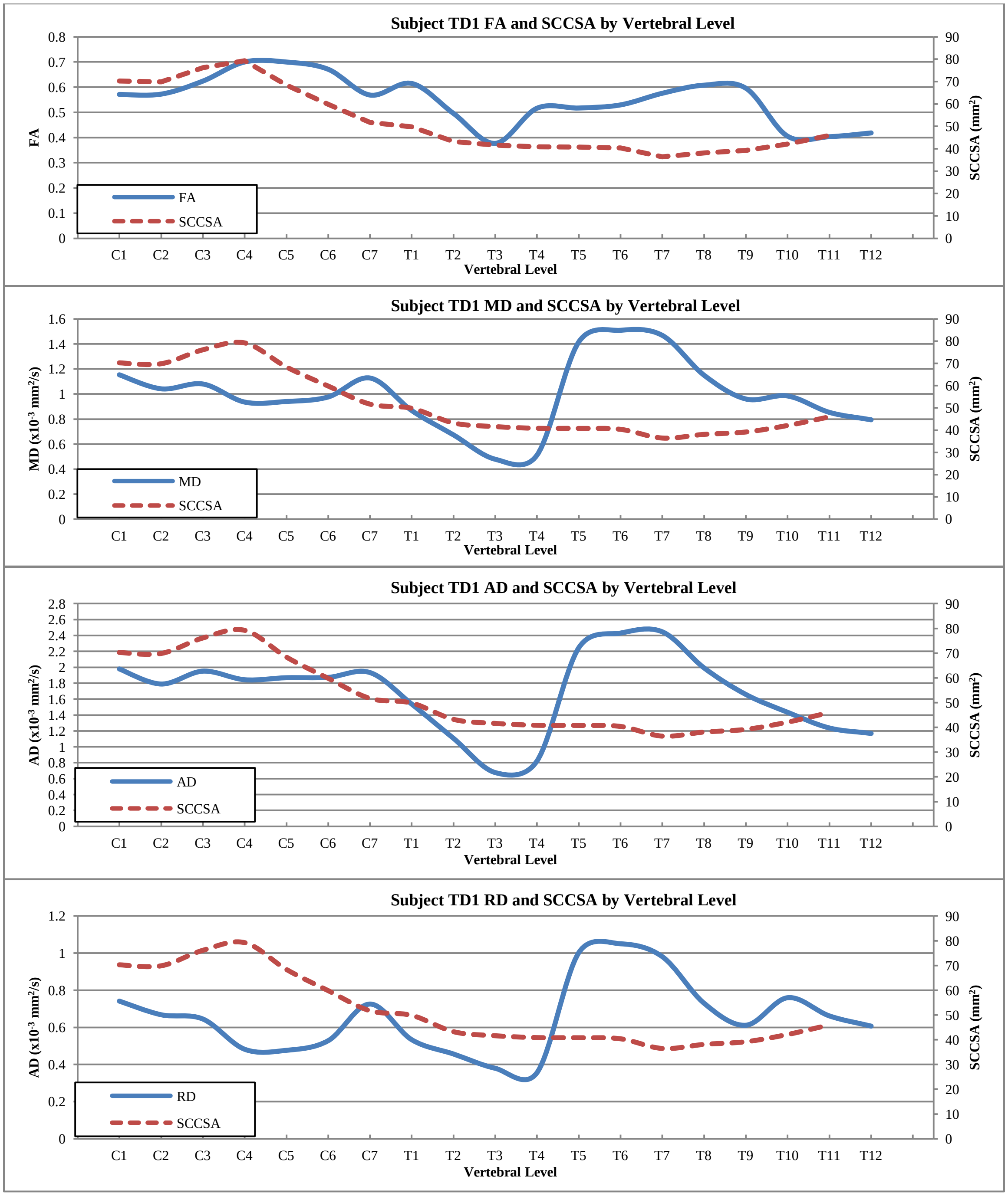

Figure A-11: FA, MD, AD, and RD with SCCSA by vertebral level for subject TD1

Subject TD2

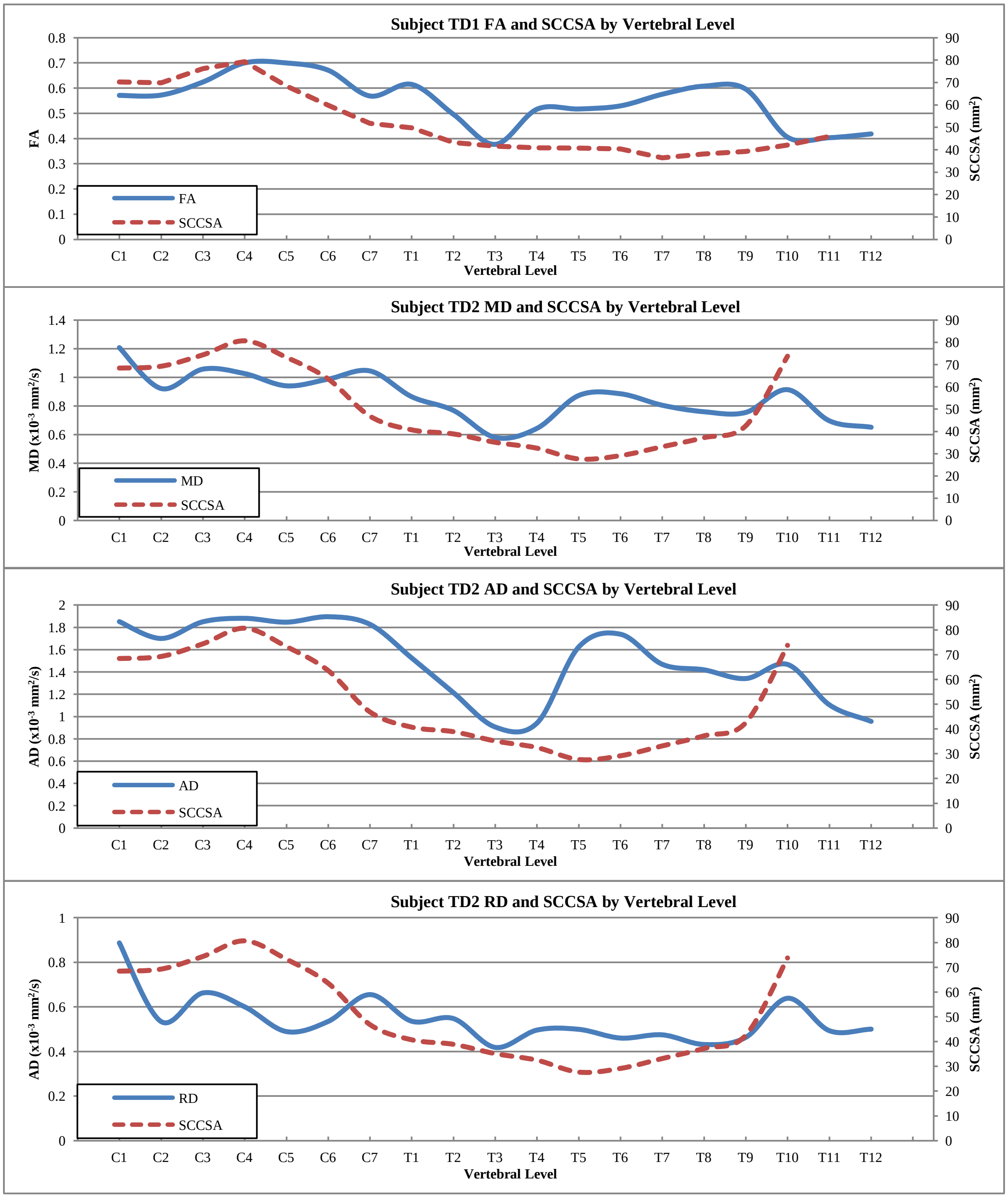

Figure A-12: FA, MD, AD, and RD with SCCSA by vertebral level for subject TD2

Subject TD3

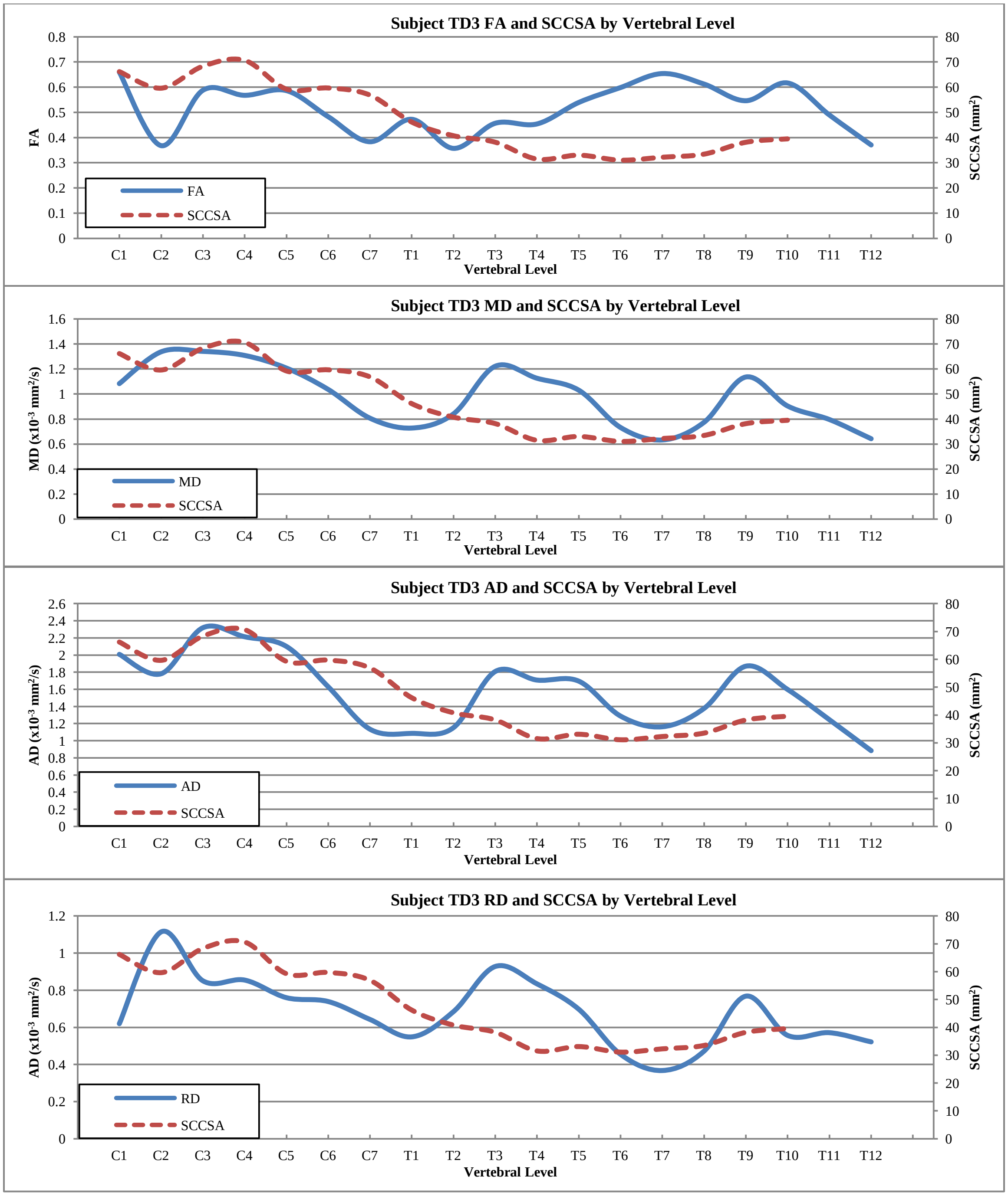

Figure A-13: FA, MD, AD, and RD with SCCSA by vertebral level for subject TD3

Subject TD4

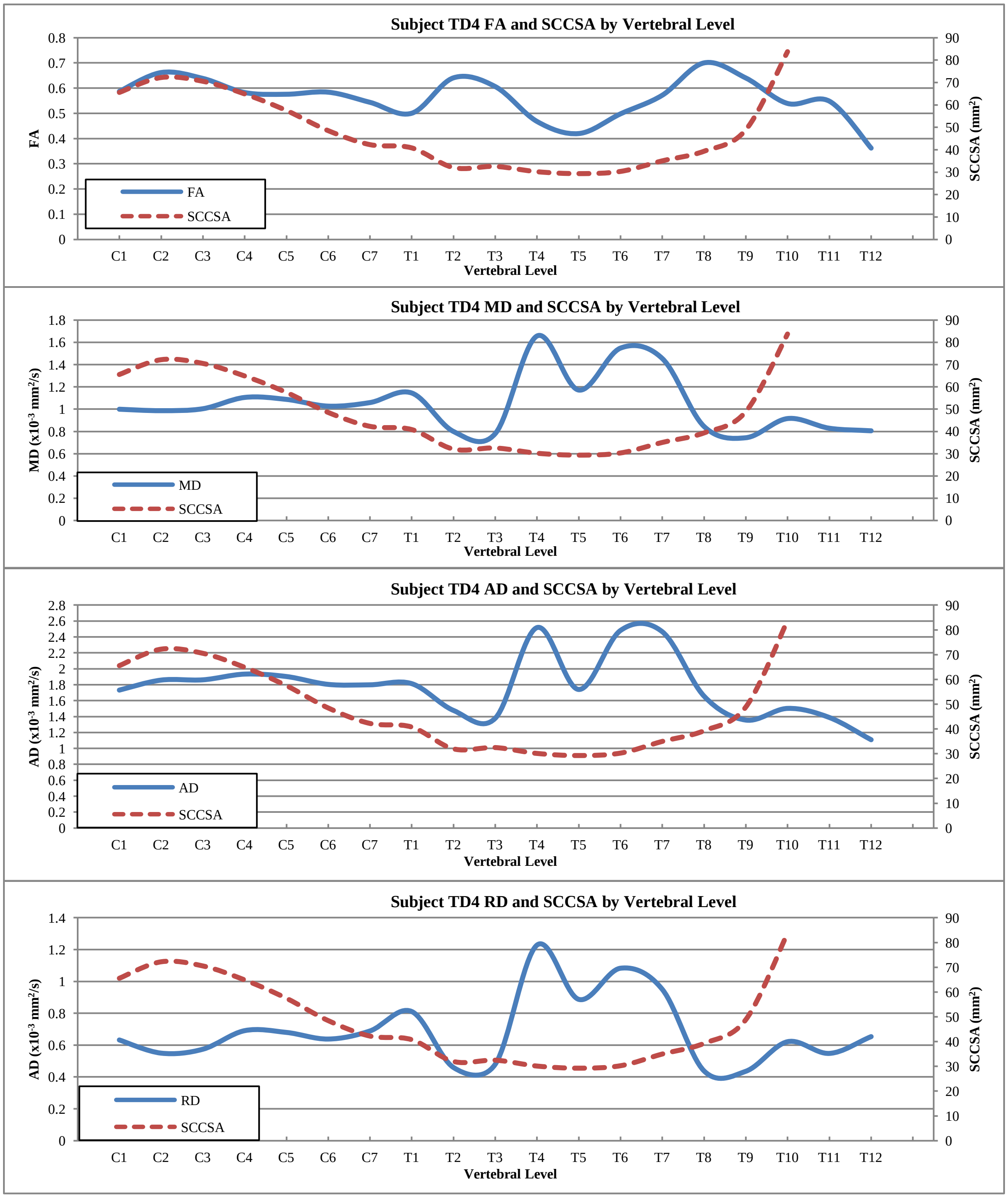

Figure A-14: FA, MD, AD, and RD with SCCSA by vertebral level for subject TD4

Subject TD5

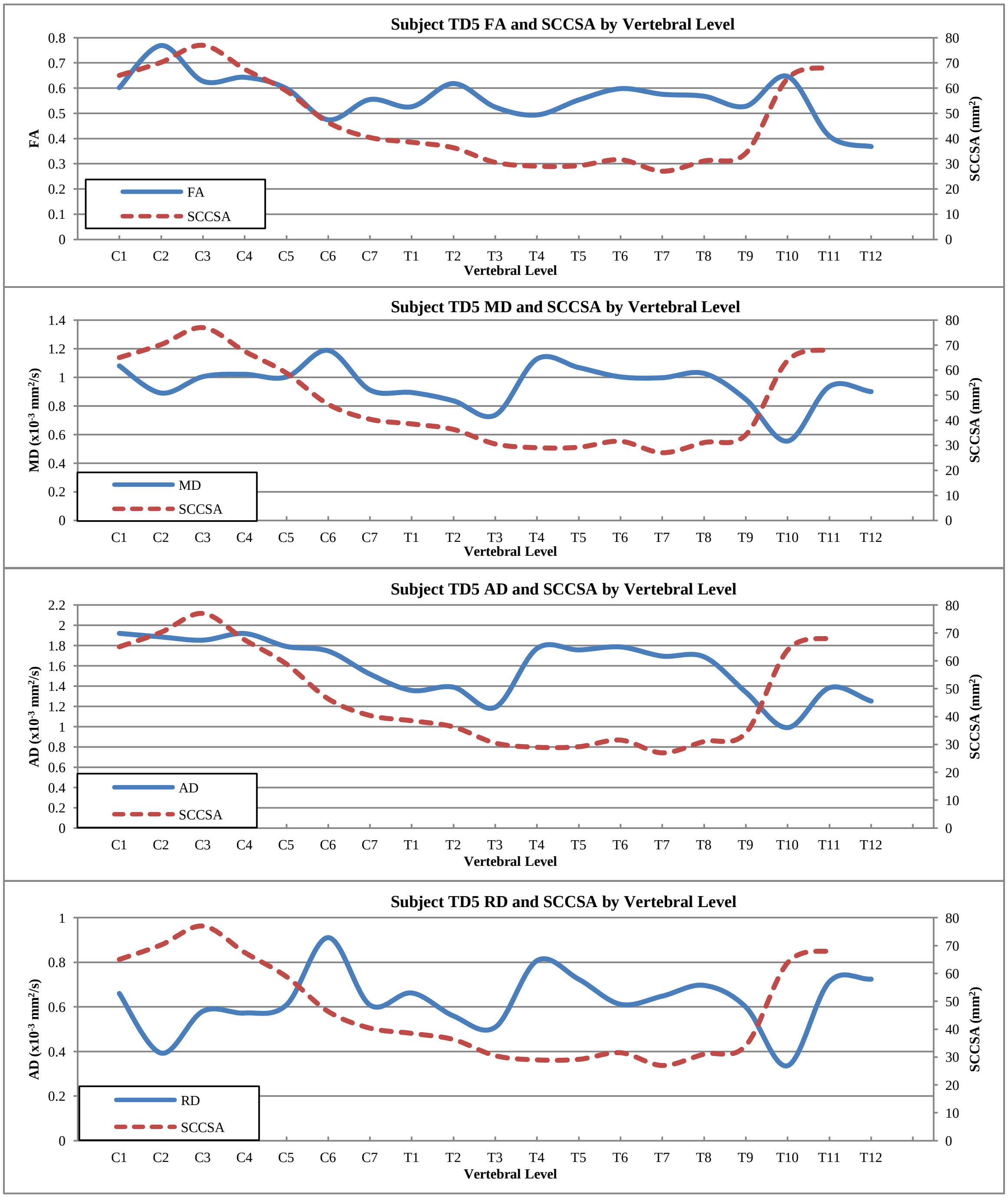

Figure A-15: FA, MD, AD, and RD with SCCSA by vertebral level for subject TD5

Subject TD6

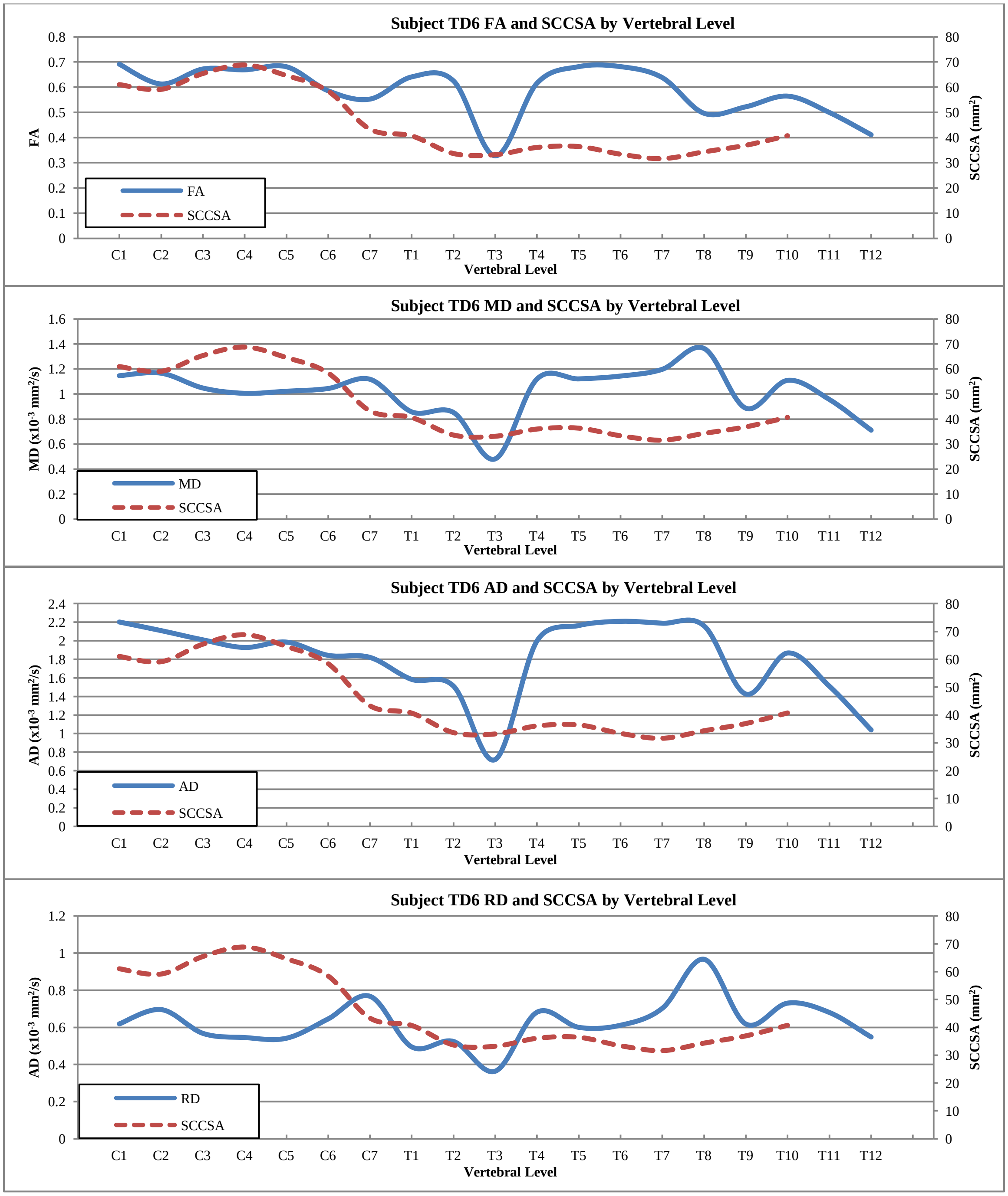

Figure A-16: FA, MD, AD, and RD with SCCSA by vertebral level for subject TD6

Subject TD7

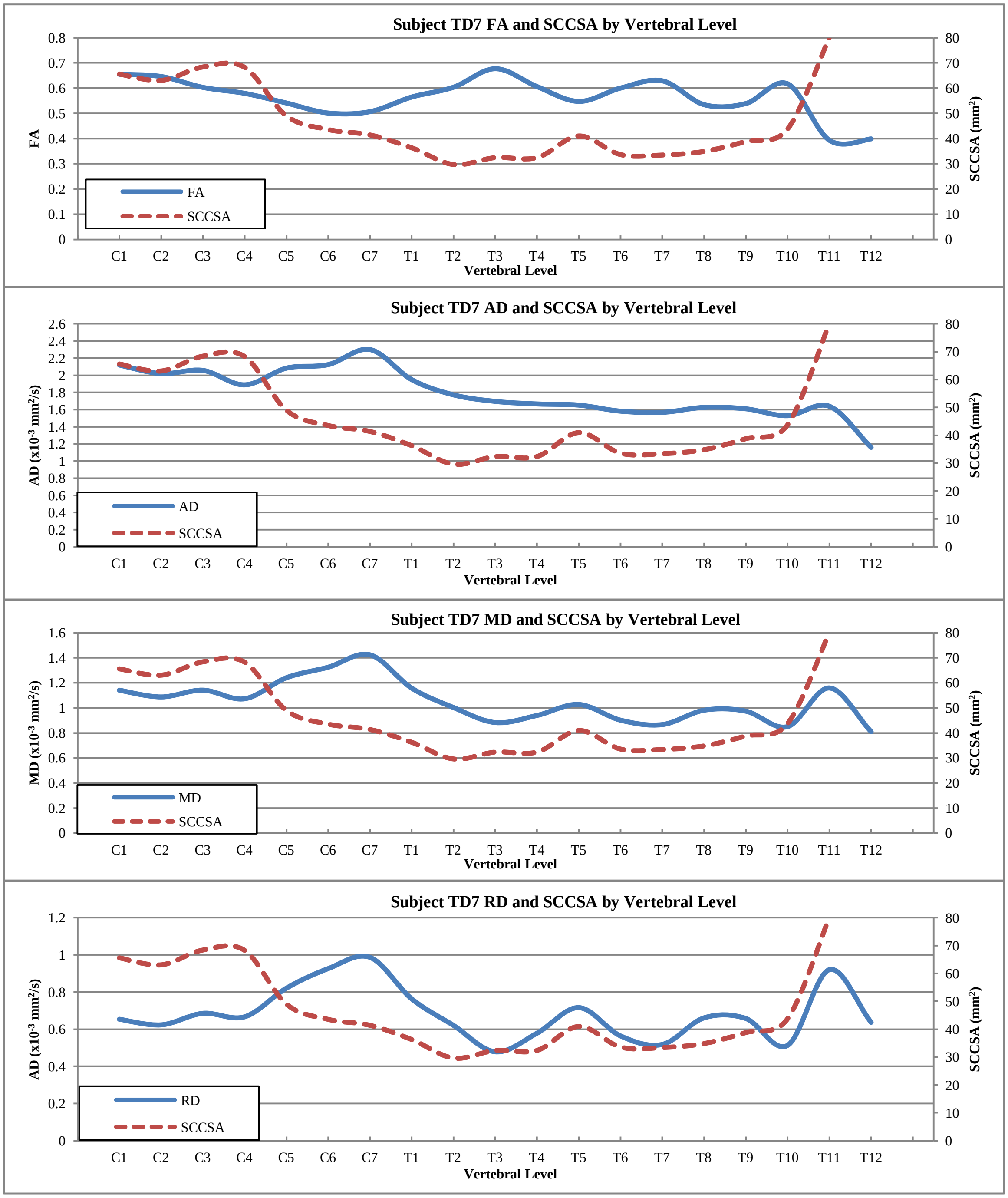

Figure A-17: FA, MD, AD, and RD with SCCSA by vertebral level for subject TD7

Subject TD8

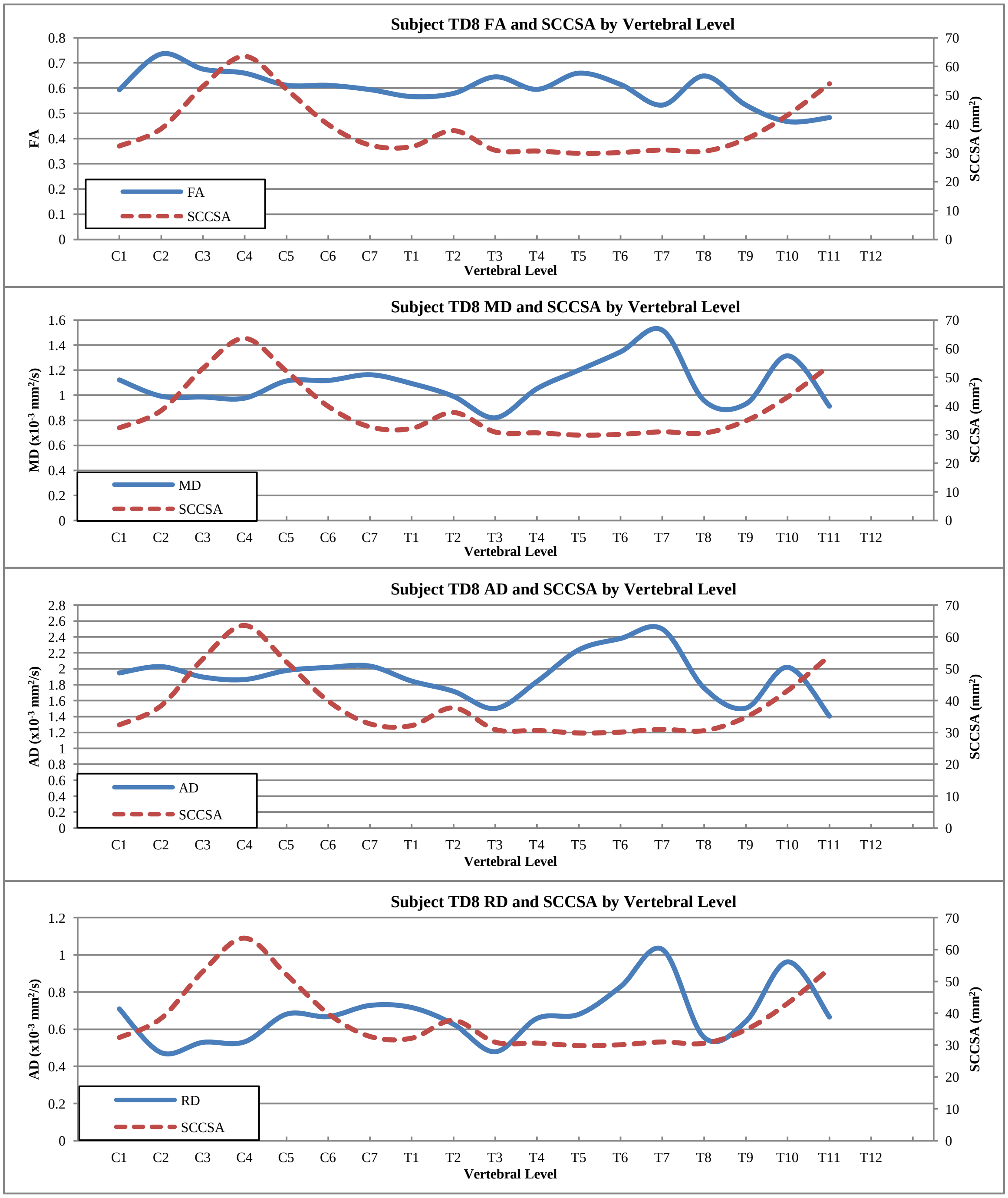

Figure A-18: FA, MD, AD, and RD with SCCSA by vertebral level for subject TD8

Subject TD9

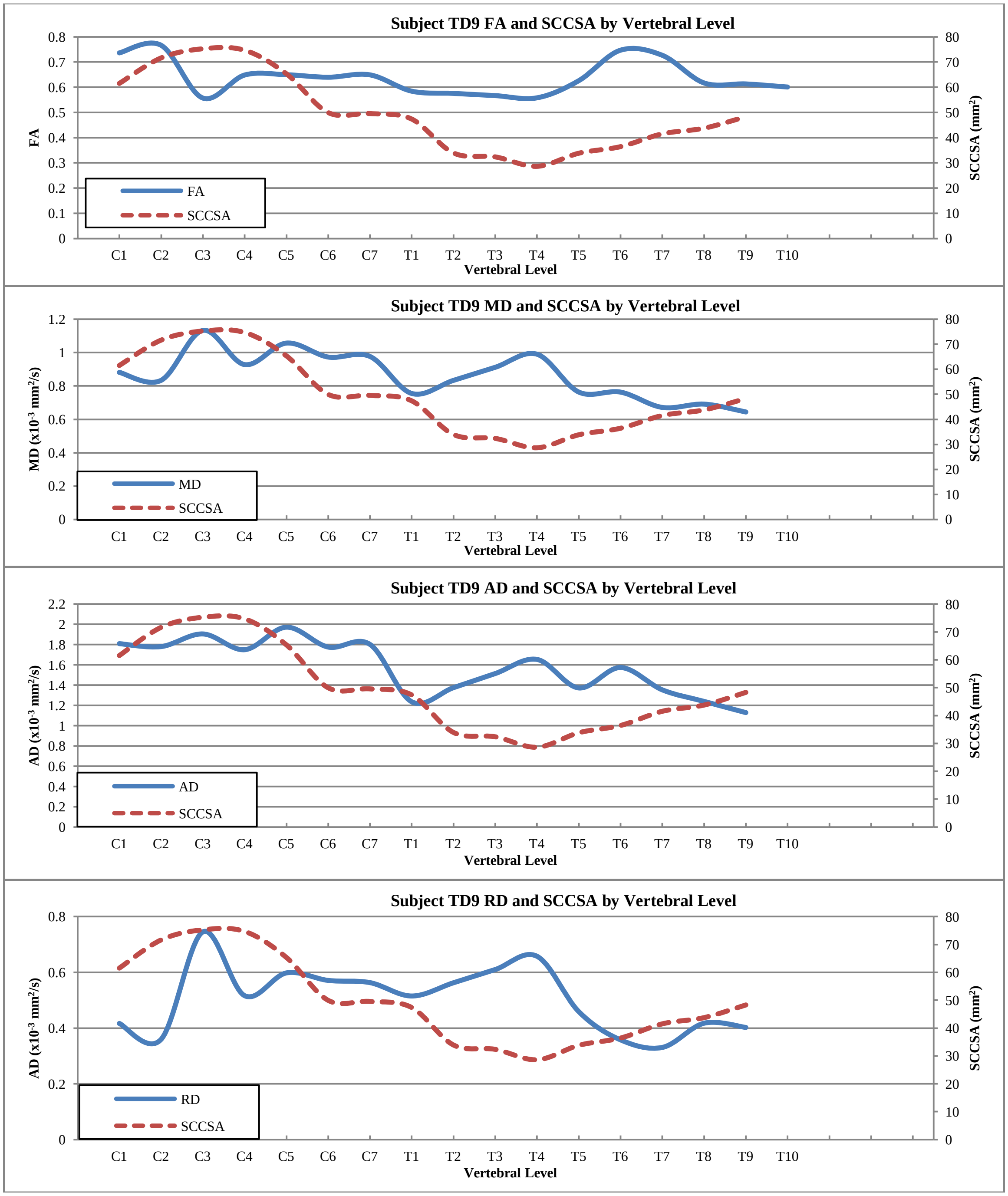

Figure A-19: FA, MD, AD, and RD with SCCSA by vertebral level for subject TD9

Subject TD10

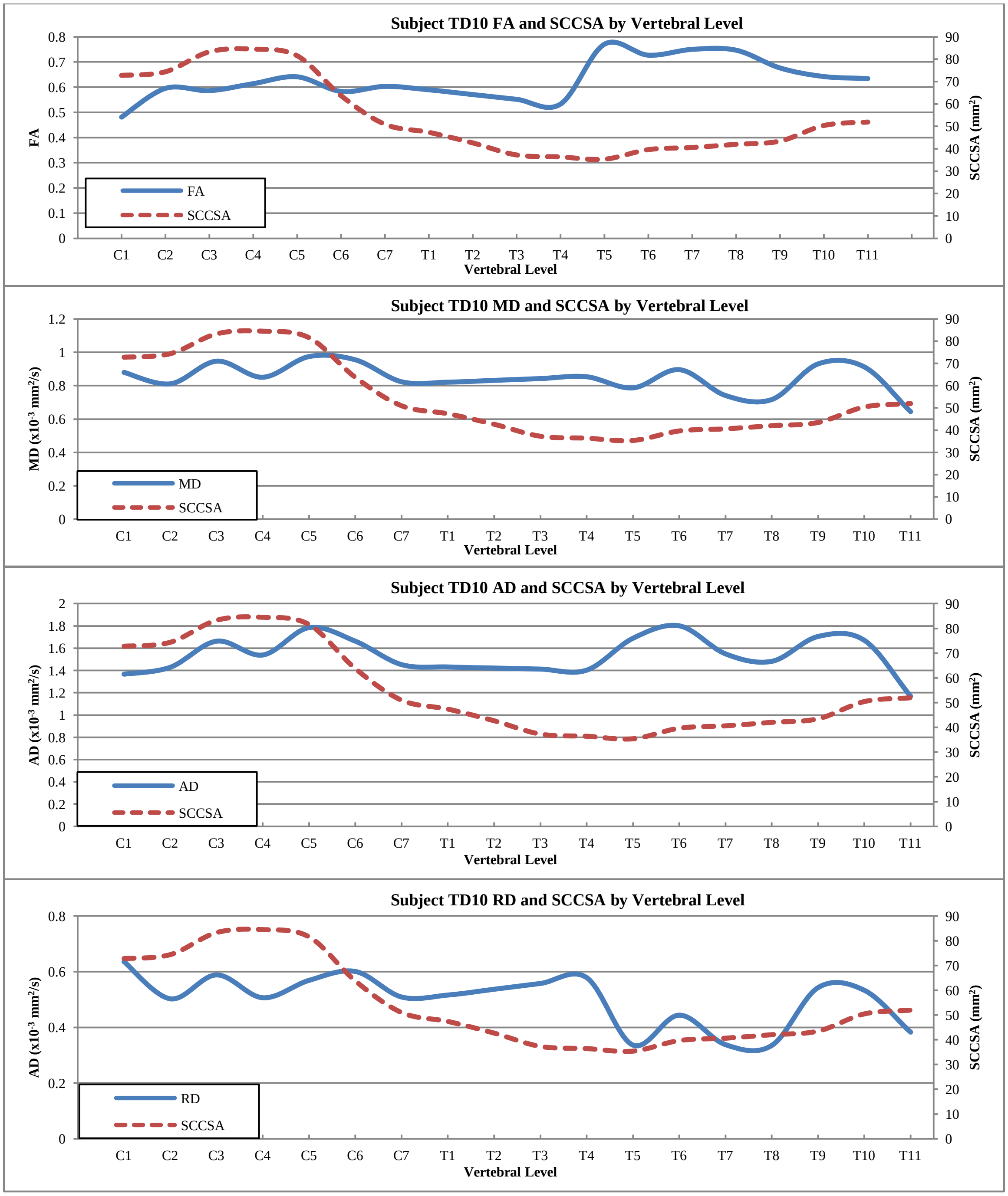

Figure A-20: FA, MD, AD, and RD with SCCSA by vertebral level for subject TD10